Golden-Ten and Related Trajectory Games

de Vos, J.C.

Publication date:
1997

Document Version
Publisher's PDF, also known as Version of record

Golden-Ten and Related Trajectory Games

Hans de Vos

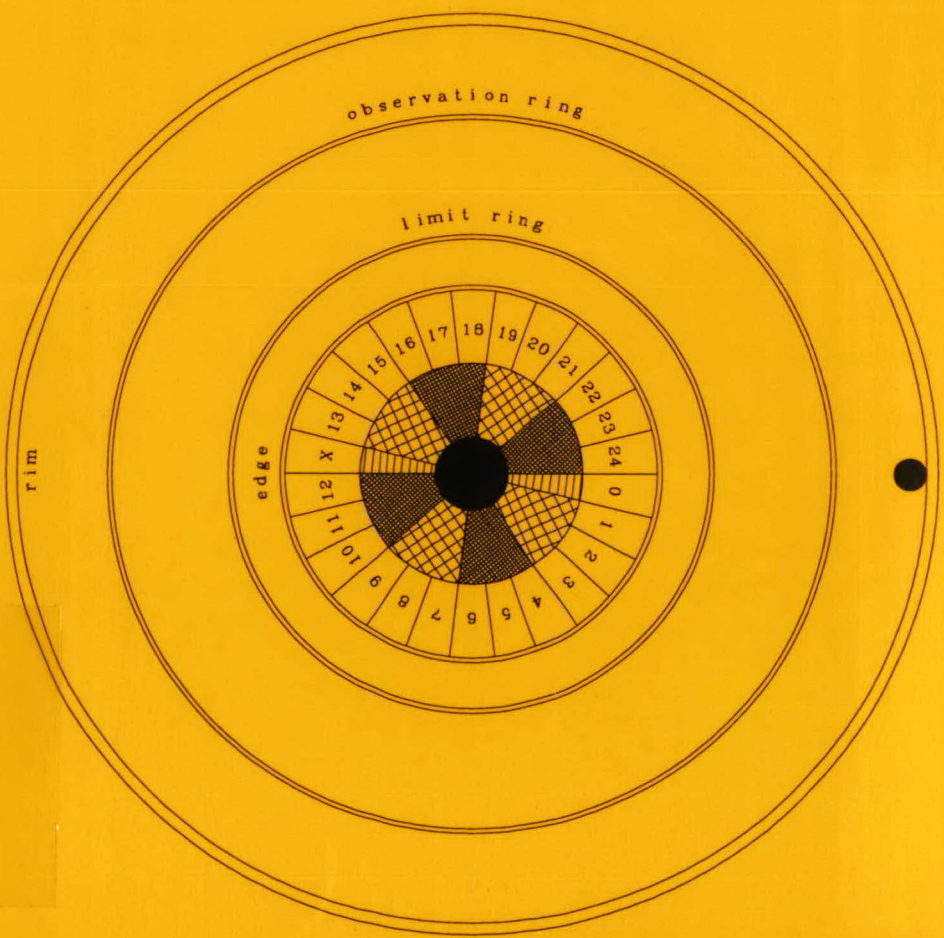

(Top-view on drum, ball and number disc)

Stellingen

behorende bij het proefschrift

Golden-Ten and Related Trajectory Games

van

Hans de Vos

3 december 1997

I

Met behulp van observatie kunnen spelers van Golden-Ten op lange termijn winst behalen.

II

De tot op heden meest gespeelde inzetstrategieën zijn qua verwachte opbrengst niet optimaal.

III

Het potentiële behendigheidsniveau van Golden-Ten, gespeeld volgens en met de hier beschreven regels en attributen, is lager dan dat van Blackjack. Op deze grond kan Golden-Ten worden geclassificeerd als een kansspel.

IV

Er bestaan kogelbaanspelen waarvan het potentiële behendigheidsniveau hoger is dan dat van Blackjack. Er kan daarom niet zonder meer worden gesteld dat alle kogelbaanspelen kansspelen zijn.

V

De baan van de kogel in een kogelbaanspel kan worden gekarakteriseerd als een spiraal van wentelende ellipsen met een periode van vijftien vakjes.

VI

Met behulp van een deterministisch model kan men de beweging van een object alleen globaal beschrijven.

VII

Bij kogelbaanspelen speelt het moment waarop het "rien ne va plus" wordt uitgesproken ten aanzien van de optimale spelersstrategie dezelfde dominante rol als de hoogte van het luchtweerstandsniveau.

VIII

"Er en is nijet sekerder op dese werelt als de doot, ende nijet onsekerder dan de uijre der selver."

Claes Pieterssen Hoondert, *Testamentaire dispositie.* Goes: notariaat Johan van Rijen (1645)

IX

Ontpoldering is een vorm van cultuurvernietiging, en dus een barbarisme.

X

Het vervangen van de term positieve discriminatie door positieve actie doet niets af aan het discriminerende karakter van deze actie.

XI

Als iedere vorm van informatie een zekere waarde vertegenwoordigt, dan zijn alle archeologische opgravingen schatgraverijen.

XII

SAS® kan alles, maar alleen als het goed wordt aangestuurd.

Golden-Ten and Related Trajectory Games

Golden-Ten and Related Trajectory Games

PROEFSCHRIFT

ter verkrijging van de graad van doctor aan de Katholieke Universiteit Brabant, op gezag van de rector magnificus, prof. dr. L.F.W. de Klerk, in het openbaar te verdedigen ten overstaan van een door het college van decanen aangewezen commissie, in zaal YZ 1 van de universiteit op woensdag 3 december 1997 om 16.15 uur

door

JOHANNES CORNELIS DE VOS

geboren op 28 september 1959 te Hoedekenskerke

Promotores: prof. dr. B.B. van der Genugten
prof. dr. ir. J. de Graaf

Copromotor: dr. ir. A.A.F. van de Ven

ISBN 90-361-0016-X

Voor Annelies,
Peter, en Frank.

TOM POES EN DE PASMUNT

Door Marten Toonder

5504 Tom Poes had genoeg gezien. Voorzichtig daalde hij het trapje af en sopte door de modder naar de vaste grond, juist op het moment dat commissaris Bulle Bas op zijn avondronde het terrein passeerde.

'Dat treft goed', zei Tom Poes. 'U moet daar binnen eens kijken!'

'Waarom?' vroeg de politiechef, terwijl hij een blik vol tegenzin op het gebouwtje wierp. 'Ik heb wel wat anders te doen dan friteskramen te inspecteren.'

'Het is geen friteskraam', zei Tom Poes. 'Het is een speelhol. Er wordt gegokt — en dat is toch verboden?'

'Huh?' hernam de commissaris. Hij fronste de wenkbrauwen en bezag de keet met nieuwe ogen, zodat nu het geluid van vallende munten en opgewonden uitroepen tot hem doordrong.

De plichtsgetrouwe beambte aarzelde niet langer; hij betrad de modder en stampte de treden op.

'Wat is hier aan de hand?' vroeg hij bars. 'Hazardspel, huh? Mag ik je papieren eens even zien?'

'Oho!' riep de ondernemer uit. 'U jaagt een arme, oude man de stuipen op het lijf! Men mag toch zeker wel een onschuldig spelletje doen? Daar heeft toch niemand last van?'

'Een onschuldig spelletje?' herhaalde de commissaris. Hij wees beschuldigend op Joost, die met een hoed vol geldstukken voor een apparaat stond en snauwde: 'Wat is dat dan?'

'Behendigheid', verklaarde de grijsaard. 'Die meneer is een héél knappe speler; hij wint altijd!'

Dank zij de welwillendheid van Toonder Studio's b.v.

Contents

Chapter 1

Introduction

1.1 Subject-matter

Golden-Ten is a modified version of Roulette. The game is played with a small ball moving down in a relatively large drum, at the bottom of which lies a stationary disc with numbered compartments. The main differences with Roulette are that the drum is a smooth conic bowl in which the ball gently spirals down, and that the players do not have to bet before the ball has reached a certain level. Golden-Ten is in fact an observation game in which the players try to predict the outcome of a trajectory by observing only the first part of it. Although the players can not control the motion of the ball, it is often claimed that the possibility to observe part of the trajectory enables the players to make a better than random guess on the outcome. For really good players this might imply that they can make money from the game. The ability to make money by playing a game is often considered as some form of "skill"; the presence of this form of skill makes Golden-Ten more attractive to players than Roulette. Furthermore, since the majority of the players is usually not very skillful, Golden-Ten can also be attractive to casino proprietors (it has been suggested, though, that Golden-Ten can only be exploitable when too highly skilled players are refused admittance).

The Dutch authorities - as well as those in other European countries, like Germany and Switzerland - consider Golden-Ten to be a game of chance. This has drastic consequences for potential exploiters, since the law (in Holland) exclusively reserves the right to exploit games of chance to the public institution of "Holland Casino's". Mainly for this reason potential exploiters often claim that Golden-Ten is not a game of chance,

but rather a game of skill. Another reason for this claim may be that recognition would exempt Golden-Ten exploiters from taxes levied on exploitation of games of chance. Holland Casino's, on the other hand, has never been inclined to exploit a second trajectory game in addition to Roulette. All this has in fact reduced the number of official Golden-Ten casino's to zero. The case seemed to be settled in 1991, when the Dutch Supreme Court proclaimed that Golden-Ten is indeed a game of chance, but since then many other trajectory games have been invented - like Eurobsgame and Dromus-24 - and the old discussion is still very much alive.

In the mean time, quite a number of research reports on skill in Golden-Ten - and other, related trajectory games - have seen the light. Some of these research works were carried out by order of (potential) private casino exploiters, and some (indirectly) by order of the government. The conclusions from these reports are not always of the same tenor. For reasons of scientific curiousity, and in an attempt to resolve the ongoing dispute, a joint research team from the two Brabantine universities KUB and TUE, decided in 1992 to submit a scientific research project to the SOBU cooperation centre. The aim of this project was to determine whether or no trajectory games like Golden-Ten involve skill, and - if so - to which extent. SOBU eventually allotted the project to the writer of this thesis. The research work was carried out between January 1993 and August 1997 (in part-time); the results are presented in this dissertation.

The main issue in this research work is the determination of the exact level of skill in Golden-Ten and related trajectory games. More specific questions are where the possible elements of skill eventually come through while playing the game, how the players can employ these skills, what they will win by doing so, and what the implications are for the exploiters. This research work eventually unfolds a number of practical players strategies, including (a practical variant of) the optimal strategy. A strategy is considered to be optimal when its players can reach the highest possible gain; the optimal strategy together with the gains of its players is crucial in the computation of the level of skill. In this research work, the level of skill is presented as an objective measure that allows all kinds of games to be compared on the same scale. This scale thus offers legislators and judges the opportunity to determine exactly which games should be classified as games of chance, or as games of skill.

The research is based on a comparison of standard theoretical models for the motion of a ball in a drum, and a vast collection of empirical

trajectories of genuine Golden-Ten balls moving in a genuine Golden-Ten drum. This comparison results in a complete simulation model for Golden-Ten, and other trajectory games. On the basis of this model, some rational and practical strategies will be developed. The gains (or losses) of these strategies will be used to determine the level of skill, in such a manner that it links up closely to the code of the applicable Act on Games of Chance. Hence, one of the interesting aspects of this research is that it is characterized by a multidisciplinary approach. First of all, the model for the motion is of a physical nature, whereas the analysis thereof involves mathematical (i.e. analytical and numerical) techniques. The construction of a simulation model and the development of players strategies are typical examples of statistical research. Gains and losses are subjects on the field of economics, whereas the determination of the level of skill is a juridical matter. This multidisciplinary approach offered the two Brabantine universities KUB and TUE, via their cooperation centre SOBU, an excellent opportunity for a joint research project.

1.2 Approach

An overview of the research results, and the conclusions thereof, is given in chapter 2. The description of the contents of this dissertation therefore starts with chapter 3, where a mechanical, deterministic model is employed to describe the motion of the ball in the drum. This model results in a set of second order, ordinary differential equations, together with a set of theoretical initial conditions. The numerical solution to this system can be found via some preliminary estimates from chapter 4, but an exact analytic solution is not available. However, the introduction of a new set of variables directly leads to an analytic solution for part of the system, whereas the use of asymptotic techniques leads to accurate approximations of the complete solution. The solution clearly shows the overall characteristics of the motion of a ball in a drum. The leading part appears to be played by the coefficient of air friction, which is in fact the small parameter on the basis of which the asymptotic analysis is performed. However, a precursory inspection of some experimental data shows that the motion of the ball is not (completely) deterministic. The asymptotic analysis is therefore extended to local solutions with different initial conditions. Most of these results have been published in De Vos and Van de Ven [11].

Chapter 4 describes the setup and the results of an experiment to

obtain a set of one thousand accurately measured Golden-Ten orbits, together with as much relevant additional environmental information as possible. This experiment was carried out with real casino attributes, which offered the opportunity to also accurately measure the attributes themselves. A thousand Golden-Ten orbits were recorded on tape. These tapes were - after the event - read out by a computer system (that was actually designed to analyse fluid dynamics, but appeared to be also capable of reading Golden-Ten orbits). The elaboration of the recorded images turned out to be a hell of a job, as a result of which only 338 out of a total of 1042 orbits could be made available for further research. These 338 orbits have become accessable as a set of time series of accurate ball coordinates. The remaining 704 orbits are still available on tape, but not as readily accessable time series. The collected environmental data for all thousand orbits are available in the shape of a dataset. The setup and the results are extensively reported and documented in De Vos [8]. The image analysis program is also discussed and published in De Vos [9].

In chapter 5, the experimental results in chapter 4 are compared to the theoretical results in chapter 3, in order to gain insight in the validity of the theoretical assumptions, as well as in the characteristics of real trajectories. This comparison first of all provides estimates for the not directly measured components of the motion (especially the spin), and secondly for otherwise immeasurable model parameters (such as the before-mentioned coefficient of air friction). It also becomes clear that the orbits are far from deterministic. The differences between the deterministic model in chapter 3 and the experimental orbits are explained, and modelled according to a set of second order, stochastic differential equations. This system is supplemented with an appropriate system for the motion along the rim, and one for the downfall into the number disc. After this, a complete simulation model for Golden-Ten has become available. Chapter 5 describes two models: a complete model for Golden-Ten as it is played with real Golden-Ten attributes under normal environmental conditions, and a basic model that corresponds to Golden-Ten played with superior materials under ideal circumstances. The essential difference between these models is the quality of the drum surface. Both models are also suited for simulation of Golden-Ten variants. Most of the contents of chapter 5 has been previously published in De Vos and Van der Genugten [10].

On the basis of simulations by the models described in chapter 5, chapter 6 develops a number of practical players strategies. These strategies

are derived from the basic model, and played in both the basic and the complete model. This gives the expected gains of the strategies, for both models. Furthermore, chapter 6 presents the optimal strategy, i.e. the one with the highest possible expected gain. Furthermore, it is demonstrated how the strategies and their expected gains can depend on the prevailing level of air friction. Since this level is usually not known to the players, chapter 6 offers two alternatives: one to employ a robust strategy, which is a strategy that acts independently of the level of friction, as well as one to estimate this level by means of observation, and then to play an appropriate strategy. This last-mentioned alternative can also be used for Golden-Ten variants. Finally, chapter 6 gives an overview of the strategies and gains of experienced players as these are reported in earlier research work by Albers [1], Boer [3], Embrechts et al. [13] and LaFors & Derksen [16], and compares them to related strategies and gains for the complete model as well as the basic model.

Chapter 2 summarizes the results and conclusions of this dissertation. The arrangement of this chapter is such that it can be easily read and understood by scientists, lawyers, players and (potential) exploiters. After a description of the attributes and the rules of Golden-Ten and related trajectory games, the text discusses the use of intuitive as well as rational strategies. The intuitive strategies are the ones that are usually (or used to be) played in practice, whereas the rational strategies are those derived in chapter 6. The rational strategies may not always offer more fun, but on the other hand do lead to higher expected gains. Although these gains depend on the level of air friction, they are positive in all cases. These conclusions are mainly of interest to players and exploiters. Then, in te last section, chapter 2 focusses the attention on the level of skill. Skill is defined as an objective, quantitative measure based on the expected gains of players. This measure allows all kinds of games - like Roulette, Blackjack and Golden-Ten - to be compared on the same scale. The level of skill of Golden-Ten appears to be clearly different from that of related trajectory games; a fact which is mainly due to variations in the quality of the drum surface. These conclusions are especially of interest to lawyers, and to the legislator. The decision on whether or no to classify Golden-Ten as a game of chance, depends on the official threshold value, which can only be set by the legislator.

Chapter 2

Playing the game

2.1 The rules of the game

2.1.1 Game attributes

The main attributes of the game are a solid little ball, made of ivory-like synthetic material, and a big, slightly grooved uncoated metal drum, at the bottom of which lies a motionless disc with twenty-six equally large, numbered compartments. The drum and the number disc are supposed to be in a perfectly horizontal position. See figures 2.1 and 2.2 for a top- and a cross-section side-view, respectively. Table 2.1 provides the exact dimensions of the attributes of the particular game that we will call "Golden-Ten". The attributes belonging to related trajectory games may be slightly different. The game starts when the ball is launched from a slit plastic arm, right in between the compartments 0 and 24, in the counter-clockwise direction, along the rim. Note that the compartments are numbered from 24 to 13, then to X, and further from 12 to 0. From now on, we renumber them consecutively from 0 to 25 (see also figure 2.1).

After rolling a few rounds alongside of the rim, the ball gradually spirals down the surface of the drum. This surface is cut on a milling-machine, and contains approximately three concentric, shallow grooves per millimeter. On the way down, the ball eventually crosses two clearly visible surface rings, which are in fact nothing but thin rings of slightly deeper cut grooves. The upper ring is called the *observation ring*, the lower one the *limit ring*. The players can start betting - on the final outcome - when the ball reaches the observation ring, and must stop betting when it reaches the limit ring (see subsection 2.1.2 for more details). In

object	attribute	dimension	value
drum	surface	inclination	4.75 deg
	rim	diameter	974 -1000 mm
	observation ring		770 - 780 mm
	limit ring		510 - 520 mm
	edge		410 mm
number disc	base	diameter	400 mm
		height	7 mm
	lamellae	length	80 mm
		width	2 mm
		height	35 mm
ball		diameter	35 mm
		weight	38 gr

Table 2.1: Dimensions of the main attributes of Golden-Ten (cf. figures 2.1 and 2.2).

the end, the ball falls off of the edge, and comes to a standstill right in between two partitioning compartment lamellae on the number disc. The number of the compartment determines the final outcome.

2.1.2 Rules of Golden-Ten

Thes rules of Golden-Ten apply to the players, the bank, and the master of the game. Note that the master is called the *bouleur*, which is French for "he who handles the ball".

1. The surface of the drum and that of the ball must always be clean, i.e. completely free of specks and dust. They may therefore never be touched with bare hands, and should be regularly cleaned with alcohol: at least once every hour.

2. The ball must be launched from a standstill on the very top of the slit plastic arm.

3. The construction of the arm must be such that the ball completes at least five, and no more than ten full rounds along the rim, before it comes loose of it and starts to descend.

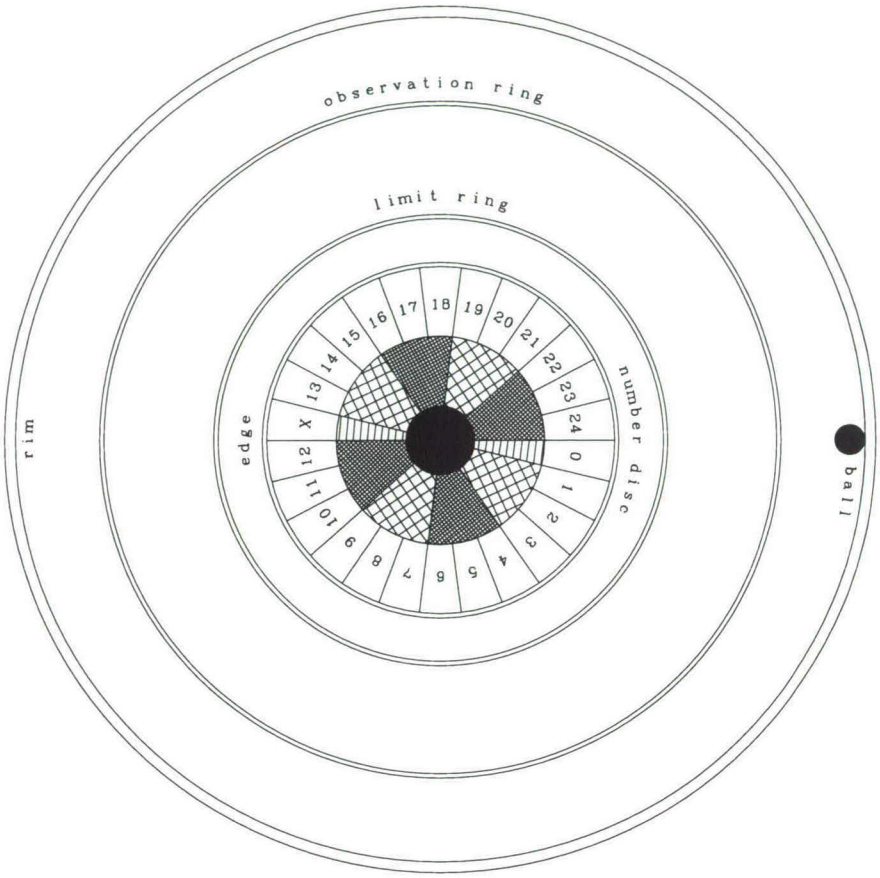

Figure 2.1: Top-view on drum, ball and number disc. Scale 1 to 8.7. (Note: from now on, the numbers 24-0 are renumbered as 0-25, counter-clockwise. See also figures 2.3 and 2.4.)

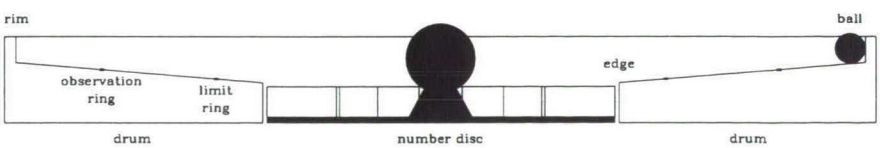

Figure 2.2: Cross-section side-view on drum, ball and number disc. Scale 1 to 8.7.

4. The players are only allowed to place bets after the orbit of the ball has intersected the outer edge of the observation ring. After the intersection has taken place, the bouleur proclaims "faites vos jeux".

5. The players can choose between five different variants of bets:

   (a) *plein*, or one single compartment number,

   (b) *cheval*, or a sector of two consecutive compartments,

   (c) *transversale plein*, or three consecutive compartments,

   (d) *carré*, or four consecutive compartments,

   (e) *transversale simple*, or six consecutive compartments,

   plus any possible combination of these five variants.

6. The players are not allowed to place bets after the orbit of the ball has intersected the inner edge of the limit ring. After the intersection has taken place, the bouleur proclaims "rien ne va plus".

7. All stakes accrue to the bank. Winning bets are payed off with twenty-four times the stake-money, divided by the number of compartments on which the stake was put.

Golden-Ten is a so-called *observation game*, which means that it challenges the players to predict the end of a trajectory by observing only the first part of it. It is in the interest of the players to be allowed to bet as late as possible, since the shorter the remaining part of a trajectory, the more reliable the prediction of the final outcome can be (see subsection 2.2.2). It therefore follows - from rule number 6 - that the bouleur plays a pre-dominating role in this game, since he in fact determines when the players have to stop observing. By stopping the observation process too soon, the bouleur will financially injure the players. This would be especially true if he would order the players to stop placing bets before the ball has reached the outer edge of the limit ring, since this would deprive the players of their essential reference point (being the intersection point with the limit ring, see section 2.2). So, in order to be able to play Golden-Ten according to the rules, the bouleur should be highly trained in observing the right moment for proclaiming "rien ne va plus".

2.1.3 Rules and attributes of related trajectory games

The game *Golden-Ten* is defined by the attributes in subsection 2.1.1, together with the rules in subsection 2.1.2. Strictly speaking, games that do not exactly conform to this combination of rules and attributes, should not be called "Golden-Ten". However, in practice some of these variants do bear this name, particularly games which are played in the same manner, and with the same kinds of attributes as those described in subsection 2.1.1. However, the dimensions of the attributes may be slightly different, even those of the drum and the ball (for details, see LaFors & Derksen [16], Teugels [24] and Van der Genugten & Borm [26]). These differences do not change the nature of the game, since - for the players - it is still a matter of predicting the final outcome through observing the first part of a trajectory. But they do change the strategies of the players (see subsection 2.2.3), as well as the corresponding gains and losses (see subsection 2.3.3).

Even the games *Roulette Opta II A*, as described by Urban [25], and *Fantasie 24*, as described by Gill & Oudshoorn [14], are played in the same manner and with the same kinds of attributes as Golden-Ten. Therefore, these games are sometimes also called "Golden-Ten". On the other hand, games like Eurobsgame and Super-Ten are also played with a ball and a grooved metal drum, but in both cases the surface of the drum differs from that of Golden-Ten. *Eurobsgame* is played with a drum with six rings (see Boer [3]), thereby increasing the number of possible reference points. This turns out to be especially useful - for players - when the bouleur is inclined to stop the betting too early, i.e. before the ball has reached the inner edge of the limit ring. *Super-Ten* is a - fictitious - game, played on a - yet to design - extremely smooth, but still slightly grooved metal drum. It is called "Super-Ten", because the gains for the players are higher than those for players of Golden-Ten (i.e. the game described in subsections 2.1.1 and 2.1.2). The purpose of defining this new game is merely to use it as an example in subsection 2.3.3 (about skill in Golden-Ten).

Numerous variants of Golden-Ten can be created through simple modifications of the attributes and the rules in subsections 2.1.1 and 2.1.2. We here mention three of them, namely Kogelspel, Euro-roulette, and Dromus-24. *Kogelspel* is described by Wagenaar & Groeneweg [33], and is played with a smooth wooden drum, instead of a grooved metal drum. This variant is partly beyond the scope of our research, since the charac-

teristics of a motion on a perfectly smooth surface may be quite different from those of a motion on a slightly rough surface (see sections 5.3 and 5.4). The same is true for the game *Euro-roulette*, which is played with a drum made out of synthetic material. On the other hand, *Dromus-24* is played with a grooved metal drum, but the limit ring on this drum is slightly elevated. The players must place their bets before the ball falls over the limit ring. This game strongly resembles Golden-Ten variants of which the rules require that the players must place their bets before the ball has left the rim. This requirement in fact reduces the number of possible reference points to zero.

2.2 Strategies for the game

2.2.1 Intuitive strategies

A naive player just bets on an arbitrary number, without any consideration, and is therefore likely to lose his stake in twenty-five out of twenty-six games. In the remaining game, the pay-off is only twenty-four times the stake, which does not compensate for the loss in the twenty-five other games. Therefore, players sometimes try to play a certain strategy, which is a plan of action based on an observed trajectory, staking money on one or more numbers in such a way as to maximize the expected gain or to minimize the expected loss. However, this does not imply that all strategies try to maximize the expected gain, since some players already consider their strategies to be satisfactory when they can enjoy playing Golden-Ten without losing too much money, or when they occasionally predict the right outcome.

When observing the orbit of a ball in a conic drum, one will notice that this orbit is in fact an elliptical spiral (the radius of the spiral does not decrease monotonously). It is sometimes believed - according to Boer [3] and Wagenaar & Groeneweg [33] - that under ideal circumstances the orbit can be a circular spiral (with a monotonously decreasing radius), but in chapter 3 it will be proven that the spiral is always elliptical. Furthermore, chapter 3 will show that the axes of the "ellipse" is rotating, a fact which seems already known (see Boer [3], LaFors & Derksen [16], NSC [19] and Van der Genugten & Borm [26]). However, as Delbaen & Haezendonck [7], Embrechts et al. [13] and Wagenaar & Groeneweg [33] have pointed out, this is often ignored. The concept of a non-rotating elliptical spiral is sketched in figure 2.3. The most common strategies in

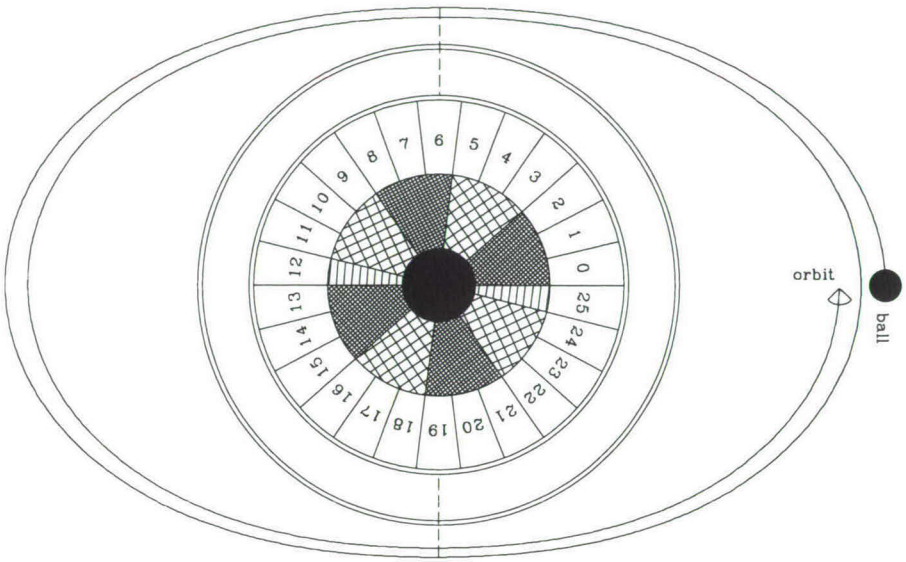

Figure 2.3: Imaginary elliptical orbit of a Golden-Ten ball.

practice are based on the idea that the ball falls off of the edge at the angular position of the minor axis of the ellipse (in figure 2.3 compartment numbers 6 and 19) and that the final outcome should therefore be predicted as one of the two diametrical numbers corresponding to this angular position. According to Boer [3] and Embrechts et al. [13], this position can be roughly estimated by observing the intersection point of the orbit with the limit ring.

To secure themselves against a possible half revolution of thirteen compartments more or less, most players (even those that seem to know that the ellipse is rotating) bet on at least two diametrical numbers. Usually they even bet on two diametrical sectors (i.e. short series of consecutive compartments). This will increase the probability of a correct prediction, but - on the other hand - it will decrease the total pay-off when the prediction actually is correct, so it is not immediately clear that this will increase the expected gain. According to Albers [1], NSC [19]

and Van der Genugten & Borm [26], the most commonly used bet is a combination of two diametrical sectors of three compartments, also known as *double transversale plein* (see subsection 2.1.2). In case of a correct prediction, this bet yields a pay-off of $24/4 = 6$ times the stake.

Other, but less common strategies are not based on observation of the intersection point with the limit ring, but - according to Embrechts et al. [13] - focus on the intersection point with the observation ring, or - according to Embrechts et al. [13], Van der Genugten & Borm [26] and Wagenaar & Groeneweg [33] - on the point where the ball comes loose of the rim. Furthermore, it is sometimes proposed - e.g. by Wagenaar & Groeneweg [33] - to observe the time span for the motion from rim to observation ring as well (although it is not explained how one could use this extra information). Finally note that seemingly only LaFors & Derksen [16] do not propose bets on diametrical sectors, although they do advise to bet on multiple numbers (i.e. on five-number sectors).

2.2.2 Rational strategies for Golden-Ten

On the basis of the general characteristics of the motion - i.e. some kind of elliptical spiral towards the edge of the drum - one can derive several practical and gainful strategies. Figure 2.4 shows an elliptical spiral, albeit one with a strongly exaggerated ellipticity. (In practice, the difference in length between the minor and the major axis is often less than 3 mm, see figures 6.3 and 6.4.) The periodicity of the motion is $15\frac{1}{16}$ compartments (see section 6.5), which is illustrated by the minor axis in figure 2.4, which moves from 6 to 21 to 10, etc. (just count the compartments). The final compartment number usually coincides with the angular position of the minor axis during the last not fully completed ellipse, since the ball falls off of the edge just before reaching this axis position, and comes down just a little bit further, due to a short free fall down onto the disc. However, when trying to predict this final outcome, one has to realize that the motion also contains random factors, which slowly accumulate, and thus disturb the motion. Hence, to eliminate as many random factors as possible, one should observe and place bets as late as possible.

A first strategy is based on the idea that by observing the compartment position of the minor axis before the orbit intersects the limit ring, one can generate a (single-number) prediction for the final outcome by adding a multiple of $15\frac{1}{16}$ compartments. The appropriate multiple de-

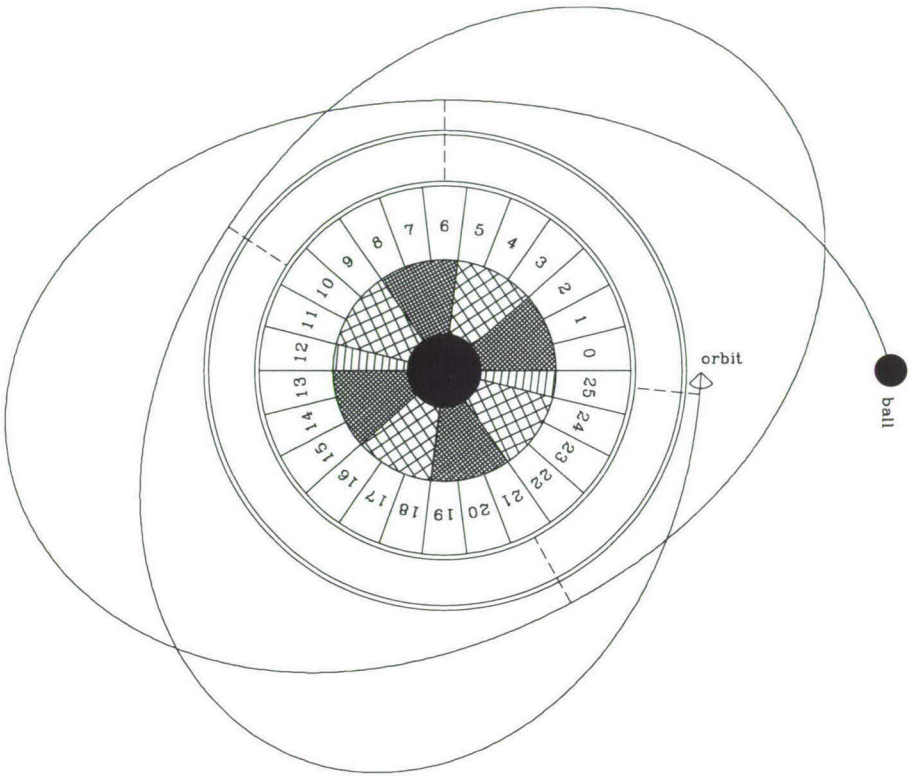

Figure 2.4: Realistic, though strongly exaggerated, elliptical orbit of a Golden-Ten ball.

pends solely on the ratio of the air friction level and the diameter of the limit ring. For the specific drum described in subsection 2.1.1, and the friction levels from the experimental setup in chapter 4, this number has already been calculated, and presented as the difference in compartment numbers (modulo 26) in table 6.1 (see section 6.1 for more explanation). This strategy is called by the name *Min*, which is short for "minimum strategy" (it is based on observation of a "minimum distance" or minor axis). In case the actual friction level is not known, or when the diameter

of the limit ring is different from that in table 2.1, the appropriate multiple of $15\frac{1}{16}$ compartments can be estimated as described in section 6.5 (according to table 6.6).

The exact position of the minor axis can be quite hard to observe, especially when the ellipticity is much smaller than suggested by figure 2.4. As an alternative to observing the ellipse itself, one may content oneself with observing only the intersection point (of the centre of the ball) with the (outer edge of) the limit ring. This intersection point lies just before the minor axis: the difference is usually two compartments. This leads to a strategy that generates a (single-number) prediction for the final outcome by adding a multiple of $15\frac{1}{16}$, plus 2 compartments. This is the "intersection strategy", or the strategy *Int*, presented in table 6.1 (for more details, see section 6.1). A refinement of *Int* is given as *Adv* (short for "advanced strategy"), also in table 6.1. It estimates the difference between the intersection point and the position of the next minor axis by also taking into account the observed "height", i.e. the length of the minor axis just before the intersection, minus the radius of the (outer edge of) the limit ring. See also figures 6.3-6.5. The advanced strategy is almost optimal, in the sense that it uses practically all available information to maximize the expected gain (i.e. the gain in the long run).

It may seem strange that all essential information of an orbit is contained in only two parameters: the intersection point with the limit ring and the (above-described) height above the limit ring. However, in section 6.2 it is demonstrated that all information is in fact contained in these two parameters plus a third one, which is the observed "rise", i.e. the difference in length between the minor axis just before the intersection, and the corresponding major axis (see also figure 6.3). To be sure, this last parameter does not influence any of the strategies, but instead appears to determine the probability of a correct prediction: for high rises, this probability is larger than for low rises, as is the expected gain. The rate of success appears to be always high enough (even for low rises) to yield a quite large positive expected gain, so all advanced players can make quite a lot of money in the long run. But those who want to get rich quickly (i.e. in as few games as possible) should stake more when the rises are high.

All of the above strategies are based on one or two observed parameters, and they maximize the expected gain - given these observations - by betting on the most likely outcome. All other possible outcomes are less likely, and by betting on these, the expected gain will decrease. On

the other hand, multiple-number strategies (that include the most likely number) do have a higher rate of success. Hence, these multiple-number strategies may offer the players more fun, but they also offer them less money. This especially holds for strategies that bet on diametrical sectors, since this presumed kind of symmetry is simply not present (see figure 2.4). If a trajectory towards the edge does not end at the predicted position, it usually skims the edge, and therefore probably ends just before it reaches the next position of the minor axis. The difference between those positions is smaller than $15\frac{1}{16}$: it appears to be usually 14 compartments, instead of 13 (see section 6.1).

2.2.3 Rational strategies for related trajectory games

All Golden-Ten strategies in subsection 2.2.2 depend on the ratio of the air friction level and the (outer) diameter of the limit ring. For the specific drum described in subsection 2.1.1, the diameter of the limit ring is known (viz. 520 mm), but under circumstances different from those described in chapter 4, the actual level of friction may not be known. All that is actually known about this level (as an empirical fact) is that it can vary much between different parts of a day, but not much within such a part (i.e. an afternoon, evening, etc.). An impression of this variation can be obtained from table 6.1, which presents the three strategies *Min, Int* and *Adv* for a high, a moderate, and a low level. If Golden-Ten is played on the particular drum described in subsection 2.1.1, but without any available information on the actual friction level, then a rational strategy is to place bets (in some proportion) on all different numbers in table 6.1 that correspond to one of the strategies, say *Int*. Table 6.4 presents this - still gainful - strategy, called *Rob*, which is short for "robust strategy" (for it is independent of the actual friction level). For details, see section 6.4.

For all trajectory games played with a drum of which the surface has a small angle of inclination, the periodicity of the motion of the ball is $15\frac{1}{16}$ compartments. This directly leads, again, to variants of the intersection strategy that predict the final outcome by adding 2 plus a certain multiple of $15\frac{1}{16}$ to the observed intersection position. The appropriate multiple can be simply estimated by counting the (rounded) number of periods (of $15\frac{1}{16}$ compartments) in a series of - say sixteen - games, and determining the most frequent one of these numbers. The correspondence with the appropriate relative final compartment number is given by table 6.6 (more details in section 6.5). In order to simplify the counting of periods

and compartments, table 6.6 also presents the corresponding number of compartments (i.e. not modulo 26). Note that this method is a better alternative than observing the time span, as proposed by Wagenaar & Groeneweg [33].

The rules of some Golden-Ten variants dictate that the players should place their bets immediately after the ball comes loose of the rim. This leads to a strategy that predicts the final outcome by adding to the observed point a multiple of $15\frac{1}{16}$ plus $\frac{1}{2} \times 15\frac{1}{16} = 7\frac{9}{16}$ compartments (since the angular position where the ball lets loose corresponds to a major, not to a minor axis). It can, however, be very hard to observe this particular position, since the beginning of the trajectory is exactly tangent to the rim. Furthermore, the rest of the trajectory is so long that the role of the random factors may become dominant, and the prediction will probably become incorrect. On the other hand, some variants - like Eurobsgame - resemble Golden-Ten more closely, in the sense that the players can observe exactly the same parameters as those described in subsection 2.2.2. By placing bets immediately after the intersection with the penultimate ring (i.e. the one before the limit ring), the players can even pre-emt the decisions of the bouleur (see subsection 2.1.2). Although placing bets at an earlier moment will slightly decrease the expected gain, this effect can pale into insignificance beside that of the actions of a not highly trained bouleur.

2.3 The skill of the game

2.3.1 A definition of skill

In the Netherlands, the exploitation of games of chance is reserved for people, organizations or institutions that have obtained an official license. Licences are granted on the basis of legislation in general, and the Act on Games of Chance in particular. Under Title I of the General Provisions, article 1 of this act literally states

> ... het is verboden gelegenheid te geven om mede te dingen naar prijzen en premies, indien de aanwijzing der winnaars geschiedt door enige kansbepaling waarop de deelnemers in het algemeen geen overwegende invloed kunnen uitoefenen, tenzij ingevolge deze wet vergunning is verleend; ...

An English translation of this code reads

> ... it is forbidden to exploit games played to compete for prize money, if the participants in general do not have a predominant influence on the probability to win, unless a license is granted under this act; ...

All games that are covered by this act are considered to be *games of chance*. All other games are called *games of skill* (see also Borm and Van der Genugten [4]). Note that all games under consideration are games for which the results of the participants can be measured in terms of money. Therefore, only this type of games will be subject to further discussion. The terminology and the lines of thought for this discussion are largely borrowed from the work of Van der Genugten et al. ([31] and [28]).

A game only involves skill if a player can improve his monetary result by learning. However, in games with chance elements, results are also influenced by a random effect, which can be judged in a very operational way: the random effect is the additional result a player would obtain if he should know the outcomes of all chance elements in the game in advance (e.g. the outcomes of all random disturbances along the way of a trajectory). It is obvious that in *games of pure chance*, there is no learning effect, since the players have no influence on the outcome. An example of such a game is Roulette. On the other hand, there are *games of pure skill*, in which there is no random effect, since the actions of the players completely determine the outcome. An example of such a game is Solitaire. However, most games are not pure, so they can appositely be called *mixed games*. When applying the law, pure games cause no problem, but mixed games do.

The main issue when interpreting the above-mentioned code of law, is that of "predominant influence". Considering the result of a player, this "influence", or skill, can be described as the contribution of the learning effect, **relative** to that of the random effect. In games of pure chance, this contribution is zero, whereas in games of pure skill it is exactly one hundred percent. It is up to the legislator to judge at which level the influence becomes "predominant", and the game in question can be called a game of skill. Typically, games with a relatively large random effect usually offer large pay-offs with small probabilities. Especially this last mentioned type of games seems to attract game addicts, see e.g. Wagenaar & Keren [34]. By the judgement mentioned above, such games will be classified as games of chance, which implies that these games will be the object of the law on gambling, and that exploitation will be

regulated.

For a more concrete description of the learning effect, the random effect, and - derived from these notions - the concept of (relative) skill, it is important to note that the prevailing underlying principle is that skill should be related to players in practice, or "participants in general", as closely as possible. To this aim, three types of players should be distinguished:

1. beginner:
   he who has almost no experience, (2.1)
2. real average player:
   he whom one is most likely to meet in reality, (2.2)
3. virtual average player:
   average player, who has been told in advance
   the outcomes of the chance elements in the game. (2.3)

Note that the virtual average player is easily imaginable, but does not exist in actual play, wherefore he is called virtual. Under definitions (2.1) - (2.3), learning can be considered as the transition from beginner to average player. This leads to the definition

$$\begin{aligned}&\text{learning effect} =\\ &\text{result real average player} - \text{result beginner}.\end{aligned} \tag{2.4}$$

Furthermore, the random effect can be considered as the advancement of the real to the virtual average player. This leads to

$$\begin{aligned}&\text{random effect} =\\ &\text{result virtual average player} - \text{result real average player}.\end{aligned} \tag{2.5}$$

With given values for the results of the three types of players in (2.1) - (2.3), the two effects in (2.4) and (2.5) can be quantified.

The following definition specifies skill as a measure of the (relative) contribution of the learning effect (as compared to that of the random effect) to the results of the players in practice:

$$\text{skill} = \frac{\text{learning effect}}{\text{learning effect} + \text{random effect}} \tag{2.6}$$

$$= \frac{\text{result real average player} - \text{result beginner}}{\text{result virtual average player} - \text{result beginner}}. \tag{2.7}$$

Clearly, this implies that

$$\underset{\text{(pure chance)}}{0} \leq \text{skill} \leq \underset{\text{(pure skill)}}{1.} \tag{2.8}$$

So, games in which the random effect dominates the learning effect, have a low skill, whereas games in which the learning effect dominates, have a high skill. Hence, the translation of "predominant influence" in the code of law is "high skill". The definition of skill in (2.7) makes the way in which games can be judged objective. All games can be measured on this scale, but only after determination of the results for the three types of players in (2.1) - (2.3).

2.3.2 Measuring skill

Although the concept of skill also applies to more-person games, the class of games under consideration in the remainder of this section is restricted to one-person games. In these games, all participants face the same opponent, namely the bank. There is no strategic interaction between the players, and the bank follows a predescribed and fixed strategy (for Golden-Ten, see subsection 2.1.2). Furthermore, it is assumed that

a. games are repeated with

  a1. objective probabilities determined by the rules of the game;

  a2. independent chance elements during repetitions;

b. players can be identified by their strategies;

c. the result of a player is the mean of his gains (in terms of money) in the long run, i.e. the expected gain of the corresponding strategy.

Under these restrictions, results of players can be described numerically. From now on, the results - as they are mentioned in assumption c - will be expressed as the expected gains per unit of stake. More formally:

$$\text{result} = \frac{\text{mean gain in the long run}}{\text{mean stake in the long run}}. \tag{2.9}$$

This definition provides a direct link to the conclusions from the analysis in chapter 6.

The mechanism for measuring skill in (2.7) can be put into operation as soon as the gains of the strategies of the three types of players in

(2.1) - (2.3) have been determined. However, especially the strategy of the type average player can be hard to determine, since there is often no consensus (among lawyers in general) about the strategy of this player in practice. A pragmatic solution to this problem is to replace the concept of the rather subjective average player with the rather objective advanced player (cf. (2.3) and (2.3)):

$2'$. real advanced player:
he who plays an advanced (almost optimal) strategy, (2.10)

$3'$. virtual advanced player:
advanced player, who has been told in advance
the outcomes of the chance elements in the game. (2.11)

This substitution yields an increased difference with the result of the beginner, but since this holds for both the real and the virtual advanced player, the relative effect on the definition of skill is presumably small. More formally:

$$\begin{aligned}
\text{skill} &= \frac{\text{learning effect}}{\text{learning effect} + \text{random effect}} \\
&= \frac{\text{result real average player - result beginner}}{\text{result virtual average player - result beginner}} \\
&\approx \frac{\text{result real advanced player - result beginner}}{\text{result virtual advanced player - result beginner}} \qquad (2.12) \\
&= \frac{\text{potential learning effect}}{\text{potential learning effect} + \text{potential random effect}}. \qquad (2.13)
\end{aligned}$$

In expression (2.13), the difference of the real advanced player with the beginner is called *the potential learning effect*, because it does not measure what an average player will learn, but what a game allows potentially to be learned. The same interpretation holds for *potential random effect* as the difference between the virtual and the real advanced player.

This quantitative way of measuring skill is quite effective as long as the strategies of advanced players can be determined. This is the case for Golden-Ten, but also for other casino games, like Blackjack (see Van der Genugten [29]). With the letter G denoting the result, or - according to (2.9) - the expected gain per unit of stake of a player or strategy (also cf. section 6.1), and the indices 0, r and v respectively representing the beginner, the real advanced player, and the virtual advanced player,

the level of skill $\mathcal{S}$ of a game can now be expressed as a simple formula:

$$\mathcal{S} = \frac{G_r - G_0}{G_v - G_0}. \tag{2.14}$$

For the card game Blackjack, as it is played in Holland Casino's, Van der Genugten [29] calculated a skill of 0.035. This rather low value expresses nicely that the game does contain a potential learning effect, but also that the potential random effect is much larger. Note that acknowledged games of skill might be expected to have a level higher than 0.035, since Blackjack is known as a game of chance. However, it is up to the legislator to set the official threshold value on this scale.

2.3.3 Skill in Golden-Ten

Like Golden-Ten, Roulette is in fact a trajectory game, except that the ends of the trajectories are practically unpredictable. Apart from the precise actions the players can take, this unpredictability leads to a level of skill equal (or close) to zero. About the real advanced player, we know that he always plays "simple" (i.e. bets on red/black or even/uneven), since then he maximizes his expected gain (i.e. minimizes his expected loss) to $G_r = -\frac{1}{74} \approx -0.014$ (when he plays American Roulette, see Van der Genugten & Borm [27] and Van der Genugten [28]). If the beginner also plays simple, then we have $G_r - G_0 = 0$, hence also $\mathcal{S} = 0$, according to (2.14). If, on the other hand, the beginner does not play simple (i.e. he bets on one or more specific numbers), then his expected gain equals $G_0 = -\frac{1}{37} \approx -0.027$, which is less than -0.014. With $G_v = 35$, since the virtual advanced player always wins $36 - 1 = 35$, this leads to a level of skill of $\mathcal{S} = (-0.014 + 0.027)/(35 + 0.027) \approx 0.00037$, which is very close to zero. These results are listed as line one in table 2.2, which gives a ranking of a number of casino games - including Roulette - according to their level of skill. This table also lists the results for Blackjack, as they can be computed from the results in Van der Genugten [30].

When the beginner has not yet developed any specific skills in playing Golden-Ten or variants like Kogelspel or Eurobsgame, he plays the game as if it were Roulette. Therefore, his expected gain **per unit of stake** is $G_0 = \frac{24}{26} - 1 = -\frac{1}{13} \approx -0.077$, no matter which bet he chooses (see the rules of the game in subsection 2.1.2, and also Borm and Van der Genugten [4]). The advanced player, who plays an advanced strategy, always bets - according to the results in section 6.1 - on a single

game	G_0	G_r	G_v	$\mathcal{S}$
Roulette	-0.027	-0.014	35	0.000
Kogelspel	-0.077	0.18	23	0.011
Golden-Ten	-0.077	$\leq$ 0.46	23	$\leq$ 0.023
Eurobsgame	-0.077	$\geq$ 0.64	23	$\geq$ 0.031
Blackjack	-0.057	0.007	1.8	0.035
Super-Ten	-0.077	$\geq$ 2.15	23	$\geq$ 0.097

Table 2.2: Ranking of some casino games, according to their level of skill (based on the expected gains of the beginner, the real and the virtual advanced player).

number. This leads to an expected gain per unit of stake of $G_r = 0.46$, or less, depending on the specific circumstances in the casino (cf. the complete model in table 6.2). With $G_r = 24 - 1 = 23$, this yields a level of skill for Golden-Ten of $\mathcal{S} = (0.46 + 0.077)/(23 + 0.077) \approx 0.023$. For Kogelspel, as it is described by Wagenaar & Groeneweg [33], we find a level of skill of 0.011, which is even smaller. As far as Eurobsgame is concerned, the data in Albers [1] yield an expected gain of experienced players of 0.64 (see also table 6.9). Since these experienced players may not yet have been advanced, this leads to a level of skill of at least 0.031.

The ranking in table 2.2 - according to the objective measure in (2.14) - shows that Kogelspel and Golden-Ten contain less skill than Blackjack, which is classified (by the Dutch Supreme Court) as a game of chance. Hence, if the threshold value on this scale is set above the level of Blackjack, both trajectory games should be classified as games of chance. This probably also holds for Eurobsgame, since its level of skill is not much higher (it may even be lower) than that of Blackjack. However, an exception must be made for the - yet to design - trajectory game Super-Ten, as defined in subsection 2.1.3. Whereas the grooves of a Golden-Ten drum are in fact quite deep (see subsection 5.6.5), thus leading to a situation (cf. the complete model in table 6.2) in which the real advanced player only reaches a gain of 0.46, the grooves of a Super-Ten drum are quite shallow and smooth (cf. the basic model in table 6.2), thus leading to a gain as high as 2.15, or a level of skill of 0.097. It then depends on the threshold value set by the legislator whether Super-Ten should still be called a game of chance.

Although the level of skill in Golden-Ten is rather low, the real advanced player can still make a fair profit of 0.46 per unit of stake. The fact that Golden-Ten casino's usually do not go broke can be explained by the fact that in practice most players are not advanced. The required skills for Golden-Ten largely involve observation skill. Whereas some players do not have such skills, others may be unaware of them, and not observe anything at all. Furthermore, it is obvious that individual players can have quite different skills. On the other hand, after reading this book, some (potential) players will become more skillful, thus reducing the profits of the casino's (should there ever be any casino's that exploit this type of trajectory games). This effect may eventually even lead to lower maximum pay-offs, but then the game can lose its attractiveness. If this happens, the game will eventually perish, but only the future can tell if this will really happen.

Chapter 3

The equations of motion

3.1 The mechanical model

The most natural model to describe the motion of the ball is a three-dimensional rigid body model, but before such a model can be constructed, we have to make some basic assumptions:

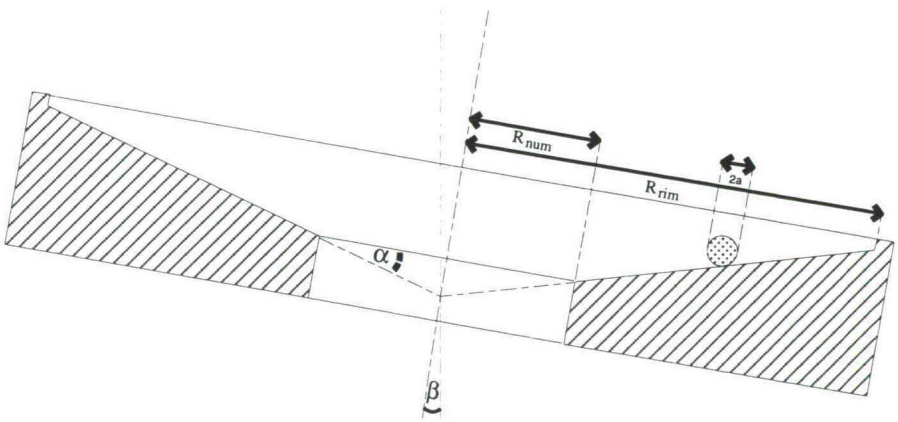

Figure 3.1: Schematic cross-section side-view on the drum and the ball; the tilt of the drum is strongly exaggerated.

a. the ball is a uniform sphere;

b. the drum is rotationally symmetric;

c. the surface of the drum - including that of the rim - is so smooth that the ball rolls without bouncing, but on the other hand so rough that the ball (after a few revolutions along the rim) rolls without slipping;

d. the motion of the ball is completely deterministic, i.e. no random factors are included.

No assumptions are made for the - preferably - horizontal position of the drum, i.e. we allow for a slightly tilted position. We denote the angle over which the drum is tilted with β. The radius of the ball is a, that of the rim is R_{rim}, whereas R_{num} denotes the radius of the edge of the drum (note that this radius is slightly larger than that of the number disc, see figure 2.2). The angle of inclination of the conical drum surface is α (as in figure 3.1). Note that $0 < \alpha \ll \pi/2$ and $0 \leq \beta \ll \alpha$.

We introduce a moving rectangular coordinate system $\{O\boldsymbol{e_1}\boldsymbol{e_2}\boldsymbol{e_3}\}$ to describe the motion of the ball on the surface of the drum (see figures 3.2 and 3.3). The origin O coincides with the apex of the drum, $\boldsymbol{e_1}$ points in the direction from O to P (being the point of contact between the ball and the drum) and $\boldsymbol{e_3}$ is parallel to the drum surface normal in P. The rotation of the three coordinate axes can thus be written as

$$\dot{\boldsymbol{e}}_\mathrm{i} = \frac{d}{dt}\boldsymbol{e}_\mathrm{i} = \boldsymbol{\Omega} \times \boldsymbol{e}_\mathrm{i}, \tag{3.1}$$

where $\boldsymbol{\Omega}$ represents the angular velocity. Calling φ the angle of rotation of $\boldsymbol{e_1}$ about the central axis of the drum, we obtain

$$\boldsymbol{\Omega} = \dot{\varphi} \sin\alpha \boldsymbol{e_1} + \dot{\varphi} \cos\alpha \boldsymbol{e_3}. \tag{3.2}$$

The position $\boldsymbol{x}_o$ of the centre of the ball o, with respect to O (see also figure 3.4), can be described by

$$\boldsymbol{x}_o = r\boldsymbol{e_1} + a\boldsymbol{e_3}, \tag{3.3}$$

where r is the distance from O to P. The velocity $\boldsymbol{v}_o$ of o is the time derivative of $\boldsymbol{x}_o$, so it equals

$$\boldsymbol{v}_o = \dot{\boldsymbol{x}}_o = \dot{r}\boldsymbol{e_1} + r\dot{\boldsymbol{e}}_1 + a\dot{\boldsymbol{e}}_3. \tag{3.4}$$

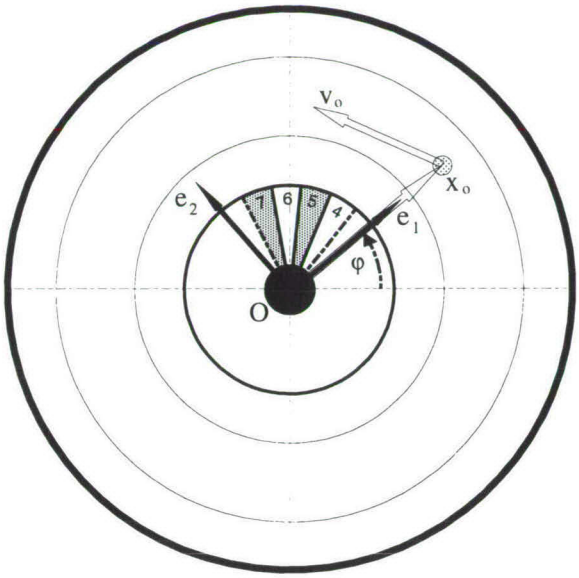

Figure 3.2: The moving frame $\{O\boldsymbol{e_1e_2e_3}\}$; top-view.

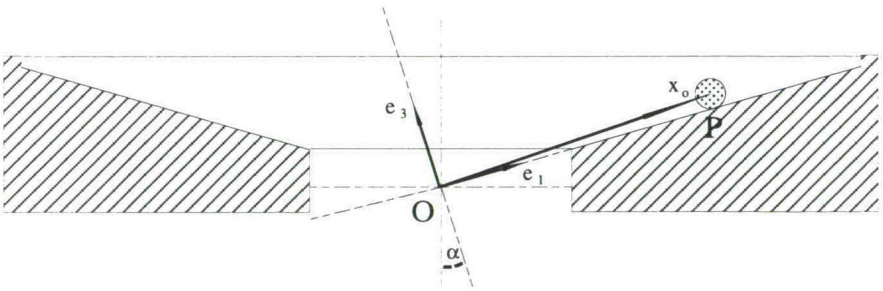

Figure 3.3: The moving frame $\{O\boldsymbol{e_1e_2e_3}\}$; side-view.

By substituting (3.1) into (3.4), and introducing

$$R = r\cos\alpha - a\sin\alpha, \tag{3.5}$$

we obtain

$$\begin{aligned} \boldsymbol{v}_o &= \dot{r}\boldsymbol{e_1} + (r\dot{\varphi}\cos\alpha - a\dot{\varphi}\sin\alpha)\boldsymbol{e_2} \\ &= \frac{\dot{R}}{\cos\alpha}\boldsymbol{e_1} + R\dot{\varphi}\boldsymbol{e_2}. \end{aligned} \tag{3.6}$$

Likewise, the acceleration of o is

$$\begin{aligned} \dot{\boldsymbol{v}}_o &= \frac{\ddot{R}}{\cos\alpha}\boldsymbol{e_1} + \frac{\dot{R}}{\cos\alpha}\dot{\boldsymbol{e_1}} + \dot{R}\dot{\varphi}\boldsymbol{e_2} + R\ddot{\varphi}\boldsymbol{e_2} + R\dot{\varphi}\dot{\boldsymbol{e_2}} \\ &= (\frac{\ddot{R}}{\cos\alpha} - R\dot{\varphi}^2\cos\alpha)\boldsymbol{e_1} + (R\ddot{\varphi} + 2\dot{R}\dot{\varphi})\boldsymbol{e_2} + R\dot{\varphi}^2\sin\alpha\boldsymbol{e_3}. \end{aligned} \tag{3.7}$$

According to assumption c, the ball purely rolls; hence the instantaneous velocity $\boldsymbol{v}_P$ of P is zero. With $\boldsymbol{\omega}$ denoting the angular velocity of the ball, this implies

$$\boldsymbol{0} = \boldsymbol{v}_P = \boldsymbol{v}_o + \boldsymbol{\omega} \times (-a\boldsymbol{e_3}). \tag{3.8}$$

Substitution of (3.6) into (3.8) yields

$$\boldsymbol{\omega} = -\frac{R\dot{\varphi}}{a}\boldsymbol{e_1} + \frac{\dot{R}}{a\cos\alpha}\boldsymbol{e_2} + \dot{\psi}\boldsymbol{e_3}, \tag{3.9}$$

where $\dot{\psi}$ denotes the third component of $\boldsymbol{\omega}$, which is called the *spin*. The time derivative of $\boldsymbol{\omega}$ follows from differentiating (3.9), and substituting (3.1) into the result:

$$\begin{aligned} \dot{\boldsymbol{\omega}} = &- \frac{\dot{R}\dot{\varphi} + R\ddot{\varphi}}{a}\boldsymbol{e_1} - \frac{R\dot{\varphi}}{a}\dot{\boldsymbol{e_1}} + \frac{\ddot{R}}{a\cos\alpha}\boldsymbol{e_2} + \frac{\dot{R}}{a\cos\alpha}\dot{\boldsymbol{e_2}} + \ddot{\psi}\boldsymbol{e_3} + \dot{\psi}\dot{\boldsymbol{e_3}} \\ = &- \frac{R\ddot{\varphi} + 2\dot{R}\dot{\varphi}}{a}\boldsymbol{e_1} + (\frac{\ddot{R} - R\dot{\varphi}^2\cos^2\alpha}{a\cos\alpha} - \dot{\varphi}\dot{\psi}\sin\alpha)\boldsymbol{e_2} \\ &+ (\frac{\dot{R}\dot{\varphi}\tan\alpha}{a} + \ddot{\psi})\boldsymbol{e_3} \end{aligned} \tag{3.10}$$

The equations of motion are implicitly contained in the law of momentum and that of moment of momentum (consult e.g. Likins [17], ch. 8).

With m representing the mass of the ball, and $\boldsymbol{F}$ the total force acting on the ball, the first law reads

$$m\dot{\boldsymbol{v}}_o = \boldsymbol{F}, \tag{3.11}$$

and the second states

$$I\dot{\boldsymbol{\omega}} = \boldsymbol{M}, \tag{3.12}$$

with I representing the central moment of inertia, so $I = \frac{2}{5}ma^2$, and $\boldsymbol{M}$ being the momentum about o. Before we can elaborate these equations by writing them out in components in the $\{O\boldsymbol{e_1e_2e_3}\}$-system, we must first specify $\boldsymbol{F}$ and $\boldsymbol{M}$. Four distinct forces act on the ball: the normal force $\boldsymbol{F_n}$, the frictional force (or dry friction) $\boldsymbol{F_d}$, the resistive force $\boldsymbol{F_a}$ (due to air friction) and the gravitational force $\boldsymbol{F_g}$. These forces combine into

$$\boldsymbol{F_n} + \boldsymbol{F_d} + \boldsymbol{F_a} + \boldsymbol{F_g} = \boldsymbol{F}. \tag{3.13}$$

Note that the forces $\boldsymbol{F_n}$, $\boldsymbol{F_a}$ and $\boldsymbol{F_g}$ act in o, whereas the line of action for $\boldsymbol{F_d}$ is through P, in the e_1e_2-plane. Hence only $\boldsymbol{F_d}$ contributes to the momentum about o.

The normal force can simply be written as

$$\boldsymbol{F_n} = N\boldsymbol{e_3}, \tag{3.14}$$

where N is a nonnegative scalar. Likewise, the frictional force - which is tangent to the drum surface in P - is given by

$$\boldsymbol{F_d} = D_1\boldsymbol{e_1} + D_2\boldsymbol{e_2}. \tag{3.15}$$

The resistive force $\boldsymbol{F_a}$ is due to the air friction the ball experiences on account of the translation. Since this force is directed opposite to $\boldsymbol{v}_o$ and its magnitude depends on v_o, we write

$$\boldsymbol{F_a} = -\mathcal{F}(v_o)\boldsymbol{v}_o = -\mathcal{F}(v_o)\left(\frac{\dot{R}}{\cos\alpha}\boldsymbol{e_1} + R\dot{\varphi}\boldsymbol{e_2}\right), \tag{3.16}$$

where $\mathcal{F}(v_o)$ is a simple function of

$$v_o = \|\boldsymbol{v}_o\| = \sqrt{(\dot{R}\cos^{-1}\alpha)^2 + (R\dot{\varphi})^2}, \tag{3.17}$$

somewhere in between a constant and a linear function. In case of a freely moving sphere, and for high Reynolds numbers, the friction force is a pure pressure drag. This drag is quadratic in v_o and of the order of

$\frac{1}{2}\rho {V_o}^2 C_d \pi a^2$, where ρ is the density of air, V_o a characteristic velocity, and C_d the drag coefficient, with $C_d \approx 1$ (cf. Dryden et al. [12], section 1.5, or Rouse [20], section 40). For $V_o \approx 0.5$ (m/sec), $\rho \approx 1.2$ (kg/m^3), and $a = 0.0175$ (m), this yields a magnitude for $\boldsymbol{F_a}$ of about 1.5×10^{-4} N. At least in order of magnitude, this corresponds with values of the resistive force found in our experiments (see section 3.2), which are of the order of 3×10^{-4} N. A linear viscous model, for low Reynolds numbers, would yield $F_a = \|\boldsymbol{F_a}\| \sim \eta V_o a C_d$ (η: viscosity of air, cf. Dryden et al. [12], section 7.6), which is of the order of 10^{-7} N, so much lower than the observed values. In the light of our experimental results we favour the quadratic model (yielding a linear $\mathcal{F}(v_o)$), although the ball is not free here, but rolls over a solid surface. However, the range of velocities traversed in practice is strongly limited, and a linear model (having constant $\mathcal{F}(v_o)$) will probably also suffice. In section 3.2 we will consider both options, and compare the results.

Considering the gravitational force, we know that it would be directed along the central axis of the drum if the position of the drum were exactly horizontal (the ideal case). We here assume that the drum is tilted about a small angle β, and that the plane of inclination is rotated about an angle φ_β, with $\varphi_\beta \in [0, 2\pi)$, so that $\boldsymbol{F_g}$ takes the form

$$\begin{aligned} \boldsymbol{F_g} = & - mg(\cos(\varphi - \varphi_\beta)\cos\alpha\sin\beta + \sin\alpha\cos\beta)\,\boldsymbol{e_1} \\ & + mg\sin(\varphi - \varphi_\beta)\sin\beta\,\boldsymbol{e_2} \\ & + mg(\cos(\varphi - \varphi_\beta)\sin\alpha\sin\beta - \cos\alpha\cos\beta)\,\boldsymbol{e_3}, \end{aligned} \tag{3.18}$$

where g respresents the acceleration of gravity. Since β is extremely small, the component of the gravitational force in the plane of the drum is of the order $F_g \approx mg\sin\alpha \approx 3 \times 10^{-2}$ (N), whereas the order of the centrifugal force is $F_c \approx m{V_o}^2/R \approx 2 \times 10^{-2}$ (N). Hence, F_g and F_c are of the same order of magnitude, but F_a is much smaller than both F_g and F_c. Therefore it is possible to introduce a small parameter in the form of the quotient of F_a and either F_g or F_c. We will return to this subject in subsection 3.3.2.

The last term to be expressed in $\{\boldsymbol{e_1 e_2 e_3}\}$-coordinates is the total momentum $\boldsymbol{M}$. $\boldsymbol{M}$ is composed of two parts: the momentum $\boldsymbol{M_d}$ caused by the frictional force $\boldsymbol{F_d}$, and the rolling resistance $\boldsymbol{M_r}$ which is assumed to be proportional to the spin (rolling resistance due to the in-plane rotations ω_1 and ω_2 is neglected). So

$$\boldsymbol{M} = \boldsymbol{M_d} + \boldsymbol{M_r}, \tag{3.19}$$

with

$$\boldsymbol{M}_{\mathbf{d}} = -a\boldsymbol{e_3} \times \boldsymbol{F}_{\mathbf{d}} = aD_2\boldsymbol{e_1} - aD_1\boldsymbol{e_2}, \tag{3.20}$$

and

$$\boldsymbol{M}_{\mathbf{r}} = -Ih\dot{\psi}\boldsymbol{e_3}, \tag{3.21}$$

where h is a friction coefficient. From (3.3), (3.6) and (3.9), we find that the motion of the ball is completely determined by the three variables R, φ and $\dot{\psi}$. By writing (3.11) and (3.12) out in components in the $\{O\boldsymbol{e_1e_2e_3}\}$-system, and by eliminating the unknown factors N, D_1 and D_2, we obtain (with $f(v_o)$ denoting $\mathcal{F}(v_o)/m$)

$$\begin{aligned}
\ddot{R} &= -\tfrac{5}{7}f(v_o)\dot{R} + R\dot{\varphi}^2\cos^2\alpha + \tfrac{2a}{7}\dot{\varphi}\dot{\psi}\cos\alpha\sin\alpha \\
&\quad -\tfrac{5g}{7}\cos\alpha(\cos\alpha\sin\beta\cos(\varphi-\varphi_\beta) + \sin\alpha\cos\beta), \\
\ddot{\varphi} &= -\tfrac{5}{7}f(v_o)\dot{\varphi} - 2R^{-1}\dot{R}\dot{\varphi} + \tfrac{5g}{7}R^{-1}\sin\beta\sin(\varphi-\varphi_\beta), \\
\ddot{\psi} &= -h\dot{\psi} - \tfrac{1}{a}\dot{R}\dot{\varphi}\tan\alpha.
\end{aligned} \tag{3.22}$$

The above system of differential equations is to be completed with a set of initial conditions. We derive these conditions by again using assumption c: when the ball is rolling along the rim (see figure 3.4), we know that the instantaneous velocity $\boldsymbol{v}_Q$ of Q (being the point of contact between rim and ball) is equal to zero, hence

$$\mathbf{0} = \boldsymbol{v}_Q = \boldsymbol{v}_o + \boldsymbol{\omega} \times a(\cos\alpha\boldsymbol{e_1} - \sin\alpha\boldsymbol{e_3}). \tag{3.23}$$

By substituting equations (3.6) and (3.9) into (3.23), we find

$$\mathbf{0} = \frac{\dot{R}(1-\sin\alpha)}{\cos\alpha}\boldsymbol{e_1} + \{a\dot{\psi}\cos\alpha + R\dot{\varphi}(1-\sin\alpha)\}\boldsymbol{e_2} - \dot{R}\boldsymbol{e_3}. \tag{3.24}$$

At $t = 0$ the ball leaves the rim; from (3.24) we conclude that at this time the ball momentarily moves in a circular orbit ($\ddot{R}(0) = \dot{R}(0) = 0$), with radius $R(0) = R_{rim} - a$. Furthermore, we may choose $\varphi(0)$ arbitrarily, so we have $\varphi(0) = \varphi_0$. To find $\dot{\varphi}(0)$ and $\dot{\psi}(0)$, we combine the second component in (3.24) with the first equation in (3.22), whence

$$\begin{aligned}
R(0) &= R_{rim} - a, \\
\dot{R}(0) &= 0, \\
\varphi(0) &= \varphi_0, \\
\dot{\varphi}(0) &= \sqrt{\frac{5g(\sin\alpha\cos\beta + \cos\alpha\sin\beta\cos(\varphi_0-\varphi_\beta))}{(7\cos\alpha - 2\tan\alpha(1-\sin\alpha))}}\Big/\sqrt{R(0)}, \\
\dot{\psi}(0) &= -\tfrac{1-\sin\alpha}{a\cos\alpha}R(0)\dot{\varphi}(0).
\end{aligned} \tag{3.25}$$

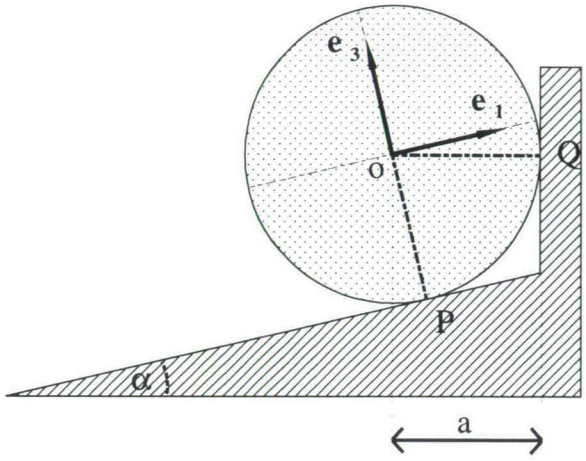

Figure 3.4: The ball rolling along the rim.

At this point we have derived a system of three nonlinear second order differential equations, and a corresponding set of initial conditions. This system, represented by (3.22) and (3.25), completely determines the motion of the ball in the drum. But, unfortunately, it does not seem to admit any standard analytic solution method.

3.2 Numerical solutions

Any system of second order differential equations can be rewritten as a system of first order differential equations by introducing some additional variables. To this end, we define

$$x_1 = R,\ x_2 = \dot{R},\ x_3 = \varphi - \varphi_\beta,\ x_4 = \dot{\varphi},\ x_5 = \dot{\psi}, \tag{3.26}$$

and regard these variables as components of the five-vector

$$\boldsymbol{x}(t) = (x_1(t), x_2(t), x_3(t), x_4(t), x_5(t)). \tag{3.27}$$

With these new variables, the equations of motion in (3.22) can be rewritten as

$$\begin{array}{rcl} \dot{x}_1 &=& x_2, \\ \dot{x}_2 &=& -\frac{5}{7}f(v_o)x_2 + x_1{x_4}^2\cos^2\alpha + \frac{2a}{7}x_4x_5\cos\alpha\sin\alpha \\ && -\frac{5g}{7}(\cos\alpha\sin\beta\cos x_3 + \sin\alpha\cos\beta)\cos\alpha, \\ \dot{x}_3 &=& x_4, \\ \dot{x}_4 &=& -\frac{5}{7}f(v_o)x_4 - 2{x_1}^{-1}x_2x_4 + \frac{5g}{7}{x_1}^{-1}\sin\beta\sin x_3, \\ \dot{x}_5 &=& -hx_5 - \frac{1}{a}x_2x_4\tan\alpha, \end{array} \tag{3.28}$$

where

$$v_o = \sqrt{(x_2\cos^{-1}\alpha)^2 + (x_1x_4)^2}. \tag{3.29}$$

Likewise, with

$$x_{0i} = x_i(0),\ i \in \{1,\ldots,5\}, \tag{3.30}$$

the initial conditions in (3.25) can be transformed into

$$\begin{array}{rcl} x_{01} &=& R_{rim} - a, \\ x_{02} &=& 0, \\ x_{03} &=& 0, \\ x_{04} &=& \sqrt{\frac{5g(\sin\alpha\cos\beta+\cos\alpha\sin\beta)}{(7\cos\alpha-2\tan\alpha(1-\sin\alpha))}}/\sqrt{x_{01}}, \\ x_{05} &=& -\frac{1-\sin\alpha}{a\cos\alpha}x_{01}x_{04}, \end{array} \tag{3.31}$$

where the values of φ_0 and φ_β have been set to zero, for the sake of simplicity. We can solve this type of differential equations by using a Runge-Kutta method. We choose the numerical values of the system parameters in (3.28) and (3.31) as follows. Since the Golden-Ten table must be positioned very carefully, the drum will be placed closely to horizontal, leaving at most a very small value for β. Therefore we will, in our present calculations, assume

$$\beta = \varphi_\beta = 0. \tag{3.32}$$

The dimensions of the drum and the ball are supplied by table 2.2.1, from which we obtain

$$\begin{array}{rcl} m = 0.038\ (\text{kg}),\ a &=& 0.0175\ (\text{m}), \\ R_{rim} = 0.487\ (\text{m}),\ R_{num} = 0.205\ (\text{m}),\ \alpha &=& 0.0831\ (\text{rad}), \end{array} \tag{3.33}$$

and

$$g = 9.81\ (\text{m/sec}^2). \tag{3.34}$$

The values (3.32) - (3.34) lead to the following initial conditions:

$$\begin{aligned} x_{01} &= 0.470 \text{ (m)}, \; x_{02} = x_{03} = 0, \\ x_{04} &= 1.13 \text{ (rad/sec)}, \; x_{05} = -28 \text{ (rad/sec)}. \end{aligned} \tag{3.35}$$

This leaves us with the unknown friction coefficient h and the unknown friction function f. As a start, we neglect the resistive force due to spin, thus assuming

$$h = 0. \tag{3.36}$$

(Note that subsection 5.2.2 provides us with an estimated h of 0.027 sec^{-1}, but for now we content ourselves with the estimate in (3.36)). For the air resistance we have two options (see section 3.1): a resistive force directly proportional to the speed v_o, in which case

$$f(v_o) = f_l, \tag{3.37}$$

or a pure quadratic model, implying

$$f(v_o) = f_q v_o. \tag{3.38}$$

Until further notice, we consider both models to be equally acceptable, so we employ them both.

At final time t_f, when the ball falls off of the edge of the drum, we have

$$x_1(t_f) = R_{num}, \tag{3.39}$$

which allows us to estimate t_f by utilizing the experimental data from chapter 4. From orbit T11B21 - which is one of the smoothest orbits, and therefore serves as an example - we obtain the value

$$t_f = 116 \text{ (sec)}. \tag{3.40}$$

We can now determine the two coefficients f_l and f_q by running two Runge-Kutta procedures (one for each friction model) for varying values of f_l and f_q, meanwhile continually checking on condition (3.39). This method eventually yields the rough estimates

$$f_l = 0.015 \text{ } (\text{sec}^{-1}), \tag{3.41}$$

and

$$f_q = 0.035 \text{ } (\text{m}^{-1}). \tag{3.42}$$

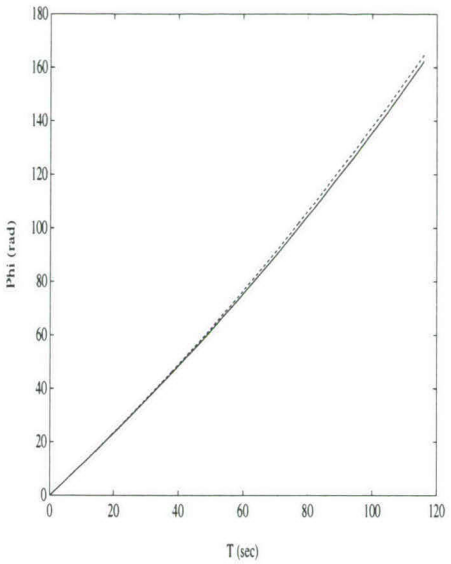

Figure 3.5: Total angle φ as function of time t.

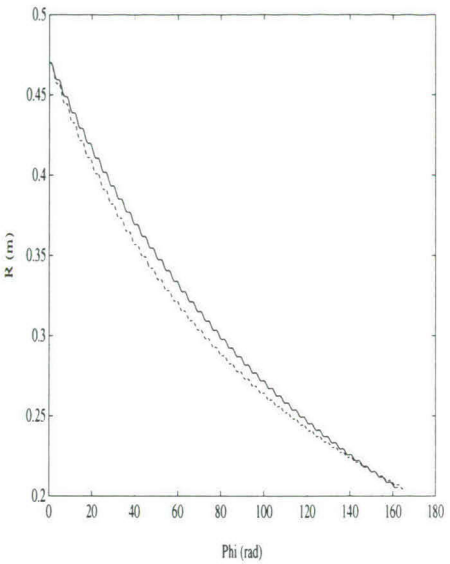

Figure 3.6: Radius R as function of total angle φ.

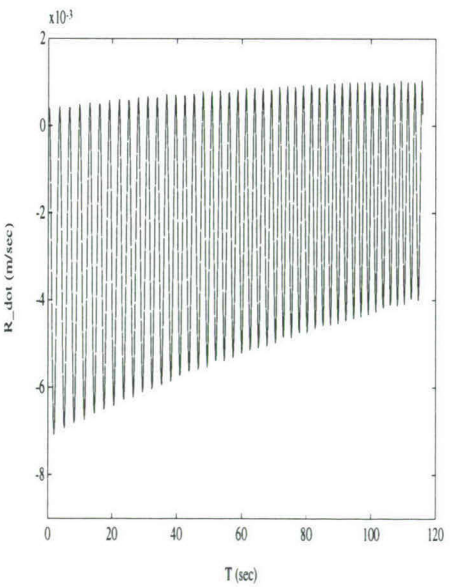

Figure 3.7: Radial velocity $\dot{R}$ (linear model).

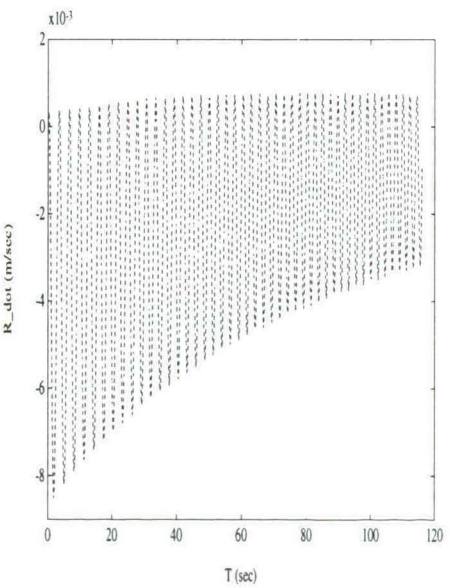

Figure 3.8: Radial velocity $\dot{R}$ (quadratic model).

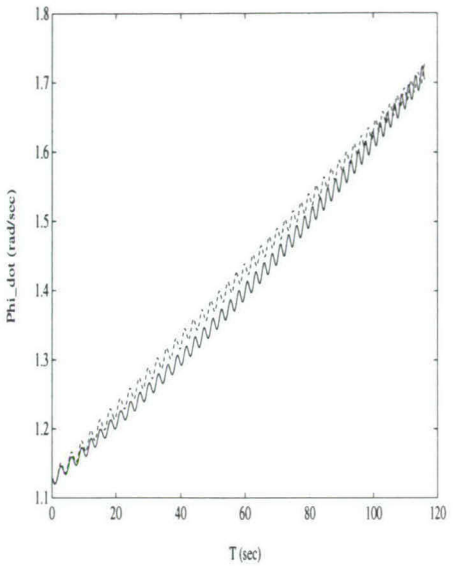

Figure 3.9: Angular velocity $\dot{\varphi}$.

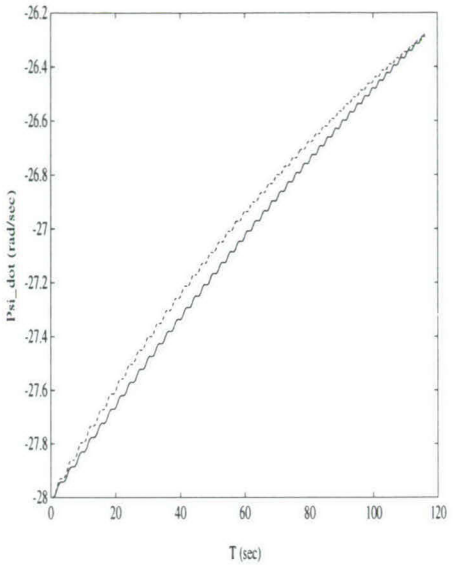

Figure 3.10: Spin $\dot{\psi}$.

With all of the above data we have run the Runge-Kutta routine ODE45, supplied by the mathematical software package MATLAB (see MathWorks [18]), where we set the error tolerance to 10^{-8}. The results are reported in figures 3.5-3.10, where the dashed graphs represent the output from the quadratic friction model. Figure 3.5 shows an almost linearly evolving total covered angle φ for both models. Therefore, and because the ball moves in orbit round the centre of the drum, we will often consider the solution as a function of φ, rather than of t. A more natural way to observe the motion of the ball - especially from a player's point of view - is thus depicted in figure 3.6. It shows that the ball slowly spirals down the drum, with clearly perceptible elliptical revolutions. The distance to the centre of the drum decreases slightly faster in the quadratic case, as does the amplitude of the corresponding oscillations (see figures 3.7 and 3.8). Finally, the angular velocity of the ball shows a gradual though oscillatory increase, whereas the spin gradually decreases (see figures 3.9 and 3.10, respectively). Although the two friction models lead to different results, the overall characteristics appear to be very similar. However, we prefer to work with the linear model. Our reasons for this preference will be stated in the next section.

3.3 Analytic solutions

3.3.1 A partial solution

In this section - as in the previous one - we neglect the spin resistance ($h = 0$), and assume that the drum is in a perfectly horizontal position ($\beta = 0$). Hence the motion of the ball depends on the gravitational force (magnitude: F_g) and the resistive force (F_a), the latter being much smaller than the former (see section 3.1). This firstly gives us the opportunity to introduce a small parameter in terms of the ratio F_a/F_g. Secondly, this ratio makes it plausible to introduce two different time scales for the global motion of the ball:

1. a typical time scale for one revolution, which is of the order $R/V_o \approx 1$ (sec). This is in accordance with the fact noted in section 3.1 that the gravitational force F_g and the centrifugal force F_c are of the same order of magnitude;

2. a time scale much larger than the first one, representing the time it takes for the air drag to become significant, of the order of $7m/(5\mathcal{F}) = 7/(5f) \approx 100$ (sec) (see $(3.22)^{1,2}$). This is due to the fact that the resistive force F_a is much smaller than both F_g and F_c.

On the basis of these two time scales we shall employ a two-variable expansion procedure as described in Kevorkian and Cole [15], chapter 3.

To rescale the equations of motion (3.22), we introduce the dimensionless variables

$$\begin{aligned}
\hat{R} &= R/R_0, (R_0 = R(0)); \hat{\omega} = \dot{\varphi}/\omega_0, (\omega_0 = \dot{\varphi}(0)); \\
\hat{\Omega} &= \dot{\psi}/\Omega_0, (\Omega_0 = -\dot{\psi}(0) = \frac{1-\sin\alpha}{a\cos\alpha} R_0\omega_0); \ \hat{t} = \omega_0 t; \qquad (3.43) \\
\hat{f} &= \tfrac{5}{7} f_l/\omega_0; \ \hat{g} = \frac{5}{7} g\sin\alpha\cos\alpha/(R_0{\omega_0}^2) = 1 - \tfrac{2}{7}\sin\alpha - \tfrac{5}{7}\sin^2\alpha,
\end{aligned}$$

where we again (see sections 3.1 and 3.2) express our preference for a linear F_a-model, since it simplifies our analytic expressions. So from now on we assume $f(v_o)$ to equal a constant f_l. The new variables, with

$h = \beta = 0$, change system (3.22) into

$$\begin{aligned} \frac{d^2\hat{R}}{d\hat{t}^2} &= -\hat{f}\frac{d\hat{R}}{d\hat{t}} + \hat{R}\hat{\omega}^2\cos^2\alpha - \tfrac{2}{7}\hat{\omega}\hat{\Omega}(1-\sin\alpha)\sin\alpha - \hat{g}, \\ \frac{d\hat{\omega}}{d\hat{t}} &= -\hat{f}\hat{\omega} - 2\hat{R}^{-1}\hat{\omega}\frac{d\hat{R}}{d\hat{t}}, \\ \frac{d\hat{\Omega}}{d\hat{t}} &= \frac{\sin\alpha}{1-\sin\alpha}\hat{\omega}\frac{d\hat{R}}{d\hat{t}}, \end{aligned} \tag{3.44}$$

with

$$\hat{R}(0) = \hat{\omega}(0) = \hat{\Omega}(0) = 1, \text{ and } \frac{d\hat{R}}{d\hat{t}}(0) = 0. \tag{3.45}$$

When air resistance is completely neglected i.e. when $\mathcal{F}(v_o) = f(v_o) = f_l = 0$, the equations of motion admit three first integrals, representing conservation of angular momentum - about two distinct axes - and conservation of energy. With $\hat{f} = 0$, (3.44) reduces to (we omit the circumflex signs):

$$\ddot{R} = R\omega^2\cos^2\alpha - \tfrac{2}{7}\omega\Omega\sin\alpha(1-\sin\alpha) - g, \tag{3.46}$$

$$\dot{\omega} = -2R^{-1}\omega\dot{R}, \tag{3.47}$$

$$\dot{\Omega} = \sin\alpha(1-\sin\alpha)^{-1}\omega\dot{R}. \tag{3.48}$$

From (3.47) we find

$$\frac{d}{dt}\{R^2\omega\} = 0, \tag{3.49}$$

reflecting conservation of angular momentum about the central axis of the drum. Combination of (3.47) and (3.48) leads to conservation of angular momentum about the axis of spin, or

$$\frac{d}{dt}\{\Omega(1-\sin\alpha) + \omega R\sin\alpha\} = 0. \tag{3.50}$$

Another quantity that is preserved in the absence of air friction is the total mechanical energy, being the sum of kinetic and potential energy. However, we do not use this quantity here because it would - due to the essential nonlinear nature of the energy - needlessly complicate our calculations.

The two remaining conservation laws imply that the most direct way to study the dependency on $\hat{f}$ is by analyzing the momentary changes in the two physical quantities in (3.49) and (3.50). To this end, we introduce three new variables

$$y_1 = \hat{R}^2\hat{\omega},\ y_2 = \hat{\Omega}(1-\sin\alpha) + \hat{\omega}\hat{R}\sin\alpha,\ y_3 = \hat{R}, \tag{3.51}$$

which results in the following form of the equations of motion:

$$\begin{aligned} \dot{y}_1 &= -\hat{f}y_1, \\ \dot{y}_2 &= \hat{f}y_1{y_3}^{-1}\sin\alpha, \\ \ddot{y}_3 &= -\hat{f}\dot{y}_3 + (1-\tfrac{5}{7}\sin^2\alpha){y_1}^2{y_3}^{-3} - \tfrac{2}{7}y_1y_2{y_3}^{-2}\sin\alpha - \hat{g}, \end{aligned} \tag{3.52}$$

and the initial conditions

$$y_1(0) = y_2(0) = y_3(0) = 1,\ \dot{y}_3(0) = 0. \tag{3.53}$$

The first equation in (3.52) is uncoupled from the rest of the system, and leads - via the corresponding initial condition in (3.53) - to the explicit solution

$$y_1 = e^{-\hat{f}\hat{t}} = e^{-\frac{5}{7}f_l t}. \tag{3.54}$$

This formula expresses the dependency of the total covered area per time unit $y_1 = R^2\dot{\varphi}$ on the air friction coefficient f_l and time t. By fitting equation (3.54) to the experimental data provided by chapter 4, we can expect to obtain an accurate estimate of coefficient f_l. A logarithmic transformation and a simple linear regression model, applied to orbit T11B21, yield the estimated value

$$f_l = 0.014\ (\text{sec}^{-1}). \tag{3.55}$$

Note that this value does not differ much from the one in (3.41). The residuals from the regression model are shown in figure 3.11. The apparently small values indicate a close fit, although the rough sine shape does not indicate a truly linear friction model. But it does not point to a truly quadratic model either, as can be seen in figure 3.12, where we used the earlier estimates of f_l and f_q to plot $\log(y_1)$ for both friction models (the dashed curve represents the quadratic model). We now definitely favour the linear model, because of its elegance and greater simplicity.

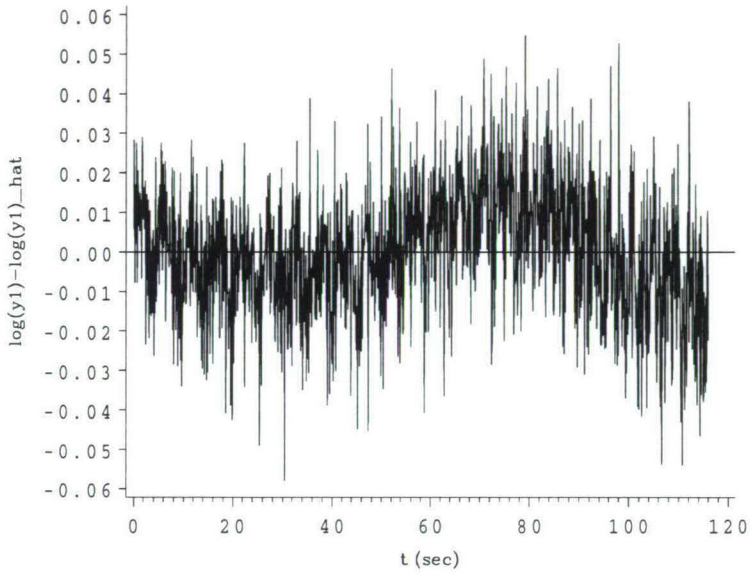

Figure 3.11: Residuals from the fitted regression equation $\log(y_1) = b_0 + b_1 t$, with $y_1 = R^2\dot{\varphi}$.

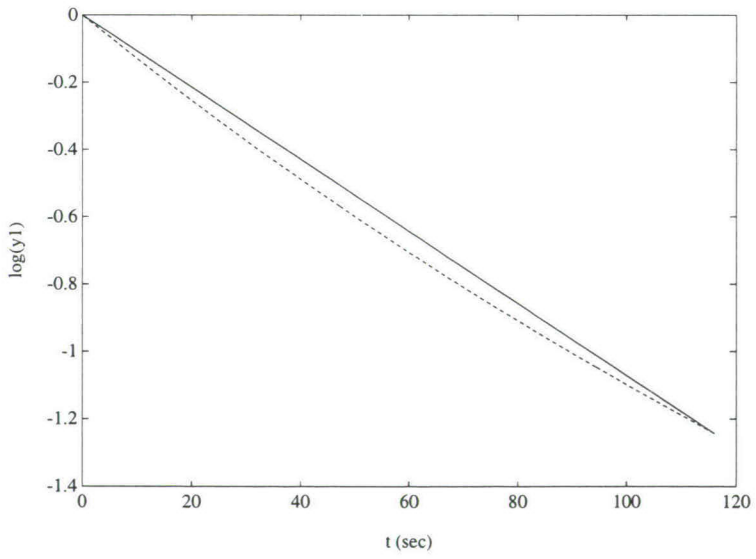

Figure 3.12: $\log(y_1)$ as function of t.

Substitution of the estimated f_l in (3.55) into the Runge-Kutta procedure, however, does not lead to an orbit that closely matches example orbit T11B21. One of the obvious reasons is that the experimentally determined initial angular velocity appears to be lower than the theoretical value of 1.13 rad/sec in (3.35): chapter 4 reports the value

$$\omega_0 = 1.09 \text{ (rad/sec)}. \tag{3.56}$$

Figure 3.13 compares orbit T11B21 to the Runge-Kutta output based on the newly estimated values of f_l and ω_0 (the dashed graph represents the Runge-Kutta output). The overall shape of the graphs appears to be quite similar, especially during the first part of the experiment. However, the second part shows a slightly varying phase shift and a small variation in amplitude. We would be able to assess the influence of the system parameters and the initial conditions on the orbit of the ball better if we supplied system (3.44) with an analytic solution. But since such a solution is not available, we are restrained to an asymptotic approximation method. In the next subsection we will present such a method, where the asymptotics will be based on the small value of f_l, or (better) $\hat{f}$.

3.3.2 Global solutions

Since the ball moves in orbit round the centre of the drum, it is only natural to replace independent variable $\hat{t}$ in system (3.52) with variable φ. This change of variables is common use in the treatment of satellite equations (cf. Kevorkian and Cole [15], section 3.4), which have a lot in common with our set of equations. The procedure we shall follow runs more or less along lines analogous to those presented in sections 3.4.1 and 3.4.2 of Kevorkian and Cole [15].

With the transformations

$$u(\varphi) = {y_3}^{-1}, \; v(\varphi) = {y_1}^{-1}, \tag{3.57}$$

we find from (3.51)

$$\hat{\omega} = \frac{d\varphi}{d\hat{t}} = \frac{u^2}{v}. \tag{3.58}$$

Furthermore, to get rid of the factor $\sin\alpha$ in $(3.52)^2$, we rewrite y_2 as

$$y_2 = 1 - w(\varphi)\sin\alpha. \tag{3.59}$$

This change of variables transforms (3.52) into the new system

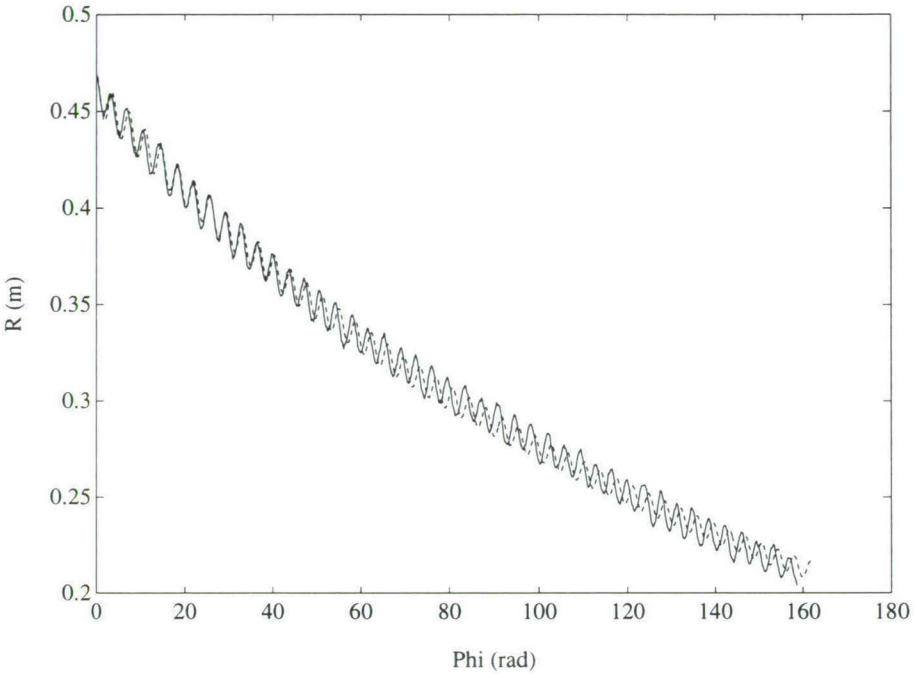

Figure 3.13: A comparison of numerical results and experimental data. The dashed line represents the numerical results, the solid line represents the data of experiment T11B21.

$$\begin{aligned}
\frac{dv}{d\varphi} &= \hat{f}\frac{v^2}{u^2}, \\
\frac{dw}{d\varphi} &= \hat{f}\frac{1}{u}, \\
\frac{d^2u}{d\varphi^2} &= -u + \frac{v^2}{u^2} - \tfrac{2}{7}\sin\alpha(\frac{v^2}{u^2} - v) + \tfrac{5}{7}\sin^2\alpha(u - \frac{v^2}{u^2} - \frac{2}{5}vw),
\end{aligned} \tag{3.60}$$

with corresponding initial conditions

$$u(0) = v(0) = 1,\ w(0) = 0,\ \frac{du}{d\varphi}(0) = 0. \tag{3.61}$$

This new set of equations reveals an explicit dependency on just two, dimensionless parameters, namely $\hat{f}$ and $\sin\alpha$, which both turn out to be small. The first one expresses, as we have seen before, the smallness of the resistive force as compared to the gravitational force (cf. Kevorkian and Cole [15], section 3.4.2). We here replace $\hat{f}$ by ε and note that

$$\varepsilon = \hat{f} = \tfrac{5}{7} f_l/\omega_0 \approx 8.8 \times 10^{-3}, \tag{3.62}$$

in accordance with $(3.35)^3$ and the estimate for f_l in (3.55). The second small parameter is due to deviations in the gravitational force, related to the slope of the drum surface (comparable to Kevorkian and Cole [15], section 3.4.1). Although the two small parameters have quite different physical origins, their influences on the equations of motion (3.60) are of the same order of magnitude. This is manifested by writing

$$\tfrac{2}{7}\sin\alpha = d_1\varepsilon, \;\; \tfrac{5}{7}\sin^2\alpha = d_2\varepsilon, \tag{3.63}$$

where d_1 and d_2 are coefficients of $O(1)$-magnitude, i.e. (from (3.33))

$$d_1 = 2.69, \text{ and } d_2 = 0.559. \tag{3.64}$$

In this way we are able to combine the two small effects in one small parameter ε, since now (3.60) can be rewritten as

$$\begin{aligned} \frac{dv}{d\varphi} &= \varepsilon\frac{v^2}{u^2}, \\ \frac{dw}{d\varphi} &= \varepsilon\frac{1}{u}, \\ \frac{d^2u}{d\varphi^2} + u - \frac{v^2}{u^2} &= \varepsilon[d_1(v - \frac{v^2}{u^2}) + d_2(u - \frac{v^2}{u^2} - \tfrac{2}{5}vw)]. \end{aligned} \tag{3.65}$$

Hence, u obeys the equation of a weakly nonlinear oscillator (cf. Kevorkian and Cole [15]), and this type of problem is well adapted for solution by the multiple-variable expansion method. As we already saw before, this problem knows two time scales, and therefore - following Kevorkian and Cole [15], section 3.2 - we introduce the fast and the slow φ-scale by

$$\varphi_1 = (1 + \varepsilon^2\omega_2 + \varepsilon^3\omega_3 + \ldots)\varphi, \tag{3.66}$$

and

$$\varphi_2 = \varepsilon\varphi, \tag{3.67}$$

respectively, where $\omega_2, \omega_3, \ldots$ are unknown coefficients (not depending on ε). However, as we are not looking for a solution valid for all posible values of φ, but only for a range up to $\varphi = O(\varepsilon^{-1})$ (see figure 3.5), these ω_i-coefficients are redundant here, and may be taken zero, i.e.

$$\omega_2 = \omega_3 = \ldots = 0 \Rightarrow \varphi_1 = \varphi. \tag{3.68}$$

Furthermore, we assume the variables u, v and w to be functions of both φ_1 and φ_2, and write them as

$$u = u(\varphi_1, \varphi_2),\ v = v(\varphi_1, \varphi_2),\ w = w(\varphi_1, \varphi_2), \tag{3.69}$$

thus finally transforming (3.65) into

$$\begin{aligned}
\frac{\partial v}{\partial \varphi_1} + \varepsilon \frac{\partial v}{\partial \varphi_2} &= \varepsilon \frac{v^2}{u^2}, \\
\frac{\partial w}{\partial \varphi_1} + \varepsilon \frac{\partial w}{\partial \varphi_2} &= \varepsilon \frac{1}{u}, \\
\frac{\partial^2 u}{\partial {\varphi_1}^2} + 2\varepsilon \frac{\partial^2 u}{\partial \varphi_1 \partial \varphi_2} + \varepsilon^2 \frac{\partial^2 u}{\partial {\varphi_2}^2} &= -u + \frac{v^2}{u^2} \\
&\quad + \varepsilon [d_1 v + d_2 u - (d_1 + d_2) \frac{v^2}{u^2} - \tfrac{2}{5} d_2 v w].
\end{aligned} \tag{3.70}$$

Without loss of generality we may assume $\varphi_1(0) = \varphi_2(0) = 0$, yielding the initial conditions

$$\begin{aligned}
u(0,0) = v(0,0) = 1,\ w(0,0) &= 0, \\
\frac{\partial u}{\partial \varphi_1}(0,0) + \varepsilon \frac{\partial u}{\partial \varphi_2}(0,0) &= 0.
\end{aligned} \tag{3.71}$$

We now expand u, v, and w into the following asymptotic power series:

$$u \sim \sum_{i=0}^{\infty} u_i(\varphi_1, \varphi_2)\varepsilon^i,\ v \sim \sum_{i=0}^{\infty} v_i(\varphi_1, \varphi_2)\varepsilon^i,\ w \sim \sum_{i=0}^{\infty} w_i(\varphi_1, \varphi_2)\varepsilon^i, \tag{3.72}$$

and we try to find solutions for u_i, v_i, and w_i - on a limited φ-scale of $O(\varepsilon^{-1})$ - by substituting the series (3.72) into (3.70) and (3.71), and by matching the terms with equal powers in ε.

For the ε^0-terms we thus obtain

$$\begin{aligned} \frac{\partial v_0}{\partial \varphi_1} &= 0, \\ \frac{\partial w_0}{\partial \varphi_1} &= 0, \\ \frac{\partial^2 u_0}{\partial \varphi_1^2} &= -u_0 + \frac{{v_0}^2}{{u_0}^2}, \end{aligned} \tag{3.73}$$

with

$$\begin{aligned} u_0(0,0) = v_0(0,0) = 1,\ w_0(0,0) &= 0, \\ \frac{\partial u_0}{\partial \varphi_1}(0,0) &= 0, \end{aligned} \tag{3.74}$$

whereas the ε^1-terms yield

$$\begin{aligned} \frac{\partial v_1}{\partial \varphi_1} &= -\frac{\partial v_0}{\partial \varphi_2} + \frac{{v_0}^2}{{u_0}^2}, \\ \frac{\partial w_1}{\partial \varphi_1} &= -\frac{\partial w_0}{\partial \varphi_2} + \frac{1}{u_0}, \\ \frac{\partial^2 u_1}{\partial {\varphi_1}^2} + 2\frac{\partial^2 u_0}{\partial \varphi_1 \partial \varphi_2} &= -u_1 + 2\left(\frac{v_0 v_1}{{u_0}^2} - \frac{{v_0}^2 u_1}{{u_0}^3}\right) + d_1 v_0 + d_2 u_0 \\ &\quad -(d_1 + d_2)\frac{{v_0}^2}{{u_0}^2} - \tfrac{2}{5} d_2 v_0 w_0, \end{aligned} \tag{3.75}$$

with

$$\begin{aligned} u_1(0,0) = v_1(0,0) = w_1(0,0) &= 0, \\ \frac{\partial u_1}{\partial \varphi_1}(0,0) + \frac{\partial u_0}{\partial \varphi_2}(0,0) &= 0. \end{aligned} \tag{3.76}$$

From $(3.73)^3$, with initial conditions (3.74), we find that both the first and the second derivative of u_0, with respect to φ_1, vanish in 0. From a quadrature of this equation it then follows that $\partial u_0/\partial \varphi_1 = 0$ for all $\varphi_1 > 0$, and hence we obtain from (3.73)

$$u_0 = U_0(\varphi_2),\ v_0 = V_0(\varphi_2),\ w_0 = W_0(\varphi_2), \tag{3.77}$$

such that

$${U_0}^3(\varphi_2) = {V_0}^2(\varphi_2), \tag{3.78}$$

and

$$U_0(0) = V_0(0) = 1,\ W_0(0) = 0. \tag{3.79}$$

Solutions for U_0, V_0 and W_0 follow from the ε^1-equations by requiring that the secular terms must equal zero (cf. Kevorkian and Cole [15]). So the first equation in (3.75) gives

$$\frac{\partial v_1}{\partial \varphi_1} = -\frac{dV_0}{d\varphi_2} + \frac{{V_0}^2}{{U_0}^2} = -{V_0}' + {V_0}^{2/3}, \tag{3.80}$$

which would result in a linear, unbounded particular solution for v_1, unless

$$-V_0{}' + V_0{}^{2/3} = 0, \tag{3.81}$$

yielding, with $V_0(0) = 1$,

$$V_0 = (1 + \tfrac{1}{3}\varphi_2)^3, \tag{3.82}$$

and

$$U_0 = (1 + \tfrac{1}{3}\varphi_2)^2. \tag{3.83}$$

Analogously, the second equation in (3.73) leads us to

$$\frac{\partial w_1}{\partial \varphi_1} = -\frac{dW_0}{d\varphi_2} + \frac{1}{U_0} = -W_0{}' + (1 + \tfrac{1}{3}\varphi_2)^{-2}, \tag{3.84}$$

or, with $W_0(0) = 0$,

$$W_0 = \varphi_2(1 + \tfrac{1}{3}\varphi_2)^{-1}. \tag{3.85}$$

Hence we see that for a complete solution of the ε^0-terms, we need the equations of the ε^1-approximation (and so on for the higher order terms). Substitution of (3.82), (3.83) and (3.85) into (3.75) results in

$$\begin{aligned} \frac{\partial v_1}{\partial \varphi_1} &= 0, \text{ or } v_1 = V_1(\varphi_2), \\ \frac{\partial w_1}{\partial \varphi_1} &= 0, \text{ or } w_1 = W_1(\varphi_2), \end{aligned} \tag{3.86}$$

and (where the last two results have already been substituted)

$$\begin{aligned} \frac{\partial^2 u_1}{\partial {\varphi_2}^2} + 3u_1 &= \tfrac{1}{3}(d_1 - \tfrac{6}{5}d_2)\varphi_2(1 + \tfrac{1}{3}\varphi_2)^2 + 2(1 + \tfrac{1}{3}\varphi_2)^{-1}V_1 \\ &=: R_1(\varphi_2). \end{aligned} \tag{3.87}$$

The solution of the latter equation reads

$$u_1(\varphi_1, \varphi_2) = U_1(\varphi_2) + A_1(\varphi_2)\sin\sqrt{3}\varphi_1 + B_1(\varphi_2)\cos\sqrt{3}\varphi_1, \tag{3.88}$$

with

$$U_1(\varphi_2) = \tfrac{1}{3}R_1(\varphi_2), \tag{3.89}$$

and, following from (3.76) and $R_1(0) = 0$,

$$A_1(0) = -\tfrac{2}{9}\sqrt{3}, \; B_1(0) = 0. \tag{3.90}$$

The functions A_1, B_1, V_1 and W_1 can be determined by matching the ε^2-terms, and equating the secular terms (which lead to unbounded solutions in φ_1) to zero. This eventually leads to an explicit expression for the apparently periodic function u_1.

The ε^2-versions of the first two equations in (3.70) lead to

$$\begin{aligned} \frac{\partial v_2}{\partial \varphi_1} &= \left[-\frac{dV_1}{d\varphi_2} + 2(1+\tfrac{1}{3}\varphi_2)^{-1}V_1 - \tfrac{2}{3}R_1\right] \\ &\quad -2A_1 \sin\sqrt{3}\varphi_1 - 2B_1 \cos\sqrt{3}\varphi_1, \\ \frac{\partial w_2}{\partial \varphi_1} &= \left[-\frac{dW_1}{d\varphi_2} - \tfrac{1}{3}(1+\tfrac{1}{3}\varphi_2)^{-4}R_1\right] \\ &\quad -(1+\tfrac{1}{3}\varphi_2)^{-4}(A_1 \sin\sqrt{3}\varphi_1 + B_1 \cos\sqrt{3}\varphi_1), \end{aligned} \tag{3.91}$$

with

$$v_2(0,0) = w_2(0,0) = 0. \tag{3.92}$$

The solutions remain bounded only if the secular terms (between square brackets in (3.91)) are equal to zero, hence

$$\begin{aligned} V_1' - 2(1+\tfrac{1}{3}\varphi_2)^{-1}V_1 &= -\tfrac{2}{3}R_1, \\ W_1' &= -\tfrac{1}{3}(1+\tfrac{1}{3}\varphi_2)^{-4}R_1, \end{aligned} \tag{3.93}$$

which leads - via $V_1(0) = W_1(0) = 0$, and R_1 as in (3.87) - to

$$V_1(\varphi_2) = -\tfrac{1}{9}(d_1 - \tfrac{6}{5}d_2)\varphi_2{}^2(1+\tfrac{1}{3}\varphi_2)^2, \tag{3.94}$$

and

$$\begin{aligned} W_1(\varphi_2) = \quad & -\tfrac{1}{3}(d_1 - \tfrac{6}{5}d_2)\varphi_2(1+\tfrac{2}{3}\varphi_2)(1+\tfrac{1}{3}\varphi_2)^{-2} \\ & +(d_1 - \tfrac{6}{5}d_2)\log(1+\tfrac{1}{3}\varphi_2). \end{aligned} \tag{3.95}$$

By substituting these results into (3.91) and solving the differential equations thus obtained, we get

$$v_2(\varphi_1,\varphi_2) = V_2(\varphi_2) + \tfrac{2\sqrt{3}}{3}A_1 \cos\sqrt{3}\varphi_1 - \tfrac{2\sqrt{3}}{3}B_1 \sin\sqrt{3}\varphi_1, \tag{3.96}$$

with

$$V_2(0) = -\tfrac{2\sqrt{3}}{3}A_1(0) = \tfrac{4}{9}, \tag{3.97}$$

and

$$\begin{aligned} w_2(\varphi_1,\varphi_2) &= W_2(\varphi_2) \\ &+ \tfrac{\sqrt{3}}{3}(1+\tfrac{1}{3}\varphi_2)^{-4}\{A_1 \cos\sqrt{3}\varphi_1 - B_1 \sin\sqrt{3}\varphi_1\}, \end{aligned} \tag{3.98}$$

with

$$W_2(0) = -\tfrac{\sqrt{3}}{3}A_1(0) = \tfrac{2}{9}. \tag{3.99}$$

The above results allow us to write out the ε^2-terms in $(3.70)^3$ as

$$\begin{aligned}
&\frac{\partial^2 u_2}{\partial {\varphi_1}^2} + 3u_2 = R_2(\varphi_2) \\
+\ &\tfrac{3}{2}(1+\tfrac{1}{3}\varphi_2)^{-2}\{2A_1B_1\sin 2\sqrt{3}\varphi_1 - ({A_1}^2 - {B_1}^2)\cos 2\sqrt{3}\varphi_1\} \\
-\ &2\sqrt{3}[{A_1}' - \tfrac{2}{3}(1+\tfrac{1}{3}\varphi_2)^{-1}A_1 - \omega_1 B_1]\cos\sqrt{3}\varphi_1 \\
+\ &2\sqrt{3}[{B_1}' - \tfrac{2}{3}(1+\tfrac{1}{3}\varphi_2)^{-1}B_1 + \omega_1 A_1]\sin\sqrt{3}\varphi_1,
\end{aligned} \tag{3.100}$$

where

$$\begin{aligned}
R_2 = \quad &(\tfrac{4}{27} + \tfrac{2}{9}{d_1}^2 + \tfrac{1}{5}d_1d_2 - \tfrac{14}{25}{d_2}^2)\varphi_2 \\
&+(\tfrac{2}{81} + \tfrac{4}{27}{d_1}^2 + \tfrac{2}{15}d_1d_2 - \tfrac{28}{75}{d_2}^2){\varphi_2}^2 \\
&+\tfrac{11}{135}d_2(d_1 - \tfrac{6}{5}d_2){\varphi_2}^3 - \tfrac{1}{81}(d_1 - \tfrac{6}{5}d_2)^2{\varphi_2}^4 \\
&-\tfrac{2}{5}d_2(d_1 - \tfrac{6}{5}d_2)(1+\tfrac{1}{3}\varphi_2)^3\log(1+\tfrac{1}{3}\varphi_2) \\
&+2(1+\tfrac{1}{3}\varphi_2)^{-1}V_2(\varphi_2),
\end{aligned} \tag{3.101}$$

and

$$\omega_1 = \tfrac{\sqrt{3}}{3}(d_1 + \tfrac{3}{2}d_2) + \tfrac{\sqrt{3}}{9}(d_1 - \tfrac{6}{5}d_2)\varphi_2. \tag{3.102}$$

In this case, the secular terms are those with $\cos\sqrt{3}\varphi_1$ and $\sin\sqrt{3}\varphi_1$. Equating these terms to zero, we find

$$\begin{aligned}
{A_1}' &= \tfrac{2}{3}(1+\tfrac{1}{3}\varphi_2)^{-1}A_1 + \omega_1 B_1, \\
{B_1}' &= \tfrac{2}{3}(1+\tfrac{1}{3}\varphi_2)^{-1}B_1 - \omega_1 A_1.
\end{aligned} \tag{3.103}$$

A straightforward solution of (3.103) under the initial conditions (3.90) yields

$$A_1(\varphi_2) = -\tfrac{2}{9}(1+\tfrac{1}{3}\varphi_2)^2\cos\Omega_1, \tag{3.104}$$

$$B_1(\varphi_2) = \tfrac{2}{9}(1+\tfrac{1}{3}\varphi_2)^2\sin\Omega_1, \tag{3.105}$$

where

$$\begin{aligned}
\Omega_1 &= \Omega_1(\varphi_2) = \int_0^{\varphi_2}\omega_1(\phi)d\phi \\
&= \tfrac{\sqrt{3}}{3}(d_1 + \tfrac{3}{2}d_2)\varphi_2 + \tfrac{\sqrt{3}}{18}(d_1 - \tfrac{6}{5}d_2){\varphi_2}^2.
\end{aligned} \tag{3.106}$$

This ultimately results in the following explicit solution for u_1:

$$\begin{aligned} u_1 &= \tfrac{1}{9}(d_1 - \tfrac{6}{5}d_2)\varphi_2(1 - \tfrac{1}{3}\varphi_2)(1 + \tfrac{1}{3}\varphi_2) \\ &- \tfrac{2}{9}\sqrt{3}(1 + \tfrac{1}{3}\varphi_2)^2 \sin(\sqrt{3}\varphi_1 - \Omega_1(\varphi_2)). \end{aligned} \tag{3.107}$$

This completes the solution up to and including the $O(\varepsilon^1)$-terms. The ε^2- and higher order terms can be found by substituting the results for A_1 and B_1 into the expressions for u_2, v_2 and w_2, from which we can derive the ε^3-versions of our equations. The functions which are still unknown, such as V_1, W_1 etc., can then be determined by equating the secular terms to zero. This process involves the same techniques as have been applied to the calculation of lower order terms; the outcomes are reported in appendix A. We have compared our asymptotic results with the numerically computed results in section 3.2. This comparison shows that the differences are indeed of order $10^{-6} = O(\varepsilon^{-3})$ for all $\varphi \in [0, \varphi_f]$, with $\varphi_f \approx 160$ (rad). This corroborates the correctness of our assumptions. We leave the conclusions for section 3.4.

3.3.3 Local solutions

Whereas the analytic results in subsection 3.3.2 form an accurate, within $O(\varepsilon^2)$-approximation of the solution to system (3.22), figure 3.14 has in fact already pointed out that this solution is considerably different from any observed orbit, even an orbit as smooth as T11B21. To gain a first insight into the course of an arbitrary orbit, it suffices to consider (3.22) only on a limited time scale of the order of one revolution. Since the players of the game are allowed - according to the rules in subsection 2.1.2 - to observe the orbits until the moment of intersection with the limit ring, the most crucial revolution is the one immediately before this intersection. We therefore start our local analysis on time t_m, in the last local minimum before the orbit intersects the limit ring.

First, we introduce the variables

$$\begin{aligned} \tilde{R} &= R/R_m,\ (R_m = R(t_m));\ \tilde{\omega} = \dot{\varphi}/\omega_m,\ (\omega_m = \dot{\varphi}(t_m)); \\ \tilde{t} &= \omega_m\,(t - t_m);\ \tilde{\varphi} = \varphi - \varphi_m,\ (\varphi_m = \varphi(t_m)); \\ \tilde{f} &= \tfrac{5}{7}f_l/\omega_m;\ \tilde{g} = \tfrac{5}{7}g\sin\alpha\cos\alpha/(R_m{\omega_m}^2), \end{aligned} \tag{3.108}$$

on the analogy of (3.43). Next, we simplify system (3.22) by observing that the role of the spin is merely marginal, since - on $[t_m, t_f]$ - both $\dot{\varphi}$ and

$\dot{\psi}$ turn out to be of the order of magnitude of 1 rad/sec, see e.g. figures 5.10 and 5.11, hence $|\frac{2a}{7}\dot{\varphi}\dot{\psi}| \ll |\frac{5g}{7}|$. We finally also assume a perfectly horizontal position, or $\beta = 0$. All this transforms system (3.22) into the system

$$\begin{aligned} \frac{d^2\tilde{R}}{d\tilde{t}^2} &= -\tilde{f}\frac{d\tilde{R}}{d\tilde{t}} + \tilde{R}\tilde{\omega}^2\cos^2\alpha - \tilde{g}, \\ \frac{d\tilde{\omega}}{d\tilde{t}} &= -\tilde{f}\tilde{\omega} - 2\tilde{R}^{-1}\tilde{\omega}\frac{d\tilde{R}}{d\tilde{t}}, \end{aligned} \tag{3.109}$$

with initial conditions corresponding to (3.25):

$$\tilde{R}(0) = \tilde{\omega}(0) = 1, \text{ and } \frac{d\tilde{R}}{d\tilde{t}}(0) = 0. \tag{3.110}$$

Following the usual working method for analyzing satellite equations (cf. Kevorkian and Cole [15], section 3.4), we introduce the transformations

$$\tilde{u}(\tilde{\varphi}) = \tilde{R}^{-1}, \ \tilde{v}(\tilde{\varphi}) = \tilde{R}^{-2}\tilde{\omega}^{-1}, \tag{3.111}$$

to change system (3.109), together with (3.110), into

$$\begin{aligned} \frac{d\tilde{v}}{d\tilde{\varphi}} &= \tilde{f}\frac{\tilde{v}^2}{u^2}, \\ \frac{d^2\tilde{u}}{d\tilde{\varphi}^2} &= -\cos^2\alpha\,\tilde{u} + \tilde{g}\,\frac{\tilde{v}^2}{\tilde{u}^2}, \end{aligned} \tag{3.112}$$

with initial conditions

$$\tilde{u}(0) = \tilde{v}(0) = 1, \ \frac{d\tilde{u}}{d\tilde{\varphi}}(0) = 0. \tag{3.113}$$

This new set of equations reveals an explicit dependence on one small parameter $\tilde{f}$, and two parameters of order 1, namely $\cos\alpha$ and $\tilde{g}$. We replace $\tilde{f}$ by $\tilde{\varepsilon}$, and introduce the constants

$$c = \cos^2\alpha, \text{ and } \delta = c - \tilde{g}. \tag{3.114}$$

Estimations of the initial conditions on time t_m are supplied by section 5.6, from which we obtain

$$R_m = 0.261 \text{ (m)}, \ \omega_m = 1.55 \text{ (rad/sec)}, \tag{3.115}$$

yielding (in accordance with (3.33) and (3.55))

$$c = \cos^2\alpha = 0.9931, \tag{3.116}$$

$$\delta = \cos^2\alpha - \tilde{g}$$

$$= \cos^2\alpha - \tfrac{5}{7} g \sin\alpha \cos\alpha/(R_m {\omega_m}^2) \approx 6.9 \times 10^{-2}, \tag{3.117}$$

$$\tilde{\varepsilon} = \tilde{f} = \tfrac{5}{7} f_l/\omega_m \approx 6.5 \times 10^{-3}. \tag{3.118}$$

With the above substitutions, (3.112) can be rewritten as

$$\begin{aligned} \frac{d\tilde{v}}{d\tilde{\varphi}} &= \tilde{\varepsilon}\frac{\tilde{v}^2}{\tilde{u}^2}, \\ \frac{d^2\tilde{u}}{d\tilde{\varphi}^2} &= -c\tilde{u} + (c-\delta)\frac{\tilde{v}^2}{\tilde{u}^2}. \end{aligned} \tag{3.119}$$

We now expand $\tilde{u}$ and $\tilde{v}$ into the following asymptotic power series:

$$\tilde{u} \sim \sum_{i=0}^{\infty} \tilde{u}_i(\tilde{\varphi})\tilde{\varepsilon}^i, \ \tilde{v} \sim \sum_{i=0}^{\infty} \tilde{v}_i(\tilde{\varphi})\tilde{\varepsilon}^i, \tag{3.120}$$

and we try to find solutions for $\tilde{u}_i$ and $\tilde{v}_i$ by substituting the series (3.120) into (3.119) and (3.113), and by matching the terms with equal powers in $\tilde{\varepsilon}$. For the zero order terms, we thus obtain (omitting the tildes)

$$\begin{aligned} \frac{dv_0}{d\varphi} &= 0, \\ \frac{d^2u_0}{d\varphi^2} &= -cu_0 + (c-\delta)\frac{{v_0}^2}{{u_0}^2}, \end{aligned} \tag{3.121}$$

with

$$u_0(0) = v_0(0) = 1, \ {u_0}'(0) = 0. \tag{3.122}$$

The first equation in (3.121), together with the second condition in (3.122), immediately yields

$$v_0 = 1. \tag{3.123}$$

Substitution of this result into $(3.121)^2$ gives

$$\frac{d^2u_0}{d\varphi^2} = -cu_0 + (c-\delta){u_0}^2, \tag{3.124}$$

which can be integrated (exactly) to

$$\frac{du_0}{d\varphi} = \pm\sqrt{\frac{u_0 - 1}{u_0}[2(c-\delta) - cu_0(u_0+1)]}, \; u_0 \neq 1. \tag{3.125}$$

The solution of (3.125) only exists if the argument of the square root is non-negative, hence only for

$$\overline{u}_0 \leq u_0(\varphi) \leq 1, \tag{3.126}$$

where

$$\begin{aligned} \overline{u}_0 &= -\tfrac{1}{2} + \tfrac{3}{2}\sqrt{1 - \tfrac{8}{9c}\delta} && (3.127) \\ &= 1 - \tfrac{2}{3c}\delta + O(\delta^2). && (3.128) \end{aligned}$$

The solution for $u_0(\varphi)$ is periodic, and moves between the bounds $\overline{u}_0$ and one. Using the fact that δ is small, we can derive the following asymptotic solution:

$$u_0(\varphi) = 1 - \tfrac{1}{3c}(1 - \cos\sqrt{3c}\varphi)\,\delta + O(\delta^2). \tag{3.129}$$

So we find that, within $O(\delta)$-approximation, $u_0(\varphi)$ represents an ellipse with eccentricity $\delta/(3c)$, and periodicity $2\pi/\sqrt{3c}$.

For the ε^1-terms we find

$$\begin{aligned} \frac{dv_1}{d\varphi} &= \frac{1}{{u_0}^2}, \\ \frac{d^2u_1}{d\varphi^2} &= -\frac{c + 2(c-\delta)}{{u_0}^3}u_1 + \frac{2(c-\delta)}{{u_0}^2}v_1, \end{aligned} \tag{3.130}$$

with

$$u_1(0) = v_1(0) = 0, \; {u_1}'(0) = 0. \tag{3.131}$$

For this $O(\varepsilon^1)$-contribution, an $O(\delta^0)$-approximation is sufficient. This approximation conforms to

$$\begin{aligned} \frac{dv_1}{d\varphi} &= 1, \\ \frac{d^2u_1}{d\varphi^2} &= -3cu_1 + 2cv_1, \end{aligned} \tag{3.132}$$

which leads to the solutions

$$\begin{aligned} v_1(\varphi) &= 1, \\ u_1(\varphi) &= \tfrac{2}{3}\varphi - \tfrac{2}{9}\sqrt{\tfrac{3}{c}}\sin\sqrt{3c}\varphi, \end{aligned} \tag{3.133}$$

via the initial conditions in (3.131). Hence, within $O(\delta)$-approximation, the contribution of $u_1(\varphi)$ is a combination of a steady descent with slope $2\varepsilon/3$, and an ellipse with eccentricity $2\varepsilon/9\sqrt{3/c}$.

3.4 Conclusions from the analysis

In a deterministic model, the orbit of the ball in the drum is completely determined by the equations of motion, which are represented by the set of ordinary differential equations in (3.22), and the initial conditions in (3.25). Under the assumption of linear air friction, part of the system of differential equations can be solved exactly. The resulting partial solution in (3.54) can be employed to estimate the unknown coefficient of air friction, viz. by fitting this solution to the experimental data provided by chapter 4. A rough impression of the total solution can be obtained by substituting some preliminary estimates into a Runge-Kutta routine: the results in figure 3.6 show a slightly elliptical, downward spiralling orbit. The slope of the descent and the periodicity of the elliptical spiral appear to be strongly dependent on the air friction force (this follows directly from the formulas in section 3.3).

Under the assumption of a zero spin friction coefficient, the differential equations in (3.22) can be expressed in terms of only two dimensionless parameters: α and ε, where α is the angle of inclination of the drum surface, and ε is a simple combination of the air friction coefficient and the ball's initial angular velocity (see (3.62)). As has been shown in (3.64), these two small effects can be combined into one small parameter, for which we have taken ε. The smallness of ε physically represents the fact that the resistive force F_{a} (due to air friction) is much smaller than both the gravitational force F_{g} and the centrifugal force F_{c}. When a linear air friction model is applied, the system of equations can be solved analytically by expanding the solution into an asymptotic power series in ε. The definitions (3.43), (3.51) and (3.57), together with the formulas in appendix A, yield

$$\begin{aligned} u = R_0/R &= (1 + \tfrac{1}{3}\varphi_2)^2 + O(\varepsilon) \\ &= (1 + \tfrac{1}{3}\varepsilon\varphi)^2 + O(\varepsilon), \end{aligned} \tag{3.134}$$

thus explicitly revealing a slowly descending orbit, the slope of which is largely determined by the value of ε. Higher order approximations reveal an elliptical spiral:

$$\begin{aligned} u = R_0/R &= (1 + \tfrac{1}{3}\varphi_2)^2 + \tfrac{1}{9}\varepsilon(d_1 - \tfrac{6}{5}d_2)(1 - \tfrac{1}{9}{\varphi_2}^2)\varphi_2 \\ &- \tfrac{2\sqrt{3}}{9}\varepsilon(1 + \tfrac{1}{3}\varphi_2)^2 \sin(\sqrt{3}\varphi_1 - \Omega_1) + O(\varepsilon^2) \\ &= (1 + \tfrac{1}{3}\varphi_2)^2\{1 + \tfrac{1}{9}\varepsilon(d_1 - \tfrac{6}{5}d_2)(3 - \varphi_2)(3 + \varphi_2)^{-1}\varphi_2\} \\ &\quad \{1 - \tfrac{2\sqrt{3}}{9}\varepsilon \sin(\sqrt{3}\varphi_1 - \Omega_1)\} + O(\varepsilon^2). \end{aligned} \tag{3.135}$$

During one revolution, and to within $O(\varepsilon)$-approximation, φ_2 is constant, hence (3.135) strongly resembles the phase plane equation of an ordinary ellipse,

$$1/r = 1/c\{1 - e\sin\theta\}, \tag{3.136}$$

with the origin situated at one of the foci, and the major axis corresponding to $\theta = \pi/2$. Apart from a scaling factor, expression (3.135) represents an elliptical curve with eccentricity e equal to

$$e = \tfrac{2}{9}\sqrt{3}\varepsilon + O(\varepsilon^2). \tag{3.137}$$

This curve is periodic with one full period Φ corresponding to

$$\Phi \approx \tfrac{2\pi}{\sqrt{3}}. \tag{3.138}$$

Note that the above results are also published in De Vos and Van de Ven [11].

Whereas the analytic solutions in subsection 3.3.2 provide a clear insight into the global conduct of an undisturbed orbit under idealized circumstances, the local solutions in subsection 3.3.3 give a rough impression of what happens to this conduct (locally) when an occasional disturbance occurs. The definitions (3.108) and (3.111), together with the formulas in subsection 3.3.3, yield

$$\begin{aligned} \tilde{u} = R_m/R &= \tilde{u}_0 + \tilde{u}_1\tilde{\varepsilon} + O(\tilde{\varepsilon}^2) \\ &= 1 - \tfrac{1}{3c}(1 - \cos\sqrt{3c}\varphi)\,\delta \\ &+ \tfrac{2}{3}(\tilde{\varphi} - \tfrac{2}{9}\sqrt{\tfrac{3}{c}}\sin\sqrt{3c}\varphi)\,\tilde{\varepsilon} + O(\tilde{\varepsilon}^2), \end{aligned} \tag{3.139}$$

thus showing an elliptical spiral of period Φ_m, where

$$\Phi_m = \tfrac{2\pi}{\sqrt{3c}} = \tfrac{2\pi}{\cos\alpha\sqrt{3}}. \tag{3.140}$$

The eccentricity e_m of the spiral around $R = R_m$ largely depends on δ (being much larger then $\tilde{\varepsilon}$). From (3.139), in combination with (3.116) and (3.117), we find

$$e_m = \tfrac{1}{3}\cos^2\alpha - \tfrac{5}{21}g\sin\alpha\cos\alpha/(R_m{\omega_m}^2) \approx \tfrac{1}{3}\delta. \tag{3.141}$$

The slope of the descent of the orbit is largely determined by the $O(\tilde{\varepsilon}^1)$-term $\tilde{u}_1$. After one full period, $\tilde{u}_1(\varphi)$ is

$$\tilde{u}_1(\Phi_m) = \tfrac{4\pi}{3\sqrt{3c}}(1 + O(\delta)). \tag{3.142}$$

This means that for the descent ΔR per full period, from $R = R_m$ on, we find (for δ and $\tilde{\varepsilon}$ small)

$$\Delta R \approx R_m - \frac{R_m}{1 + \tilde{\varepsilon}\tilde{u}_1(\Phi_m)} \approx \tilde{\varepsilon} R_m \tilde{u}_1(\Phi_m) \approx \frac{20\pi f_l}{21 \cos\alpha\sqrt{3}} R_m/\omega_m. \quad (3.143)$$

These local asymptotic results - especially (3.140), (3.141) and (3.143) - will play a major part in the development of strategies in chapter 6.

Chapter 4

Experimental data

4.1 The experimental setup

4.1.1 Required data

The main goal of our experimental setup was to collect a large number of accurately measured ball orbits, together with as much additional environmental information as possible. Each orbit should consist of a long time series of (two-dimensional) ball coordinates. A large database of orbits is the only guarantee for an accountable, statistically based comparison of theoretical models with empirical data.

From previous research in 1991 by Van der Genugten & Borm [26] we know that the motion of the ball in the drum is certainly not deterministic, as would have been the case if the factors that determine this motion were fixed and not subject to small fluctuations and (probably) random perturbations: different experiments often show remarkable dissimilarities. The only way to gather more information about the nature of these fluctuations and perturbations is to conduct a large number of experiments, and simply measure the orbits of the ball. A large number of accurately measured orbits allows for a thorough comparison of classical mechanical models on the one hand, and extensions of these models with random components on the other. In the end, we hope to acquire an appropriate model for describing and predicting the motion of the ball in the drum.

The data from the above-mentioned previous research in 1991 would have been a perfect basis for further research. However, the database turned out to be very difficult to access, and the concerning data ap-

peared not to meet our requirements of accuracy. For these reasons, we decided to conduct an extra thousand experiments on a real, frequently used Golden-Ten drum, made available by Casino Service Breda. The experiments were carried out in june 1993, at the Laboratory of Mechanical Engineering at TUE (Eindhoven University of Technology). The measurements were later processed at the division of Fluid Dynamics & Heat Transfer, Department of Technical Physics. The final elaboration of the data took place at the Department of Econometrics at Tilburg University (KUB). The complete results of this work are published in De Vos [8].

According to classical mechanical theory, the motion of the ball is completely determined by the forces that act on it. The forces in their turn depend on the physical characteristics of the ball itself, and those of the drum and the environment in which the game is played. These characteristics can be divided into two categories: those that can be measured directly, and those that have to be measured indirectly, i.e. estimated through use of a mechanical model. The environmental conditions can even be harder to measure, especially factors like "presence of dust particles on the drum surface", or "greasy fingerprints on the ball".

The dimensions of the drum can be measured by means of some suitable instrument; this also applies to the radius and the mass of the ball. The air temperature - one of the environmental conditions that may have its influence on the experiments - can also be measured directly. Other environmental factors can only be measured by fitting an appropriate theoretical model to experimentally acquired data. However, some of the secondary characteristics - like "strange sounds" and "heavy traffic passing by" - can only be noticed by mere observation.

4.1.2 Conducting the experiments

First of all we had to be sure that, during the experiments, the drum was permanently in a perfectly horizontal position. To achieve this, we installed the drum on a solid tripod and waited for a couple of days for the drum to settle. After that, the position was adjusted by means of a straight metal bar and a levelling instrument with an accuracy of 0.5 mm per m. The dimensions of the drum were measured with a marking gauge moving over the straight metal bar, and a spring rule. The marking gauge was also used to measure the diameter of the ball, and the weight was measured with a scale.

As a tracking system for the ball, we used a computer system for

digital image analysis. Because this type of systems requires a sharp contrast between the object to track and its background, a major problem was raised: the colour of the ball is whiteish, and the surface of the drum is bright unpolished steel. This problem was tackled by designing a special illumination setup, owed to advertising photographers Korff & Van Mierlo: in a large black flannel tent a ring of light bulbs was placed just outside and above the rim of the drum. The shadow of the rim prevented the surface to reflect any light, and only the top half of the ball was illuminated. A cardboard cylinder in the centre of the drum granted an even distribution of light, whereas adhesive black felt prevented the rim from reflecting. The tops of the light bulbs were covered with black cardboard, so that the bulbs would not come into vision when the total configuration was looked upon from above. At four points along the rim of the drum we attached small light bulbs; these four lights served as marker points for the computer system.

Perpendicular above the centre of the drum we fixed a Panasonic F10 CCD-camera to register the orbits. The camera images were recorded on Super VHS tape (type PDM-625) by using the available Panasonic AG-6200 video tape recorder. The recorded image was checked on-line with TIM software, version 3.36, running on a 386 personal computer with 3 MB of extended memory and a PCVISIONplus frame grabber expansion board. This computer system did not allow for real-time image analysis, it merely functioned as a means to check for possible changes in illumination, or in camera position. The experiments could later be identified trough the numbered notes that were placed in the lower right corner of the image.

After the recordings, the images were digitized and analysed with DigImage software version 1.2 (see Dalziel [5]), running on a 486 personal computer with a DT-2861 frame grabber expansion board and 8 MB of extended memory, connected to a Panasonic AG-7350 super VHS video tape recorder. Although DigImage was especially designed for image processing of fluid dynamics, we found that it was also capable - with a suitable adjustment of the system parameters - to trace one or more white balls in a dark environment. After being processed by DigImage, the data were further transformed and modified with SAS software version 6.04 (see SAS Institute [21]). SAS is a statistical package with a considerable amount of data management tools; it was run on a 486 personal computer with 2 MB of expanded memory.

4.1.3 Refining the setup

In spite of our meticulous preparations, we did anticipate some deformations and variations in our recorded images. For this reason we designed two (slightly different) layouts of single ball positions. These positions were measured directly by means of a straight wooden ruler, as well as indirectly by the computer system. One layout was laid down and recorded before the experiments were carried out, the other afterwards. By recording two series, we acquired a means to check for changes in the environmental setup during the experiments. The resulting pairs of measurements for both layouts were meant to serve as a mapping function from the recorded images to real-world coordinates. The layouts are plotted in figures 4.1 and 4.2.

In order to be able to eliminate possible secondary effects - like cleaning effects and effects of different balls or different video tapes - we divided our experiments into thirty runs of (approximate) size thirty-five. The video tapes were changed after every two runs, and the ball was changed after every set of six runs. At the beginning of each run, the drum and the ball were cleaned with alcohol. The ball was regularly cleaned with a dry paper towel, and was only touched with special, clean gloves. For every experiment, we recorded the temperature of the air at the beginning of the experiment, the outcome of the experiment, any audible or visible irregularities, possible variations in the launching of the ball, and irregularities during the fall into the numbered compartments.

4.2 Transformations and calibrations

4.2.1 The theory of central projection

The recordings consist of a large number of images of a ball moving in a three-dimensional object space, which is bounded by the drum. Every image is a perspective transformation of this object space: it is the result of a projection through a system of lenses on the image plane of the camera. This transformation can be found by applying the theory of central projection, which is usually condensed into the *collinearity principle:* every point in the object space can be connected to exactly one point in the image space by means of a straight line through the centre of projection (see Schwidefsky & Ackermann [23]).

To determine the coordinates in the object space, we use a cartesian

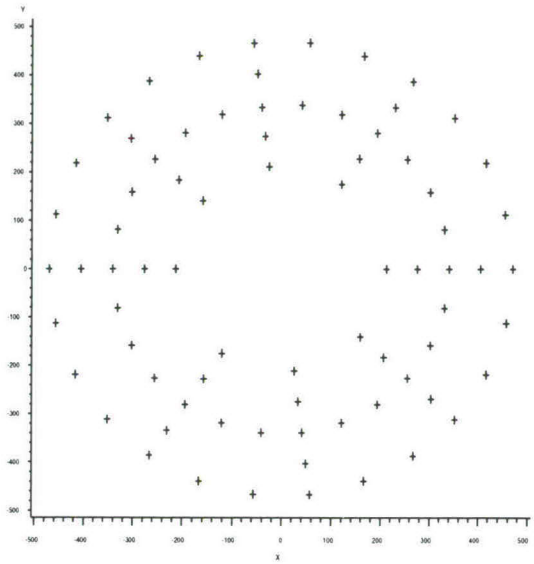

Figure 4.1: First layout of single ball positions (in mm).

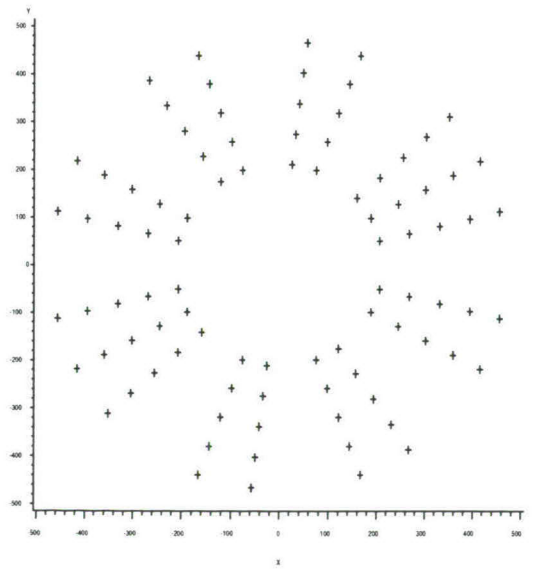

Figure 4.2: Second layout of single ball positions (in mm).

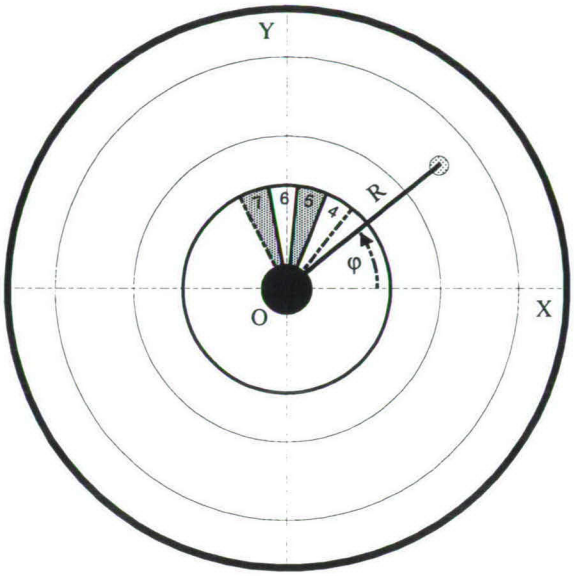

Figure 4.3: The coordinate system $\{OXYZ\}$; top-view (cf. figure 3.2).

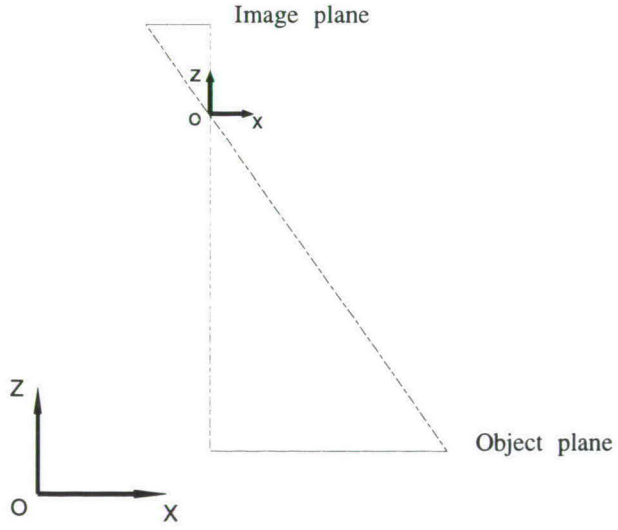

Figure 4.4: Two coordinate systems.

coordinate system $\{O_{XYZ}\}$ (see figure 4.3). For the coordinates in the image space, we use a similar system $\{o_{xyz}\}$, where o is the centre of projection, lying just below the image plane (see figure 4.4). The x- and the y-axis are fixed by the image processing system, but for the X- and the Y-axis we still have full freedom of choice. By choosing these axis as in figure 4.3, we let X, Y, and Z, respectively point in (almost) the same direction as x, y, and z.

In an ideal setup, where the illumination is perfectly uniform, and $\{o_{xyz}\}$ is a translation of $\{O_{XYZ}\}$, we have the simple set of relations

$$\begin{aligned} \frac{X - X_0}{Z - Z_0} &= \frac{x}{-c}, \\ \frac{Y - Y_0}{Z - Z_0} &= \frac{y}{-c}, \end{aligned} \tag{4.1}$$

where (X_0, Y_0, Z_0) are the coordinates of the centre of projection o in the system $\{O_{XYZ}\}$, and c is the distance from o to the image plane. The constant c is usually called the *camera constant*. In a more general setup, where the illumination is still uniform, but the $\{o_{xyz}\}$ system may have been rotated and rescaled, we have a more intricate set of equations:

$$\begin{aligned} \frac{X - X_0}{Z - Z_0} &= \frac{a_{11}x + a_{12}y - a_{13}c}{a_{31}x + a_{32}y - a_{33}c}, \\ \frac{Y - Y_0}{Z - Z_0} &= \frac{a_{21}x + a_{22}y - a_{23}c}{a_{31}x + a_{32}y - a_{33}c}, \end{aligned} \tag{4.2}$$

where $\{a_{ij}\}$ is the matrix of successive rotations over ζ, η and ϑ around the x-axis, and the rotated y- and z-axis, respectively:

$$\{a_{ij}\} = \begin{pmatrix} \cos\eta\cos\vartheta & \cos\zeta\sin\vartheta + \sin\zeta\sin\eta\cos\vartheta & \sin\zeta\sin\vartheta - \cos\zeta\sin\eta\cos\vartheta \\ -\cos\eta\sin\vartheta & \cos\zeta\cos\vartheta - \sin\zeta\sin\eta\sin\vartheta & \sin\zeta\cos\vartheta + \cos\zeta\sin\eta\sin\vartheta \\ \sin\eta & -\sin\zeta\cos\eta & \cos\zeta\cos\eta \end{pmatrix} \tag{4.3}$$

Scaling factors automatically cancel out, provided that the camera constant is measured in the same units as the distances in the image plane itself.

A non-uniform distribution of light can seriously deform the camera image. To a lesser extent, this is also true for uncertain factors like fluctuations in the power supply, weak spots in the magnetic video tape, warming-up effects in the computer hardware, etc. Without further knowledge of the nature of these effects, it is impossible to find an exact

relation between the image and the real world. The most obvious way to proceed is to allow for more variation in the parameters in (4.2). For estimation of the desired mapping function, we will therefore use equation set (4.4), with more general parameters $\{b_{ij}\}$:

$$\begin{aligned} \frac{X - X_0}{Z - Z_0} &= \frac{b_{11}x + b_{12}y + b_{13}}{b_{31}x + b_{32}y + b_{33}}, \\ \frac{Y - Y_0}{Z - Z_0} &= \frac{b_{21}x + b_{22}y + b_{23}}{b_{31}x + b_{32}y + b_{33}}. \end{aligned} \tag{4.4}$$

The only constrained parameter in (4.4) is b_{33}: we will use it as a scaling factor for the rest of the parameters.

4.2.2 Processing the image

DigImage is an image processing system that consists of several modules, one of which is especially designed for particle tracking. This last module enables the user to trace up to 4095 white particles in a dark background, and to track them for a time period of arbitrary length. The user can change a number of system parameters to adjust the tracking program to different experimental setups. Appendix B contains a listing of the settings we used. Only the first three parameters (file name, experiment name, and total tracking time) varied from experiment to experiment; the other parameters were fixed.

Because of possible synchronisation errors due to the technical limitations of both the video tape recorder and the frame grabber board, DigImage will only process video tapes that contain special audio pulses. These pulses can be added to the tape after the images have been recorded. Optimally recorded audio pulses, requiring a tape of a better than average quality, guarantee a hundred percent reliable timing.

After an image has been captured, DigImage searches the image for the (user-defined) permanent reference points. In our setup, these points were the four small light bulbs on the outside of the drum. After the reference points have been identified, the captured image is shifted over an integer number of positions, in order to match the user-defined points as closely as possible. If the differences fall within certain limits, the image is kept and further analysed; otherwise the image is dropped and recaptured. All this implies that the difference between the analysed image and the real-world situation is small, but still subject to certain perturbations. This is especially true in our situation, since the small

light bulbs appeared not to be fastened tightly enough to prevent them from sagging slightly.

During the analysis phase, DigImage searches the image for particles. Each particle is compared to every particle in the previous image, and only particles that seem to match are considered for further tracking. During the experimental phase we found that at least two balls are needed before any matches can be found. We fixed this problem by placing a motionless ball on top of a small cylinder, positioned right above the top of the drum. Furthermore, it appeared that the moving ball could only be tracked for exactly one time step. This was long enough for the system to save the corresponding coordinates, but unfortunately not long enough to allow us to use any more of the available tracking utilities.

Eventually we were able to generate, from every series of experiments, a set of four files of which the first serves as an index to the second, and the second contains the ball coordinates (usually of both balls). The record structure of the first file is such that the record numbers correspond to the total elapsed time, and that the two next numbers are the corresponding record numbers in the second file. The second file is a direct access binary file containing two-byte, unsigned integer values, representing rescaled ball coordinates. We used SAS software to read these two files and to combine them, thus to render a time series of ball coordinates.

Two-byte, unsigned integer values range from 0 to 65535, whereas video screen coordinates - which are measured in rectangular *pixels* - range from 0 to 511 (horizontally and vertically). DigImage rescales the pixel coordinates to a user-defined, rectangular tracking window, and then rescales them again to user-defined world coordinates. The coefficients of the first mapping function - which is a linear transformation - can be found in the third tracking file. The coefficients of the second transformation are recorded in the fourth file; they should represent the mapping function that was described in equation set (4.4). However, since none of the offered alternatives for a mapping function matched, we chose not to use this feature. However, on some occasions we used it accidentally, in which case we caused a reflection of coordinates. So we had to check the last tracking file as well.

Note that due to a restricted lease contract, we were not allowed to analyse more than four tapes. On these four tapes we recorded 350 experiments, which is approximately one third of the total number. The rest of the experiments still remains available on tape, but from these experiments only some very basic information has been extracted. See

De Vos [8].

4.2.3 Transforming the image

Parameter	Estimate	Asymptotic Std. Error	Asymptotic 95 % Confidence Interval Lower	Upper
X0	105.592291	60.76114623	-14.3575723	225.5421549
Y0	-305.620485	76.97893737	-457.5862328	-153.6547368
Z0	3788.291936	629.22828644	2546.1190702	5030.4648010
B11	1.003212	0.16828105	0.6710048	1.3354191
B12	0.001356	0.00145866	-0.0015233	0.0042358
B13	-82.386070	28.37007459	-138.3920346	-26.3801063
B21	0.004365	0.00095288	0.0024834	0.0062456
B22	0.996788	0.16819614	0.6647481	1.3288272
B23	145.803185	27.64348536	91.2315957	200.3747737
B31	-0.046473	0.00576468	-0.0578527	-0.0350923
B32	0.088860	0.00576032	0.0774881	0.1002312

Table 4.1: Estimated transformation coefficients.

The twelve unknown coefficients of the non-linear mapping function in equation set (4.4) can be estimated using the data from the two layouts in figures 4.1 and 4.2. However, because of some small changes in illumination, and because of the sagging reference lights, we can expect the results for the two layouts to be slightly different. To eliminate possible start-up effects, we use the second layout for the actual estimation, and the first layout to check the results.

Although we do not impose any constraints on the parameters $\{b_{ij}, (i,j) \neq (3,3)\}$, we do want to check the estimations against the original formulas in equation (4.3), in order to get some idea of the errors we make. First of all this requires an estimate of the *aspect ratio:* the ratio of horizontal to vertical size of the pixels that compose the image. Since an incorrect aspect ratio would deform an actual circle to an apparent ellipse, we use the equation

$$((x - x_0)/\lambda)^2 + ((y - y_0)/\mu)^2 = 1, \tag{4.5}$$

and a simple least squares procedure, to fit an ellipse to the first round of the ball on every one of the four tapes. Note that (x_0, y_0) is the midpoint of the apparent ellipse, and λ/μ is the ellipticity. Although this method

does not take into account the deformations due to equation set (4.4), the resulting estimate of

$$\mu/\lambda = 1.447 \pm 0.001 \tag{4.6}$$

turns out to be accurate enough to serve our purpose.

After multiplying the x-coordinate with 1.447, we proceed by simultaneously fitting the equations in (4.4) to the data from layout number two. Since equation (4.3) implies that the estimates of a_{11} and a_{22} should be close to one, we fix the value of b_{33} to -1802.5764, thus causing the corresponding estimates of b_{11} and b_{22} to be as close to one as possible. The results of the estimation procedure are presented in table 4.1, where distances are expressed in millimeters and angles in radians. The estimated 95% confidence intervals in this table indicate a relatively large inaccuracy, but the residual plots in figures 4.5 and 4.6, where the position of the ball is expressed in polar coordinates (R, φ) in the xy-plane (see figure 4.3) show that the errors are not systematic, except maybe for the innermost region of the drum, near the angles 4.3 and 6.0 rad. In this region we seem to underestimate the angle φ, in the second we seem to overestimate the distance R.

Table 4.1 also indicates that the camera and illumination setup were far from ideal. From the estimated values of X_0 and Y_0 we find that the camera may have been positioned at more than 30 centimeters distance from the main axis of the drum. We also find - from the estimated b_{32}, b_{31} and b_{21} - that the camera was probably rotated around the x-, the y- and the z-axis over the angles 0.09, -0.05, and 0.004 rad, respectively.

Application of the estimated transformation to layout number one results in the somewhat surprisingly shaped graph in figure 4.7. The roughly parabolic shape is caused by two effects: one is the sagging of the four reference lights (which is in fact a warming-up effect), the other is a warming-up effect of the computer hardware: since we knew the lights sagged, we redefined our four reference points at the beginning of each computer run, thus superimposing an extra shift on the data. We can try to eliminate both effects by shifting the data back into the proper direction, but since the recorded orbits are also afflicted with this defect, and because the orbits contain much more data than the layouts, we apply the shift directly to the orbits themselves.

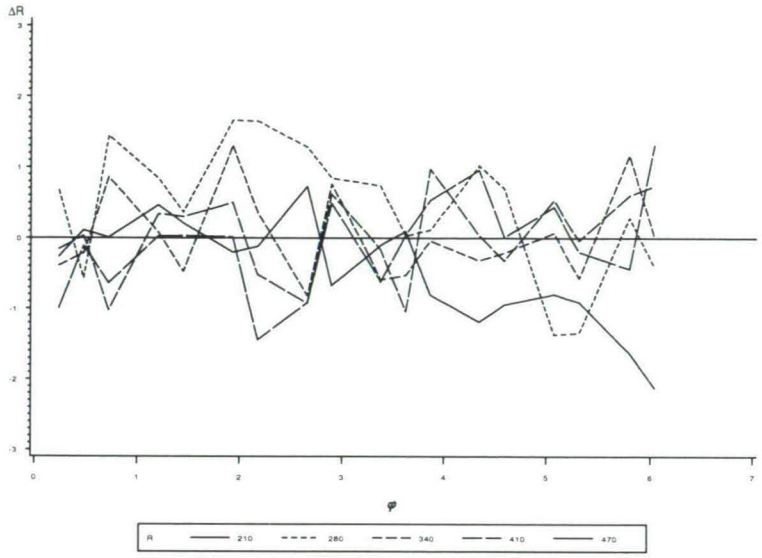

Figure 4.5: Estimated residual distances (second layout).

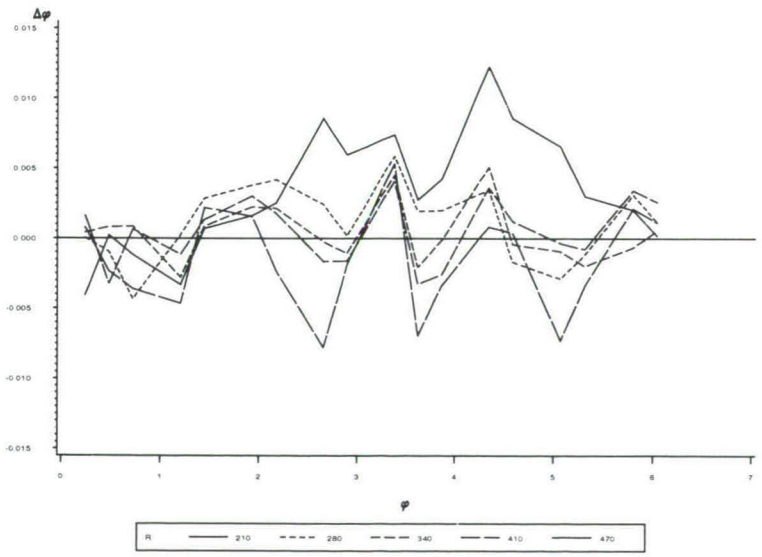

Figure 4.6: Estimated residual angles (second layout).

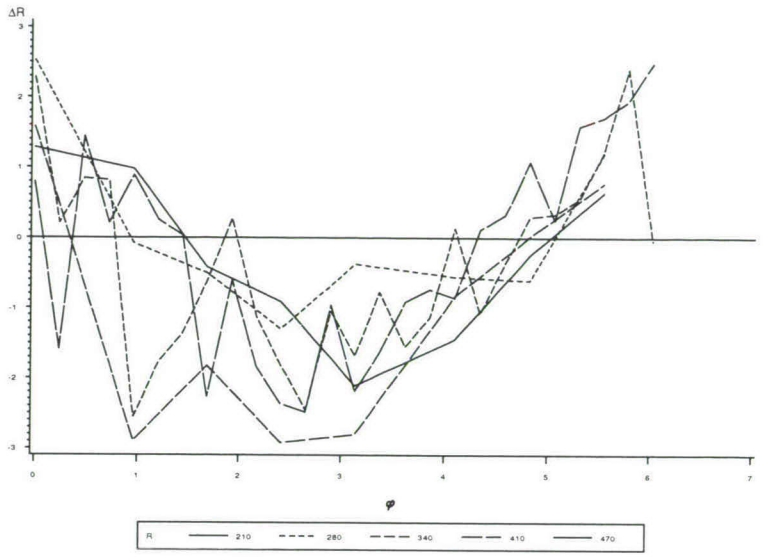

Figure 4.7: Estimated residual distances (first layout).

4.2.4 Shifting the image

The mapping function in equation set (4.4) can be rewritten as

$$\begin{aligned} X &= X_0 + (Z - Z_0)\frac{b_{11}x + b_{12}y + b_{13}}{b_{31}x + b_{32}y + b_{33}}, \\ Y &= Y_0 + (Z - Z_0)\frac{b_{21}x + b_{22}y + b_{23}}{b_{31}x + b_{32}y + b_{33}}. \end{aligned} \tag{4.7}$$

Given matrix $\{b_{ij}\}$ and vector (X_0, Y_0, Z_0), we have at our disposal a mapping function from (x, y, z) to (X, Y, Z), provided that we also know Z. For the centre of the ball, this third coordinate equals

$$Z = \sqrt{X^2 + Y^2}\tan\alpha + a/\cos\alpha, \tag{4.8}$$

since the ball is constrained to move on the surface of the drum. Note that constant α has the value $0.0831 \approx \arctan(1/12)$, see subsection 4.3.1. The second factor in (4.8) can be eliminated by adding this same factor to Z_0, as we in fact already did to obtain the results in table 4.1. Substitution of (4.8) into (4.7) yields a system of two quadratic equations in the two

unknown factors X and Y. This system can be solved by requiring that the value of Z must always be greater than zero.

This leaves the problem of estimating the shift caused by the two warming-up effects. For every orbit, we estimate this effect by using the first round of the ball along the rim. We know that this round is a perfect circle with a radius of approximately 470 mm (see subsection 4.3.1), so we estimate the shift (x_s, y_s) by using the equation

$$\begin{aligned} 470^2 = \{X_0 \quad + \quad (\tfrac{470}{12} - Z_0)\frac{b_{11}(x - x_s) + b_{12}(y - y_s) + b_{13}}{b_{31}(x - x_s) + b_{32}(y - y_s) + b_{33}}\}^2 + \\ \{Y_0 \quad + \quad (\tfrac{470}{12} - Z_0)\frac{b_{21}(x - x_s) + b_{22}(y - y_s) + b_{23}}{b_{31}(x - x_s) + b_{32}(y - y_s) + b_{33}}\}^2, \end{aligned} \quad (4.9)$$

and minimizing the sum of squared errors. We then subtract from the resulting estimates the corresponding values we find when we use the first eighteen data points of the second layout (these eighteen points are also positioned along the rim). The residual distances from this procedure appear to show the same error structure as in figure 4.5. Figure 4.8 shows the corresponding structures for both the second layout and an arbitrary orbit (T15B02, see subsection 4.3). Note that the horizontal axis represents the estimated angle φ', not the actual angle φ.

The encouraging results invite us to also try to shift the images of the first layout, thus allowing for a visual comparison of layouts number one and two. This is a somewhat precarious endeavor though, since we have only twenty-four data points at our disposal, some of which have not exactly been positioned along the rim. Figure 4.9 shows the results. By comparing figures 4.5 and 4.8, we find that the residual distances roughly have the same structure, except for the outermost region of the drum in between the angles 0 and 1.7 rad. This deviation may have been caused by illumination effects, but it may also be a result of our measurement method.

One last remark on the estimated shifts seems necessary here. In figures 4.10 and 4.11 we plotted the estimated x- and y-shift (in pixels) against the experiment number. The vertical lines in the graph indicate a change of tapes. Besides the two warming-up effects, two other effects are revealed here: a tape effect (when crossing the vertical lines), and an effect caused by the tracking software, appearing as an extra shift over exactly one or two positions.

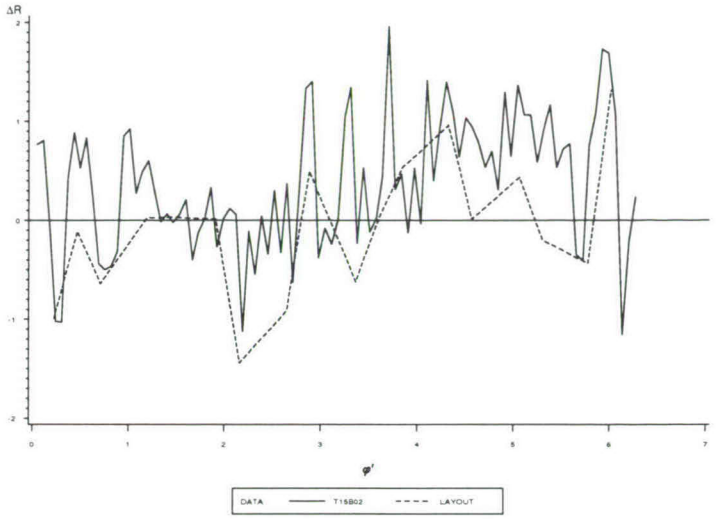

Figure 4.8: Estimated residual distances along the rim; the solid line represents the first round of T15B02, the dashed line corresponds to figure 4.5 (the second layout).

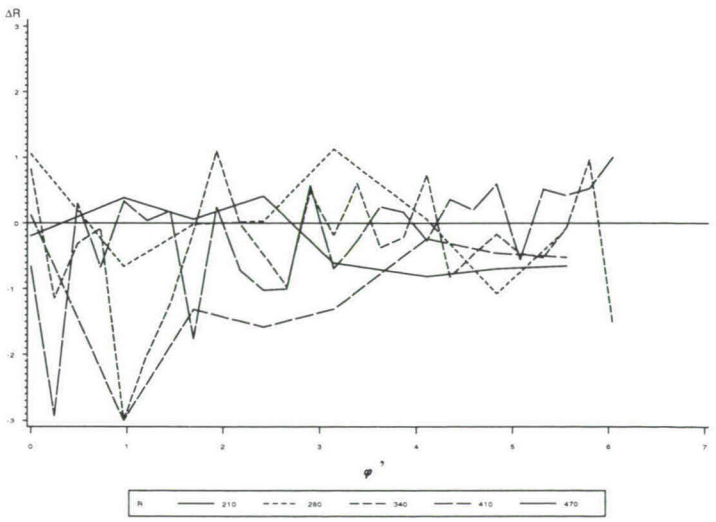

Figure 4.9: Estimated residual distances (shifted first layout).

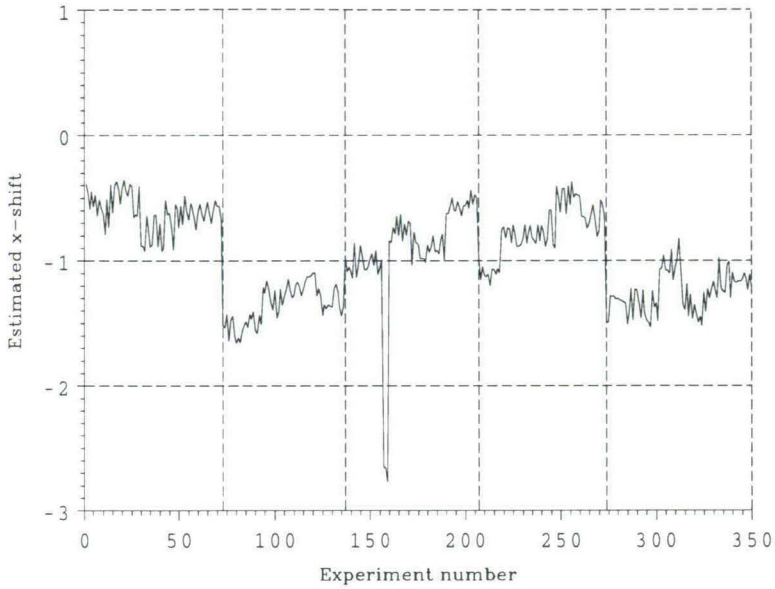

Figure 4.10: Estimated x-shift (in pixels).

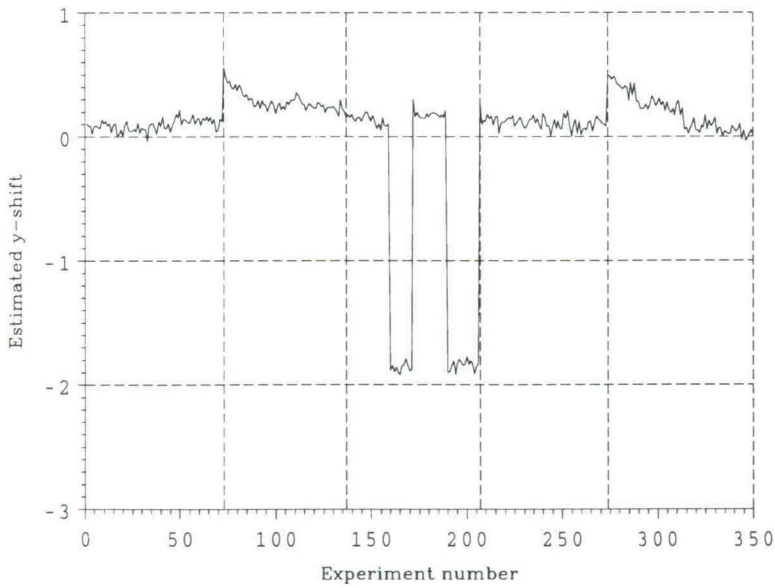

Figure 4.11: Estimated y-shift (in pixels).

4.2.5 Correcting the time code

The last complication we encountered when composing the time series was brought on by the unexpectedly large time code errors. As stated before in subsection 4.2.2, the tracking program produced a file containing an indicator of the total elapsed time. Since the quality of our tapes was only just average, the timing of the system appeared to be quite messy. The errors were eventually dealt with in two steps.

First, we checked every fifteenth record number, since at these numbers the system paused to rewind and replay the tape. We then used a rough estimator to predict the next ball position, and used the difference between the predicted and the actual position to correct the time code. This algorithm performed reasonably well, but we still had to use a second step, during which we plotted the approximate angular velocity $\Delta\varphi/\Delta t$ against the total covered angle φ, and watched for conspicuous anomalies. The remaining errors were corrected manually. During this process we found that the time code errors ranged from -0.16 to $+0.08$ seconds, depending on the tape number. Furthermore, tape number twelve appeared to contain four experiments that were too messy to correct. There also appeared to be one such experiment on tape number fifteen.

Appendix C contains a listing of the SAS program we used to transform the raw data into the required time series. First of all, this program reads the user-supplied filenames, and then it reads the corresponding four data files. It then merges the files, and removes the positions of the motionless ball. After this - while counting the number of subsequent experiments - it tries to correct the time codes as accurately as possible. Next, it splits off the different experiments, and for every experiment it uses the first round to estimate the shift. Finally, it applies the estimated shift, produces two graphs for every orbit, and writes a simple ASCII file. See also De Vos [9].

4.3 Experimental results

4.3.1 Physical dimensions

We experimented with five different Golden-Ten balls. The measurements of these balls are listed in table 4.2. The estimated mean values of the radius and the weight of the ball are found to be 17.45 mm, and 38.3 gr. The corresponding 95% confidence interval for the weight is $(37.9, 38.7)$ gr.

object	dimension	value					accuracy	unit
drum	inclination angle	0.0831					0.0003	rad
	rim	(974,1000)					0.5	mm
	observation ring	(770,780)					0.5	mm
	limit ring	(510,520)					0.5	mm
	edge	410					0.5	mm
disc	diameter	400					0.5	mm
ball	diameter	34.9	34.9	34.9	34.9	34.9	0.005	mm
	weight	38.2	38.2	38.5	38.1	38.4	0.2	gr

Table 4.2: Physical dimensions of the drum and the five balls (cf. table 2.1).

Table 4.2 also sums up the measurements for the dimensions of the drum. Note that the observation ring and the limit ring are in fact two 5 mm-wide, relatively deeply grooved tracks on the surface. The diameters have all been measured in the xy-plane (see figure 4.3). Furthermore, note that the estimated angle of inclination of the drum surface is very close to arctan(1/12). Since the drum was manufactured on a lathe, we can assume that this lathe was manually adjusted to a ratio of 1/12.

4.3.2 Environmental conditions

As was stated before in subsection 4.1.1, we have tried to collect as much environmental information as possible. De Vos [8] summarizes the concerning data in a table of 1042 experiments, grouped together by the tape they were recorded on. The experiments were coded from T01B01 to T15B77: the first number - ranging from 01 to 15 - indicates the tape (T for Tape), and the second number - roughly ranging from 01 to 75 - identifies the experiment (B for Ball). The data concerning the environmental conditions are electronically stored as a SAS dataset, named ENVIRONM. The structure of this file is given in table 4.3.

The second and third column of the table report the outcome of the experiment, and the air temperature (in degrees Celsius), respectively. The fourth column represents some - unfortunately unavoidable - changes in the setup, the fifth column indicates the quality of the launch, and the last column reports possible recording errors. The rest of the columns indicate observed irregularities, mostly audible. The first irregularity column indicates an eventual collision with a compartment lamella. Fur-

Data Set Name: MYDIR.ENVIRONM Type:
Observations: 1042 Record Len: 130
Variables: 20
Label:

-----Alphabetic List of Variables and Attributes-----

#	Variable	Type	Len	Pos	Format	Label
19	BAND	Num	8	121	3.	
1	ID	Char	6	4		
7	IRREG	Char	1	32		
6	LAMELLA	Char	1	31		
5	LAUNCH	Char	1	30		
2	OUTCOME	Num	8	10	2.	
11	PHI1	Num	8	57	4.2	
13	PHI2	Num	8	73	4.2	
9	PHISPECK	Num	8	41	4.2	
20	RECERROR	Char	1	129		
10	RHO1	Num	8	49	3.	
12	RHO2	Num	8	65	3.	
8	RHOSPECK	Num	8	33	3.	
14	ROUND1	Num	8	81	3.	
15	ROUND2	Num	8	89	3.	
16	ROUND3	Num	8	97	3.	
17	ROUND4	Num	8	105	3.	
18	ROUND5	Num	8	113	3.	
4	SETUP	Char	4	26		
3	TEMP	Num	8	18	4.1	

Table 4.3: SAS dataset structure.

thermore, there is a column for the code of the irregularity, two for the roughly estimated position (in polar coordinates) of a removed speck of dust, four columns for two audible local irregularities, five columns for irregular rounds, and finally one column for a complete irregular band. The codes for these changes, errors and irregularities are explained in tables 4.4 and 4.5.

4.3.3 Time series

At the end of experiment T01B17, we discovered that the compartment ring was slightly thrusting out above the drum surface, so we readjusted

code	launch	lamella	irregularity
1	firm	along	stain on drum
2	limp	against	drill in lab
3	with side	across	speck on ball
4	ideal	-	speck on drum
5	-	-	skid along rim
6	-	-	odd orbit

Table 4.4: Codes for (observed) irregularities concerning the motion of the ball.

code	setup	recording error
1	surface cleaned	booth not closed
2	ball changed	speck on rim
3	compartment ring adjusted	fluctuating camera
4	reference light adjusted	light ring pushed
5	iris adjusted	power fault
6	camera switched off, on	wrong numbered note
7	tape recorder adjusted	-

Table 4.5: Codes for changes and errors in the experimental setup.

the position of the ring at the beginning of T01B18 (as can be seen in De Vos [8]). This implies that the first seventeen experiments are largely unusable, which leaves us with a total of $1042 - 17 = 1025$ properly conducted experiments.

Due to a limited lease contract, we could not analyse more than six tapes. We took the six last tapes, but later discovered that one of these (tape 13) had a really poor quality and was largely unusable. In the end, we managed to extract - out of the above-mentioned 1025 experiments - a total of 350 time series of ball coordinates (i.e. polar coordinates). From every time series we created two graphs: both the distance R and the approximate angular velocity $\Delta\varphi/\Delta t$ were plotted against the total covered angle φ. Figures 4.12 and 4.13 display the two graphs for the first available experiment on tape 15 (i.e. T15B02). Since adding the rest of the graphs would extend this subsection with an extra 698 pages, we decided to move these graphs to two supplementary reports (i.e. two

addendums to De Vos [8]).

As can be seen in figures 4.5 and 4.6, we know that the errors in the distance R approximately range from -2 to $+2$ mm, and those in the angle φ roughly within $\pm$ 0.01 rad. Furthermore, we can deduce from the first graphs of experiments T11B65, T12B24, T12B41, T12B63, T15B01, T15B72 and T15B77, that the corresponding orbits have not been processed to their full extent. In addition, from the second graphs of T12B12, T12B22, T12B25, T12B55, and T15B40 we learn that the time codes for these orbits are very unreliable (although the errors do not seem to be systematic). In the end, this leaves us with exactly 338 accurately measured, completely registered orbits.

All the above-mentioned 338 orbits are accessible through DigImage files, as well as through 338 corresponding ASCII files. The names of the ASCII files exactly match the names of the experiments; the extensions all equal "DAT". As an example, we included in table 4.6 a listing of the first and the last part of T15B02.DAT. The general structure of the files is described in table 4.7. Note that the columns are separated by a double space.

0.00	468.919	0.215
0.04	468.296	0.284
0.08	468.264	0.353
0.12	468.914	0.422
0.16	469.250	0.490
	...	
120.64	160.886	166.873
120.68	160.561	166.873
120.72	160.734	166.873
120.76	160.369	166.873
120.80	161.616	166.870

Table 4.6: First and last part of T15B02.DAT.

column	variable	positions	decimals	units
1	t	6	2	sec
2	R	7	3	mm
3	φ	7	3	rad

Table 4.7: ASCII file structure (of T15B02.DAT, see table 4.6).

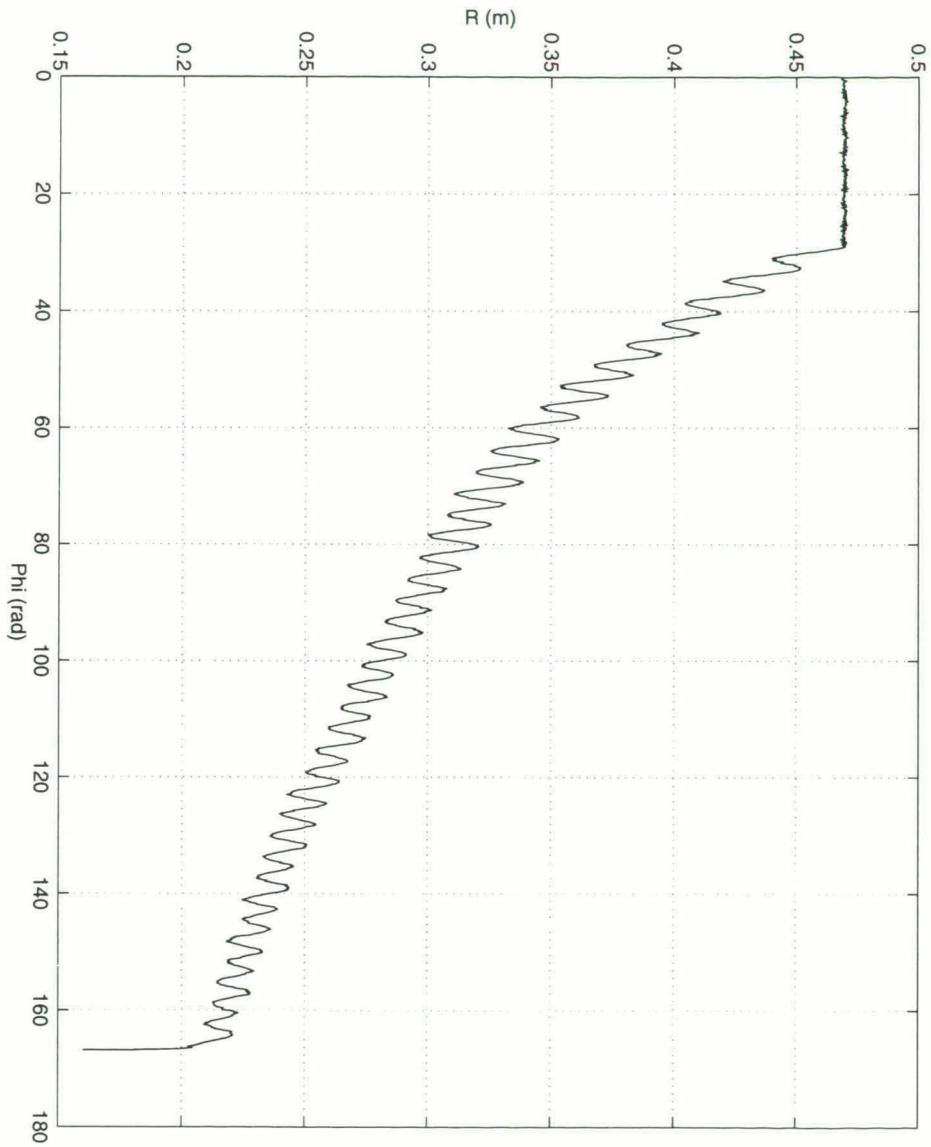

Figure 4.12: First graph of T15B02.

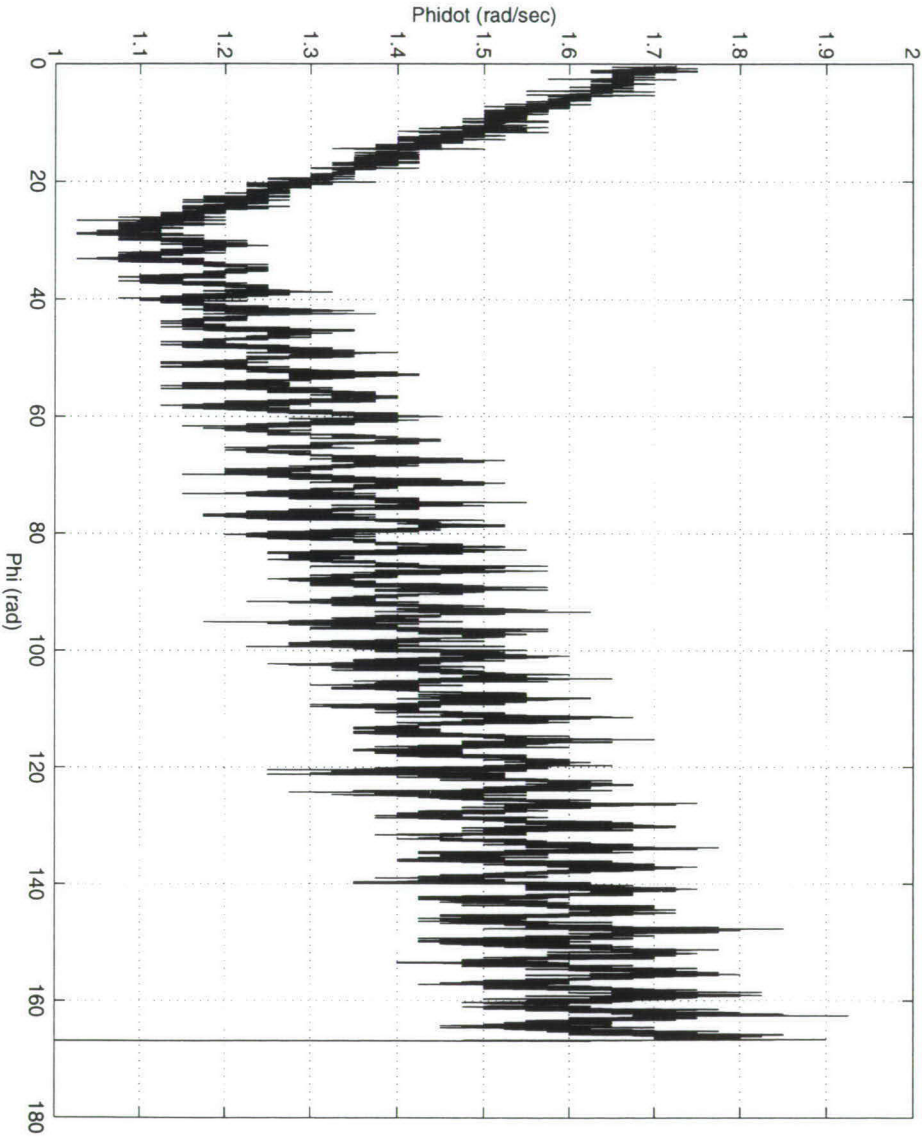

Figure 4.13: Second graph of T15B02.

Chapter 5

Stochastic modelling

5.1 Deliberation of possible models

Whereas chapter 3 describes the analytical properties of the equations of motion of the ball in the drum, based on the principal laws of mechanics, chapter 4 reports the experimental design and the observed orbits of a concrete experiment. However, a deterministic model does not fit to the experimental data (see e.g. figure 3.13), due to apparent disturbances of a random nature. In this chapter we describe the construction of a stochastic model that fits the data. In the next chapter, we will use this stochastic model to derive optimal prediction strategies for players, together with their (long term) gains.

Because of the smooth surface of the drum, one might expect that the orbit of the ball (from launch up to and including the downfall) is deterministic, which would continuously yield the same outcome. The experimental data in chapter 4, however, show an almost uniform distribution of outcomes. This is illustrated in figure 5.2, which presents the frequencies of the relative outcomes of our 338 orbits (the relative numbers are counted from rim to number disc, modulo 26). Figure 5.2 shows neither extremely high nor extremely low levels, and does not show any clear structure. This suggests that the odds in Golden-Ten are basically the same as those in Roulette. Considering the rules of the game in subsection 2.1.2, there is one major diference however: the players can start betting when the ball reaches the observation ring, and have to stop betting at the limit ring. Hence the players can observe part of the ball's orbit, which might enable them to make a better than random guess on the outcome. This would make that Golden-Ten, unlike Roulette, con-

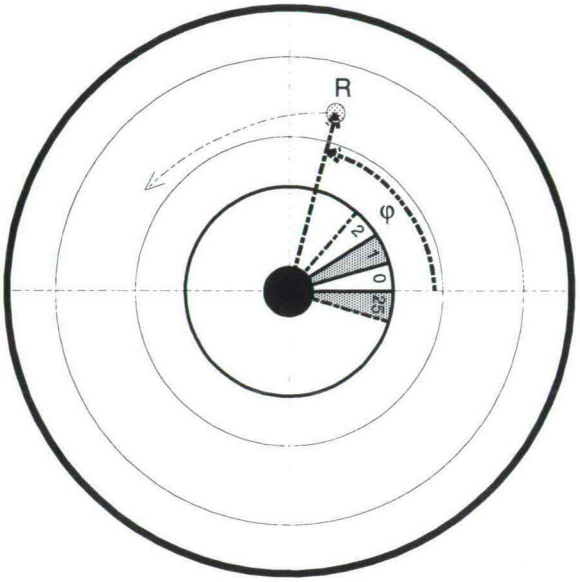

Figure 5.1: Schematic top-view on the drum and the ball. Note that the compartments 24-0 have been renumbered as 0-25, counter-clockwise (cf. figure 2.1).

tains elements of skill.

Figure 5.3 shows a histogram of the difference in compartment numbers (modulo 26) between the limit ring intersection point and the final outcome. Although the distribution shows a peak at relative number 17, it still does not show a clear structure. This implies that a reliable prediction strategy requires much more information. For that reason we first present the shortcomings of a deterministic model. Figures 5.4 to 5.7 show the main components of such a model, with parameters estimated from a nice, smooth orbit (orbit T11B21, see chapter 4). As opposed to this, figures 5.8 to 5.11 present the corresponding components of an average experimental orbit (T11B38, see chapter 4). This illustrates that the overall characteristics are quite similar - except maybe for the spin (in figures 5.7 and 5.11) - but also that the local differences are relatively large. However, small differences may eventually have large effects on the final outcome.

The erratic behaviour shown in figures 5.9 and 5.10 may be caused by

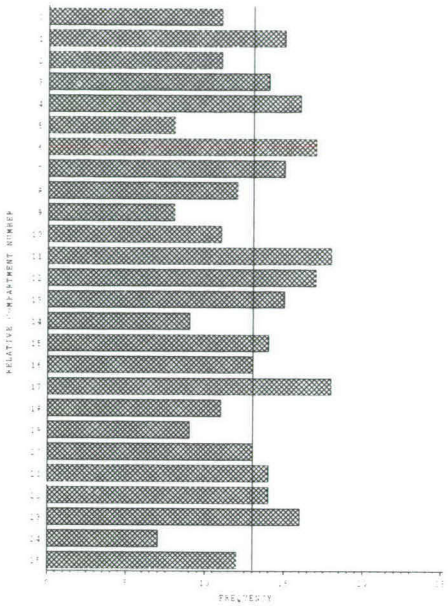

Figure 5.2: Total number of compartments (modulo 26), from rim to number disc.

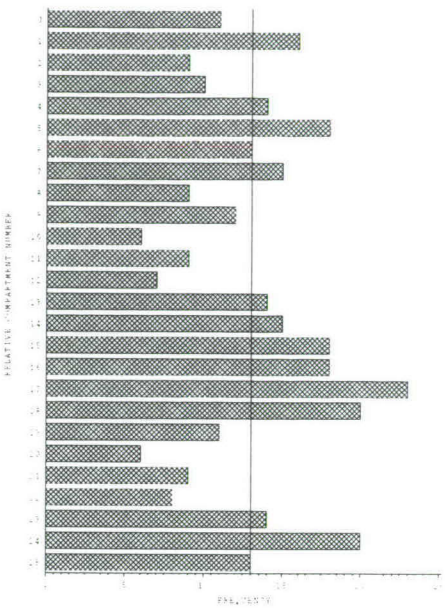

Figure 5.3: Total number of compartments (modulo 26), from limit ring to number disc.

irregularities on the surface of both drum and ball, or perhaps by varying conditions of the surrounding air (due to the ponderous illumination setup described in chapter 4). However, they may also be explained from failing model assumptions in chapter 3, such as the one concerning rolling without slipping. Furthermore, we know that the surface of the drum in question is slightly grooved. The concentric grooves can cause the ball to get stuck in a kind of trench, as is demonstrated in figure 5.13, where the ball apparently gets stuck in a trench with radius 0.43 m. Apart from that, the grooves may also account for the odd behaviour of the experimentally determined spin in figure 5.11 (see also subsection 5.5.3). These types of peculiarities have to be taken into account, because, however slightly, they will eventually influence the final outcome.

The aim of this chapter is to construct a complete stochastic model

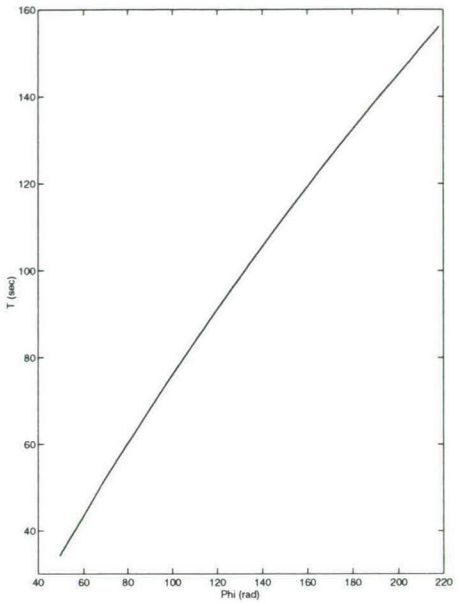

Figure 5.4: Theoretical, deterministic time.

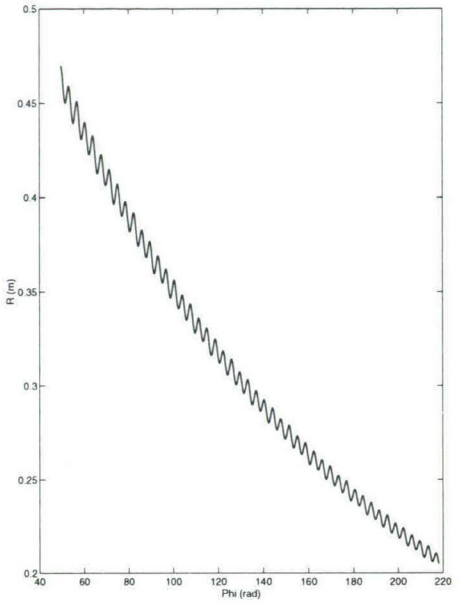

Figure 5.5: Theoretical radius.

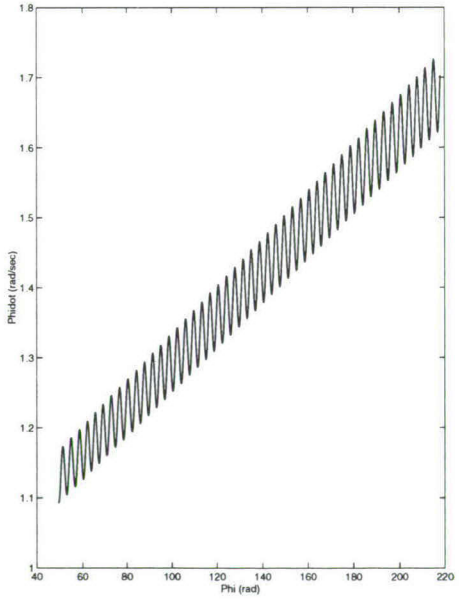

Figure 5.6: Theoretical angular velocity.

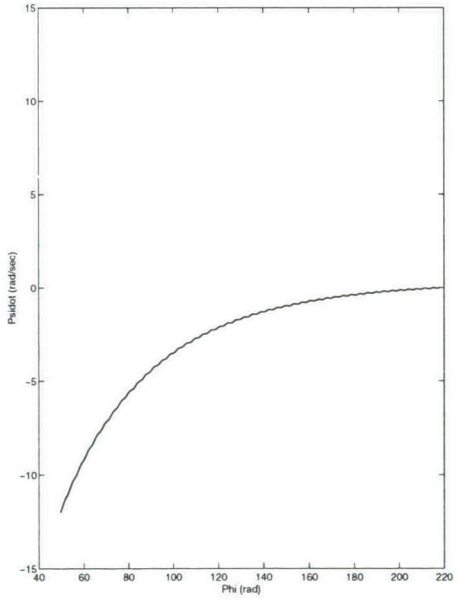

Figure 5.7: Theoretical spin.

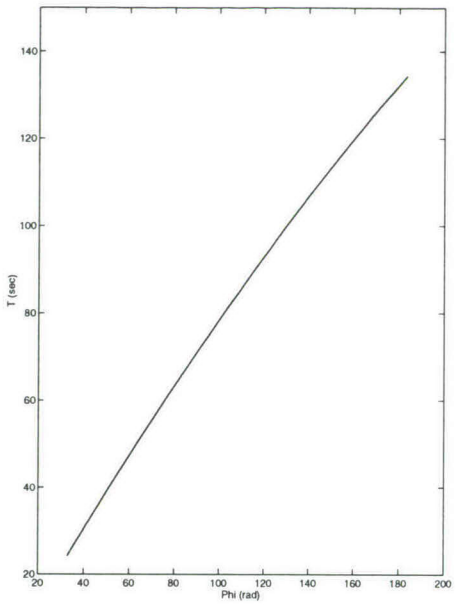

Figure 5.8: Observed time.

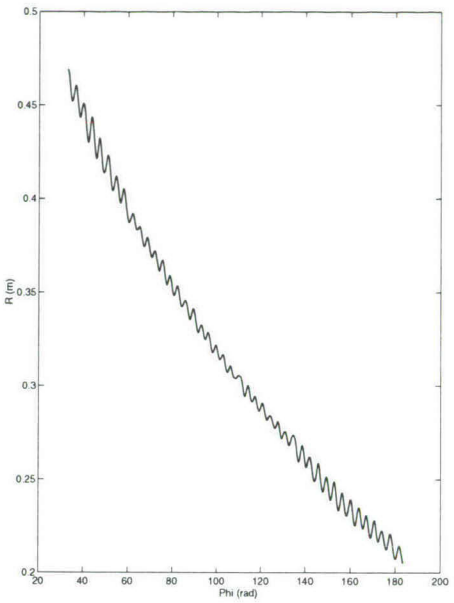

Figure 5.9: Observed radius.

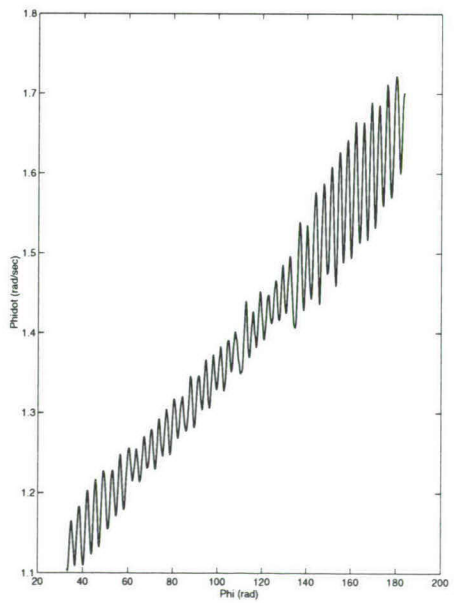

Figure 5.10: Observed angular velocity.

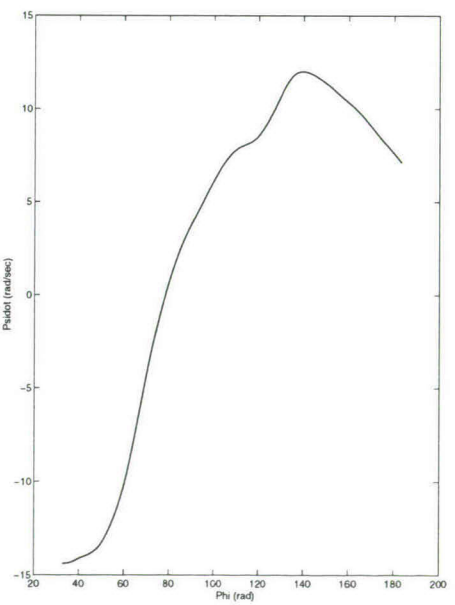

Figure 5.11: Observed (i.e. estimated) spin; all T11B38.

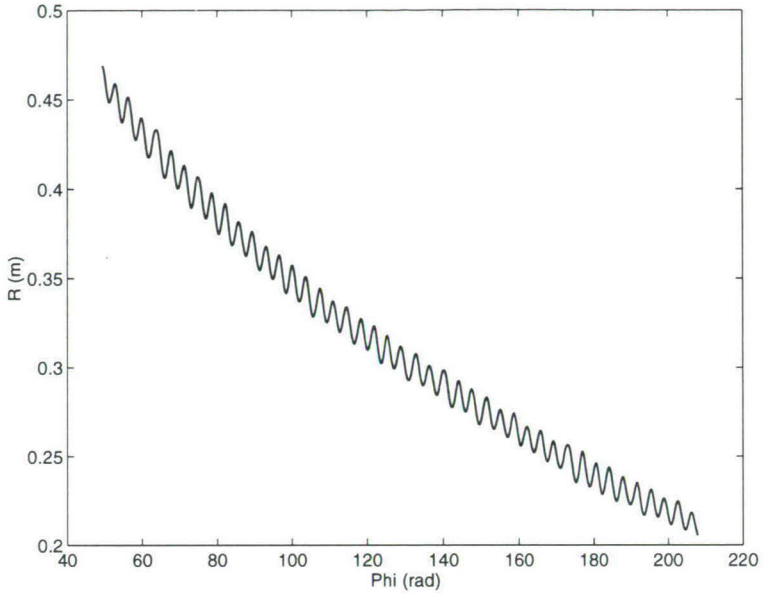

Figure 5.12: The smooth orbit T11B21.

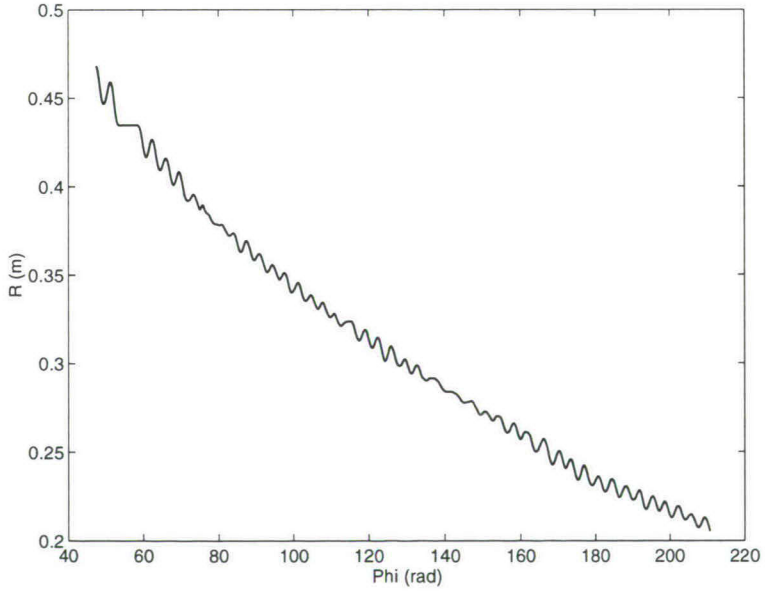

Figure 5.13: The trenched orbit T11B03.

that fits the experimental data. In order to grasp the main effects, we start off on a discussion of the deterministic model. The parameters in this model will be estimated from the experimental data. Since the estimates can differ from experiment to experiment, we consequently use the smooth orbit T11B21 (see figure 5.12) for the particular estimates, and the rest of the experiments to get a rough impression of the range. This deterministic model is described in section 5.2. The next step will be the extension of this model to a basic stochastic model for a general Golden-Ten setup without any peculiarities (see section 5.3). Finally, the model will be extended with some particular factors related to the special experimental setup in chapter 4. We will conclude this chapter with a first impression of the simulation results.

5.2 The deterministic model

The total motion consists of three basic stages, each one of which can be subdivided into one or more smaller stages. Each small stage is given an index, ranging from 0 to $n+1$. The same index is given to the starting time of a stage, as well as to the corresponding initial conditions. Index 0 thus indicates the stage where the ball rolls along the rim, after the launch, and stage 1 is the part where the ball leaves the rim, but still moves in a circular orbit. This stage is called the *first trench*, although it does not neccessarily have to be caused by the presence of surface grooves: it merely expresses the fact that the ball usually slips along the rim for some time, before it actually starts to descend.

When it comes out of the first trench, the ball rolls down on the surface until radius R reaches a local minimum. This is stage 2; the next stages where the ball moves between two local extrema are numbered from 3 to $n-1$. Some of these stages may represent trench motions. The penultimate stage - from the last extremum to the edge of the drum - is given index n, and the last stage - where the balls falls off of the edge into the number disc - has index $n+1$. The final conditions of the last stage are indicated with index $n+2$. Furthermore, we denote the duration of the i^{th} stage as

$$\tau_i = t_{i+1} - t_i,\ i \in \{0, 1, ..., n+1\}. \tag{5.1}$$

5.2.1 Rolling along the rim

While the ball is rolling along the rim, the radius R is constantly given by

$$R = R_0 = R_{rim} - a. \tag{5.2}$$

When the ball is launched from the slit plastic arm onto the surface, it will - at least for some time - slip along the rim. We assume that after a few revolutions along the rim the slipping has ended, and we start observing the game at the beginning of stage 0: when the ball passes the compartment lamella between the numbers 25 and 0 for the third time (see also figure 5.1). The observed initial conditions (of T11B21) are

$$\begin{array}{lll} t_0 = 0 & , & \dot{\psi}_0 = -46 \text{ (rad/sec)}, \\ R_0 = 0.4695 \text{ (m)} & , & \dot{R}_0 = 0, \\ \varphi_0 = 0 & , & \dot{\varphi}_0 = 1.877 \text{ (rad/sec)}. \end{array} \tag{5.3}$$

The initial angular velocity is not fixed; its value lies somewhere in the interval $(1.63, 2.14)$ rad/sec (see subsections 2.1.2 and 5.3.1).

During stage 0, on $[t_0, t_1)$, the motion of the ball is determined by the system

$$\begin{aligned} \ddot{R} &= \dot{R} = 0, \\ R\ddot{\varphi} &= -f_r R\dot{\varphi} + g_r \sin\beta \sin(\varphi - \varphi_\beta), \\ a\dot{\psi} &= -\tfrac{1-\sin\alpha}{\cos\alpha} R\dot{\varphi}, \end{aligned} \tag{5.4}$$

where f_r denotes a friction coefficient, g_r represents the contribution by gravity:

$$g_r = \tfrac{5\cos^2\alpha}{7\cos^2\alpha + 2(1-\sin\alpha)^2}\, g, \tag{5.5}$$

$a = 0.0175$ (m) (see table 2.1), and

$$\beta = 0.004, \ \varphi_\beta = 3.66 \text{ (rad)}, \tag{5.6}$$

conforming to the estimates in subsection 5.5.1. Note that β is extremely small. For f_r and g_r, the experimental data yield the estimates

$$\begin{aligned} f_r &= 0.0161 \pm 0.004 \text{ (sec}^{-1}\text{)}, \\ g_r &= 5.64 \pm 0.01 \text{ (m/sec}^2\text{)}. \end{aligned} \tag{5.7}$$

The first stage of the motion ends when the angular velocity reaches the theoretical value

$$\dot{\varphi}_1 = \sqrt{\tfrac{5g(\sin\alpha\cos\beta + \cos\alpha\sin\beta\cos(\varphi_1 - \varphi_\beta))}{7\cos\alpha - 2\tan\alpha(1-\sin\alpha)}} \Big/ \sqrt{R_1}, \tag{5.8}$$

(see equation system (3.25)), with

$$R_1 = R_0. \tag{5.9}$$

Use of this condition leads to the final values of stage 0:

$$\begin{array}{lll} t_1 = 31.42 \text{ (sec)} & , & \dot{\psi}_1 = -28 \text{ (rad/sec)}, \\ R_1 = 0.4695 \text{ (m)} & , & \dot{R}_1 = 0, \\ \varphi_1 = 46.31 \text{ (rad)} & , & \dot{\varphi}_1 = 1.128 \text{ (rad/sec)}. \end{array} \tag{5.10}$$

When the ball leaves the rim, it immediately gets stuck in the first trench. This is stage 1 of the motion, starting from the conditions in (5.10). On the analogy of system (5.4), taking $\beta = 0$, we pose the simplified model (on $[t_1, t_2)$)

$$\begin{aligned} R &= R_1, \\ \varphi &= \varphi_1 + \tfrac{1}{f_{t1}}\dot{\varphi}_1\{1 - e^{-f_{t1}(t-t_1)}\}, \\ \dot{\psi} &= \dot{\psi}_1 e^{-h_{t1}(t-t_1)}, \end{aligned} \tag{5.11}$$

where coefficients f_{t1} and h_{t1} are estimated as

$$\begin{aligned} f_{t1} &= 0.0115 \pm 0.002 \text{ (sec}^{-1}), \\ h_{t1} &= 0.3 \pm 0.2 \text{ (sec}^{-1}). \end{aligned} \tag{5.12}$$

The final conditions, obtained from the experimental data, are

$$\begin{array}{lll} t_2 = 34.32 \text{ (sec)} & , & \dot{\psi}_2 = -12 \text{ (rad/sec)}, \\ R_2 = 0.4695 \text{ (m)} & , & \dot{R}_2 = 0, \\ \varphi_2 = 49.50 \text{ (rad)} & , & \dot{\varphi}_2 = 1.093 \text{ (rad/sec)}. \end{array} \tag{5.13}$$

These values vary strongly, since they depend on the actual value of $\dot{\varphi}_0$ (cf. (5.3)). Due to possible variation, the final angle φ may range from 35 to 65 rad, and the final time from 25 to 40 sec. Furthermore, we have observed a strong influence, especially on final angular velocity $\dot{\varphi}_2$, of the actual size of trench time τ_1. The time range of $(0, 4)$ sec induces a typical range for $\dot{\varphi}_2$ of $(1.07, 1.13)$ rad/sec, see also subsection 5.3.1.

5.2.2 Rolling on the surface

After leaving the trench along the rim, the ball starts rolling on the surface. The equations of motion on $[t_2, t_{n+1})$ are, cf. (3.22) and (3.37)

$$\begin{aligned} \ddot{R}/\cos\alpha &= -\tfrac{5}{7}f_l\dot{R}/\cos\alpha + R\dot{\varphi}^2\cos\alpha + \tfrac{2}{7}a\dot{\varphi}\dot{\psi}\sin\alpha \\ &\quad -\tfrac{5}{7}g(\sin\alpha\cos\beta + \cos\alpha\sin\beta\cos(\varphi-\varphi_\beta)), \\ R\ddot{\varphi} &= -\tfrac{5}{7}f_l R\dot{\varphi} - 2\dot{R}\dot{\varphi} + \tfrac{5}{7}g\sin\beta\sin(\varphi-\varphi_\beta), \\ a\ddot{\psi} &= -ha\dot{\psi} - \dot{R}\dot{\varphi}\tan\alpha, \end{aligned} \tag{5.14}$$

where f_l represents an air friction coefficient, and h a spin friction coefficient. Anticipating on the stochastic model in subsection 5.3.2, we have redimensioned the equations in chapter 3, such that all factors in the system represent forces (setting aside the constant mass m). Note that the left-hand sides of $(5.14)^{1,2}$ represent forces acting along the surface, whereas that of $(5.14)^3$ is a perpendicular force. The coefficients in (5.14) are estimated from the experimental data as

$$\begin{aligned} f_l &= 0.0139 \pm 0.003 \ (\text{sec}^{-1}), \\ h &= 0.027 \pm 0.02 \ (\text{sec}^{-1}). \end{aligned} \tag{5.15}$$

Since we are considering a deterministic model, we assume that the ball does not get stuck into any more trenches. The final conditions of the part where the ball rolls on the surface can therefore be found by numerically solving equation system (5.14), in combination with the set of initial conditions (5.13). This yields

$$\begin{aligned} t_{n+1} &= 156.06 \ (\text{sec}) \quad , \quad \dot{\psi}_{n+1} = 0, \\ R_{n+1} &= 0.2050 \ (\text{m}) \quad , \quad \dot{R}_{n+1} = -0.0098 \ (\text{m/sec}), \\ \varphi_{n+1} &= 218.12 \ (\text{rad}) \quad , \quad \dot{\varphi}_{n+1} = 1.70 \ (\text{rad/sec}), \end{aligned} \tag{5.16}$$

and, according to figure 5.5,

$$n = 94. \tag{5.17}$$

Due to the large variation in the initial conditions (5.13), and also - albeit to a lesser extent - due to the variation of the coefficients in (5.7), (5.12) and (5.15), the final conditions in (5.16) may vary enormously. The experimental data show a typical range for n of $(65, 110)$, for t_{n+1} of $(120, 170)$ sec, and for φ_{n+1} of $(160, 240)$ rad.

5.2.3 Falling down into the number disc

The difference between the compartment number where the ball leaves the surface, and the game's final outcome, appears to vary from 1 to 3 (modulo 26). We can express the expected relation (operative on $[t_{n+1}, t_{n+2}]$) as

$$\varphi_{n+2} = \varphi_{n+1} + \tfrac{2}{13}\pi. \tag{5.18}$$

Finally, the relation between angles and compartment numbers is given by

$$N = [\tfrac{13}{\pi}\varphi \bmod 26]. \tag{5.19}$$

From the final angle in $(5.16)^3$, and the extra jump in equation (5.18), we find the outcome N_{n+2} of our deterministic model to be

$$N_{n+2} = 20. \tag{5.20}$$

However, due to the large variation of the angle in $(5.16)^3$, the strategy to always bet on this particular number is absurd. From the almost uniform distribution in figure 5.2, we conclude that a deterministic model is simply not appropriate. In the next section we present a better model.

5.3 The basic stochastic model

5.3.1 Rolling along the rim

The first stage of the motion (stage 0) starts off with a more or less arbitrary angular velocity $\dot{\varphi}_0$, and ends when $\dot{\varphi}$ reaches the theoretical value $\dot{\varphi}_1$ in (5.8). During this stage, on $[t_0, t_1)$, the ball moves according to system (5.4). Under the assumption that $\beta = 0$, the explicit solution for the angular velocity on $[t_0, t_1)$ is

$$\dot{\varphi} = \dot{\varphi}_0 e^{-f_r(t-t_0)}. \tag{5.21}$$

According to the rules of the game (see subsection 2.1.2), the ball should complete five to ten rounds before it leaves the rim. This implies

$$\dot{\varphi}_0 \in (\dot{\varphi}_1 + 10\pi f_r, \dot{\varphi}_1 + 20\pi f_r) = (\dot{\varphi}_1 + 0.506, \dot{\varphi}_1 + 1.012) \text{ (rad/sec)}, \tag{5.22}$$

according to $(5.7)^1$. At time t_1 we have $\dot{\varphi}_1 = 1.127$ (rad/sec) (computed from (5.8) with $\beta = 0$), wherefore we can take

$$\dot{\varphi}_0 \sim U(1.63, 2.14) \text{ (rad/sec)}. \tag{5.23}$$

t	.	.	.	.	-1.476
$P(\eta \leq t)$	.	.	.	.	0.000
t	-1.350	-1.050	-0.750	-0.450	-0.150
$P(\eta \leq t)$	0.017	0.054	0.131	0.330	0.576
t	0.150	0.450	0.750	1.050	1.350
$P(\eta \leq t)$	0.713	0.840	0.913	0.955	0.978
t	1.650	1.950	2.250	2.550	2.850
$P(\eta \leq t)$	0.990	0.994	0.998	0.999	1.000

Table 5.1: Cumulative distribution of corrected trench times η.

In other words: with the initial anglar velocity $\dot{\varphi}_0$ randomly taken from the interval $(1.63, 2.14)$ rad/sec, the final velocity $\dot{\varphi}_1 = 1.127$ (rad/sec) will be reached somewhere (i.e. randomly) in between five to ten rounds.

The actual value of $\dot{\varphi}_0$ in (5.23) and the final value $\dot{\varphi}_1$ in (5.8) determine stage 0. The final conditions of stage 0 in turn are the initial conditions of stage 1. For the duration τ_1 of this stage, in the first trench (from t_1 to t_2), we pose

$$\tau_1 = 1.476 + \eta_1 \text{ (sec)}, \tag{5.24}$$

where η_1 follows the distribution $\mathcal{L}(\eta)$ in table 5.1. We call η_1 the *corrected trench time*, since the total trench time is τ_1. The distribution in table 5.1 is also suited for corrected times of other than the first trench motion (see subsection 5.4.1). The making of this table is described in subsection 5.5.5.

5.3.2 Rolling on the surface

The motion of the ball on the surface is influenced by a conglomerate of small, random forces and momentums. This can be modelled by transforming the equations of motion (5.14) on $[t_2, t_{n+1})$ into the system of

stochastic differential equations

$$\begin{aligned}
\ddot{R}/\cos\alpha &= -\tfrac{5}{7}f_l\dot{R}/\cos\alpha + R\dot{\varphi}^2\cos\alpha + \tfrac{2}{7}a\dot{\varphi}\dot{\psi}\sin\alpha \\
&\quad -\tfrac{5}{7}g(\cos\alpha\sin\beta\cos(\varphi-\varphi_\beta)+\sin\alpha\cos\beta)+\sigma_1\varepsilon_1, \\
R\ddot{\varphi} &= -\tfrac{5}{7}f_l R\dot{\varphi} - 2\dot{R}\dot{\varphi} + \tfrac{5}{7}g\sin\beta\sin(\varphi-\varphi_\beta)+\sigma_2\varepsilon_2, \\
a\ddot{\psi} &= -ha\dot{\psi} - \dot{R}\dot{\varphi}\tan\alpha + \sigma_3\varepsilon_3,
\end{aligned} \tag{5.25}$$

where the integrated $\varepsilon_i = \varepsilon_i(t)$ represent three independent processes of standard Brownian motion (see e.g. Schuss [22]). The estimated standard deviations are

$$\begin{aligned}
\sigma_1 &= 4.0\times10^{-3}\ (m/sec^2), \\
\sigma_2 &= 2.9\times10^{-3}\ (m/sec^2), \\
\sigma_3 &= 0,
\end{aligned} \tag{5.26}$$

see subsection 5.5.4. As was noted before in subsection 5.2.2, the equations of motion have been redimensioned such that they all represent forces (setting aside mass m). Hence, the random factors in $(5.37)^{1,2}$ can be considered as forces acting along the surface.

The motion on the surface ends when the ball falls down into the number disc, i.e. when

$$R_{n+1} = R_{num} = 0.2050\ (\mathrm{m}), \tag{5.27}$$

(see table 2.1: $R_{num} = 410/2 = 205$ (mm)). This determines the final conditions for this stage of the motion, which are the initial conditions for the next, and final one.

5.3.3 Falling down into the number disc

The ball falls down from the surface into the disc at angle φ_{n+1}. Let γ denote the fractional compartment position at the time of the fall:

$$\gamma = \tfrac{13}{\pi}\varphi_{n+1} - [\tfrac{13}{\pi}\varphi_{n+1}], \tag{5.28}$$

Furthermore, let ν represent the jump from the edge of the drum into the final compartment, or

$$\nu = (N_{n+2} - N_{n+1}) \mod 26, \tag{5.29}$$

and let ν^* represent the (unobserved) underlying continuous variable, which can be thought of as representing the continuous difference in compartment numbers, without the constraint that the motion has to stop exactly in the middle of some compartment. The values of ν are roughly the rounded values of ν^*, or - more precisely -

$$\nu = \begin{cases} 1 & & & \nu^* & < & 1\frac{1}{2} \\ 2 & \text{if} & 1\frac{1}{2} & \leq \nu^* & < & 2\frac{1}{2} \\ 3 & & 2\frac{1}{2} & \leq \nu^* & & \end{cases} . \tag{5.30}$$

For ν^*, we estimated the relation

$$\nu^* = -9.279 + 31.63 R_{n+1}\dot{\varphi}_{n+1} + 1.198\gamma + \sigma^* Z, \tag{5.31}$$

where

$$\sigma^* = 0.2938, \tag{5.32}$$

and Z follows the standard normal distribution $N(0,1)$. For more details, consult subsection 5.5.6.

5.4 The complete stochastic model

5.4.1 Rolling through a trench

The motion of the ball along the rim is modelled in the same manner as in subsection 5.3.1. This also holds for the downfall into the number disc, see subsection 5.3.3. However, the motion on the surface is different, since the ball will - from time to time - get stuck in a *local trench.* This can happen only when the ball momentarily moves in a circular orbit or - equivalently - when radius R has a local extremum. Because of different local characteristics of the surface, the probability P_t that stage i will become a trench motion (as in figure 5.14) depends on the momentary position (R_i, φ_i), as well as on the nature of the extremum (i.e. $sgn(R_i - R_{i-1})$). Since the characteristics of the observation ring and the limit ring are different from those of the rest of the surface, we composed four probability tables: two for local maxima of R - i.e. one for the rings (table 5.3) and one for the rest of the surface (table 5.2) - and, likewise, two for local minima (tables 5.5 and 5.4). These tables give the conditional probabilities

$$P_t = P(R_{i+1} = R_i | R_i, \varphi_i, sgn(R_i - R_{i-1})), \tag{5.33}$$

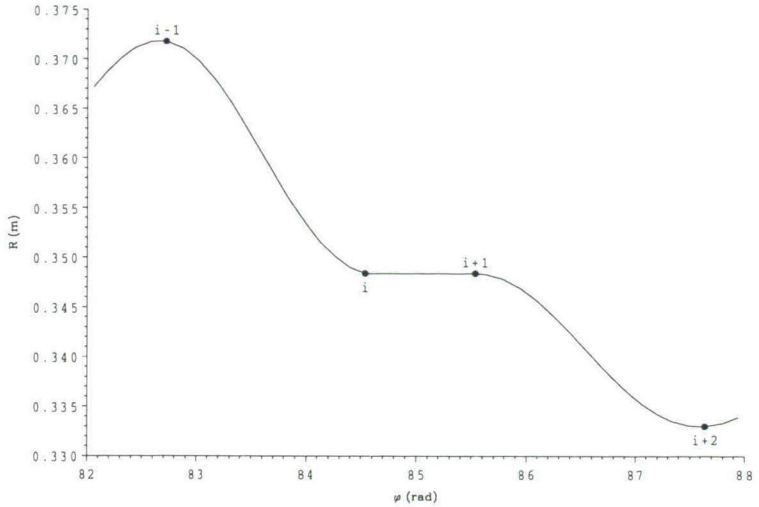

Figure 5.14: Example of a trench motion during stage i.

for those indices $i \in \{3, 4, ..., n-1\}$ with $sgn(R_i - R_{i-1}) \neq 0$. Note that these probabilities are given per segment, where the rings are divided into 56 segments each, and the rest of the surface is divided into 4×56 segments.

Let K denote the subset of indices that represent a trench, and let $k \in K$. Then the motion during stage k for general k closely resembles that through the first trench (along the rim), which is in fact the stage with $k = 1$. On the analogy of system (5.11) we pose on $[t_k, t_{k+1})$

$$\begin{aligned} R &= R_k, \\ \varphi &= \varphi_k + \tfrac{1}{f_t}\dot{\varphi}_k\{1 - e^{-f_t(t-t_k)}\}, \\ \dot{\psi} &= \dot{\psi}_k e^{-h_t(t-t_k)}, \end{aligned} \tag{5.34}$$

where

$$\begin{aligned} f_t &= 0.0113 + 0.0017 sgn(R_k - R_{k-1}) \ (\text{sec}^{-1}) \\ h_t &= 0 \end{aligned} \quad , \ k > 1. \tag{5.35}$$

More information on these estimates is given in the middle part of subsection 5.5.5. For the duration of stage k, with $k > 1$, we take

$$\tau_k = 0.4301 + 1.699 R_k \dot{\varphi}_k - 0.3149 \, sgn(R_k - R_{k-1}) + \eta_k, \tag{5.36}$$

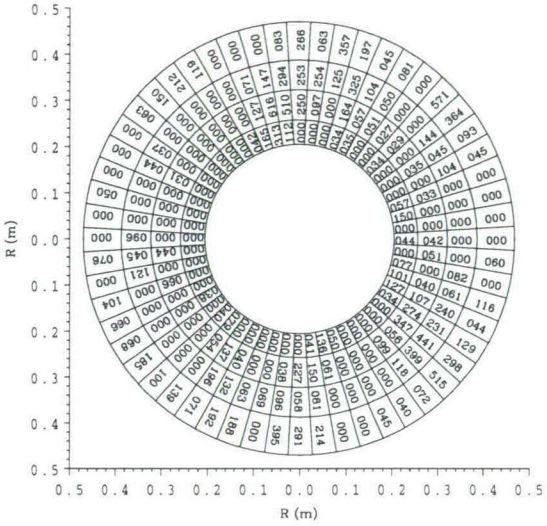

Table 5.2: Trench probabilities $P_t \times 1000$ for local maxima outside the rings.

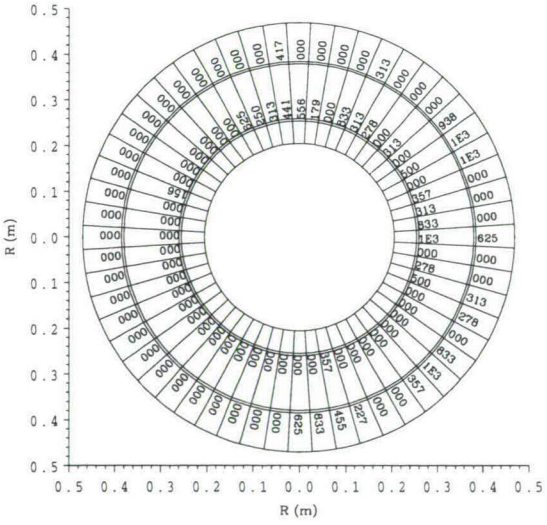

Table 5.3: Trench probabilities $P_t \times 1000$ for local maxima inside the rings.

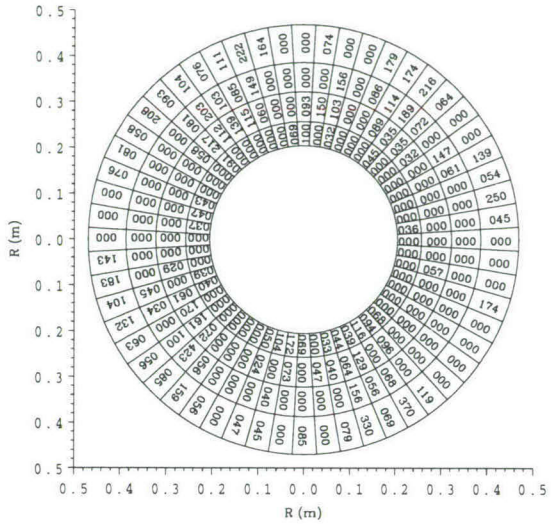

Table 5.4: Trench probabilities $P_t \times 1000$ for local minima outside the rings.

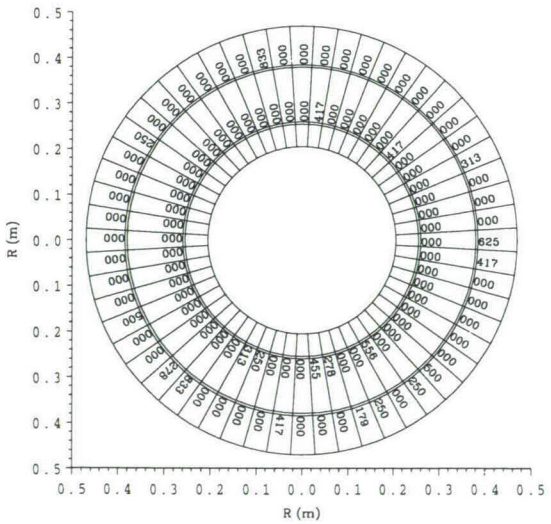

Table 5.5: Trench probabilities $P_t \times 1000$ for local minima inside the rings.

where η_k follows the distribution $\mathcal{L}(\eta)$ in table 5.1. More explanation is given in the last part of subsection 5.5.5.

5.4.2 Rolling freely on the surface

All further extensions to the basic model in section 5.3 concern the stages where the ball moves on the surface, without rolling through a trench. Let ℓ, with $\ell \notin K$, represent such a stage. The system of stochastic differential equations on $[t_\ell, t_{\ell+1})$ now generalizes from (5.25) to

$$\begin{aligned} \ddot{R}/\cos\alpha &= -\tfrac{5}{7}\mathcal{F}(R)\dot{R}/\cos\alpha + R\dot{\varphi}^2\cos\alpha + \tfrac{2}{7}a\dot{\varphi}\dot{\psi}\sin\alpha \\ &\quad -\tfrac{5}{7}g(\cos\alpha\sin\beta\cos(\varphi-\varphi_\beta)+\sin\alpha\cos\beta) + \sigma_1\varepsilon_1, \\ R\ddot{\varphi} &= -\tfrac{5}{7}\mathcal{F}(R)R\dot{\varphi} - 2\dot{R}\dot{\varphi} + \tfrac{5}{7}g\sin\beta\sin(\varphi-\varphi_\beta) + \sigma_2\varepsilon_2, \\ a\ddot{\psi} &= -ha\dot{\psi} + wR\dot{\varphi} - \dot{R}\dot{\varphi}\tan\alpha + \sigma_3\varepsilon_3. \end{aligned} \tag{5.37}$$

Here friction coefficient f_l has been made R-dependent according to

$$\mathcal{F}(R) = 0.1506\ R^2 - 0.09886\ R + 0.03091\ (\text{sec}^{-1}), \tag{5.38}$$

(see subsection 5.5.2), and a winding term with coefficient w has been added. The value of w has been estimated as

$$w = 0.0095\ \pm 0.0008\ (\text{sec}^{-1}). \tag{5.39}$$

The winding term $wR\dot{\varphi}$ in (5.37)[3] accounts for the curious behaviour of the spin in figure 5.11. The nature of this term is explained in subsection 5.5.3.

5.5 Estimation of the model parameters

Considering the deterministic system in (5.14), we note that only three of the parameters - viz. gravity coefficient g, angle α and radius a - are measured directly, i.e. independently of the actual motion. Whereas subsection 3.3.1 presented a way to estimate air friction coefficient f_l from the data in chapter 4, it simply posed that spin friction coefficient h is equal to zero. This assumption turns out to be unrealistic, since

complementary experiments with a Golden-Ten ball on a metal surface show us that

$$h = O(0.1) \ (\text{sec}^{-1}). \tag{5.40}$$

However, estimation of h from the experimental data in chapter 4 is complicated by the fact that observations of the spin itself are not available.

The residuals from the estimation procedure for coefficient f_l in subsection 3.3.1 contain two clearly systematic components, both of which are periodic (see figure 3.11). The component with an approximate period of six seconds - or approximately 2π radians (according to the estimated angular velocity $\dot{\varphi}_2$ in (5.13) - points to a slightly tilted position of the drum. This indicates that β and φ_β are not equal to zero, as was assumed in subsection 3.3.1 (note that subsection 4.1.2 reported $\beta \leq 5 \times 10^{-4}$ (rad)). The component with an approximate period of ninety seconds points to a non-linear physical friction model. This complicates the estimation procedure to such an extent that standard statistical methods - such as Least Squares or Maximum Likelihood - are rendered useless. We will therefore resort to more heuristic procedures, and examine the components of the motion one at a time.

As part of our heuristic procedures we will make frequent use of smoothing splines (cf. De Boor [6]) to determine the first and second order time derivatives of both radius R and angle φ. The smoothing parameter p is taken close to one, in order to prevent loss of information, but not too close to one, since the data in chapter 4 include relatively large measurement errors. For orbits with a sampling frequency of 1 per 0.08 sec, like T11B21, we take the more or less arbitrary value $p = 0.992$. The appropriateness of this value is corroborated by the results, see e.g. figure 5.10, which shows the time derivative of φ.

5.5.1 The drum position

By differentiating the smoothing splines for R and φ twice, we obtain estimates for the second order time derivatives $\ddot{R}$ and $\ddot{\varphi}$. By substituting these into equation $(5.14)^2$, together with the estimated value for f_l in $(5.15)^1$ (see also subsection 3.3.1) and the preliminary estimate $\beta = 0$, we compute the residuals

$$e_2 = R\ddot{\varphi} + \tfrac{5}{7} f R\dot{\varphi} + 2\dot{R}\dot{\varphi}. \tag{5.41}$$

This enables us to check the assumption of a horizontal drum position in the following manner.

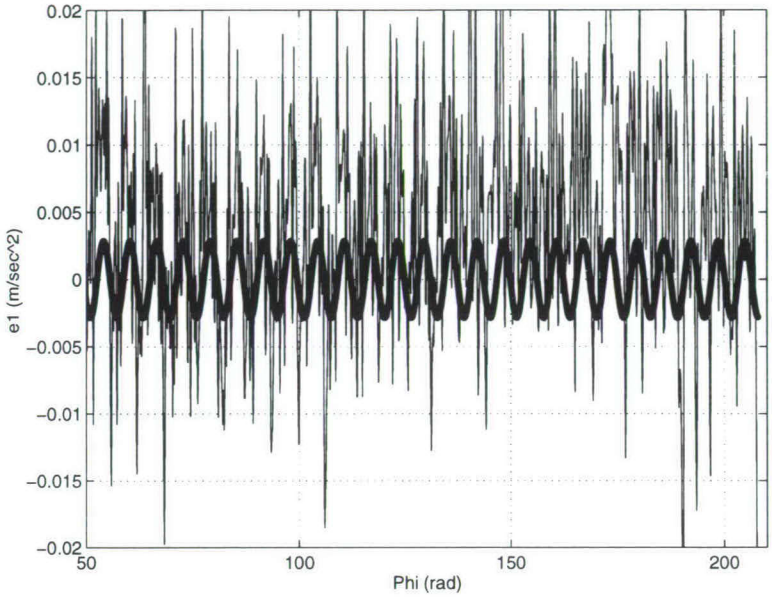

Figure 5.15: Residuals from the first equation of motion.

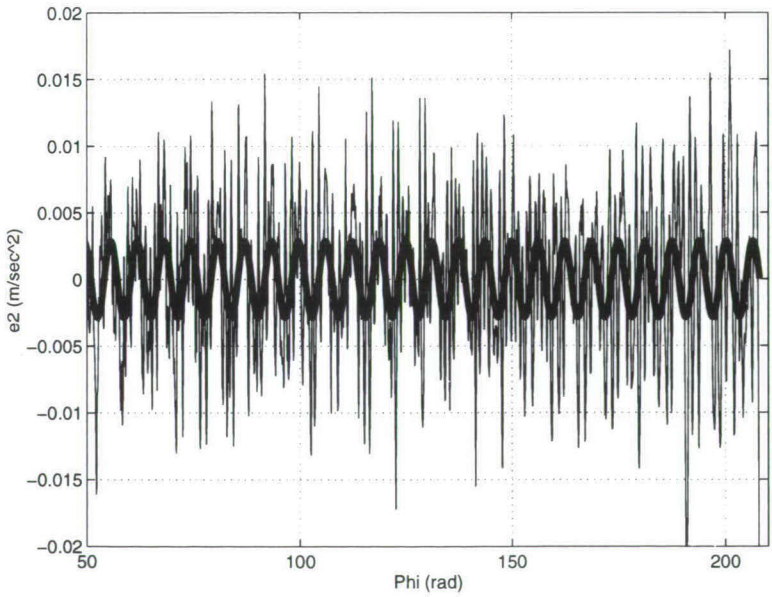

Figure 5.16: Residuals from the second equation of motion.

The residuals for experiment T11B21 have been plotted as the thin line in figure 5.16, where the thick line represents the term $\frac{5}{7}g\sin\beta\sin(\varphi-\varphi_\beta)$, with

$$\beta = 0.000409 \text{ (rad)}, \quad \varphi_\beta = 3.6633 \text{ (rad)}. \tag{5.42}$$

These estimated values for β and φ_β are the mean values from a standard nonlinear LS- regression procedure, applied to each of the 338 available orbits. Before we can apply the same method to equation $(5.14)^1$, we need a preliminary estimate of the spin. A rough estimate can be obtained by determining the outcome of a Runge-Kutta routine with f_l according to $(5.15)^1$, h equal to 0.1 sec^{-1}, and the theoretical initial conditions from (3.35) in section 3.1. This procedure yields the residuals

$$e_1 = \ddot{R}/\cos\alpha + \tfrac{5}{7}f\dot{R}/\cos\alpha - R\dot{\varphi}^2\cos\alpha - \tfrac{2}{7}a\dot{\varphi}\dot{\psi}\sin\alpha + \tfrac{5}{7}g\sin\alpha. \tag{5.43}$$

Figure 5.15 contains a graph of e_1, and one of $-\frac{5}{7}g(\cos\alpha\sin\beta\cos(\varphi-\varphi_\beta)-\sin\alpha(1-\cos\beta))$, thereby showing the same tilted position as in figure 5.16. Apart from that, figure 5.15 also shows that the preliminary spin estimate performs very poorly. We will return to this subject in subsection 5.5.3.

5.5.2 The air friction coefficient

Now that the values of β and φ_β have been estimated, we can try to determine the value of friction coefficient f_l more accurately than in $(5.15)^1$. From the spline data, we obtain one estimate for f_l for every point of time in an orbit (like T11B21). The results are represented by the stars in figure 5.17. Since the graph shows a certain curvature, we are inclined to estimate f_l as a function of R. The curvature can be explained from the experimental setup in section 4.1: the ring of light bulbs around the drum and the black flanel tent above it caused a strong flow of air, especially near the edges of the drum. As a consequence, the resistance due to air friction is larger when the ball is near the rim or near the number disc, than anywhere in between. A polynomial LS-fit yields the estimated function in (5.38).

The last term in (5.38) acts as a scale factor, which can vary from experiment to experiment. Re-estimation for other orbits than T11B21 indeed shows that this term, or level, is variable. The variation is not only due to possible small estimation errors, but also to relatively large differences in friction levels. We will return to this subject in section 6.3. Finally note that, according to the explanation in the previous paragraph,

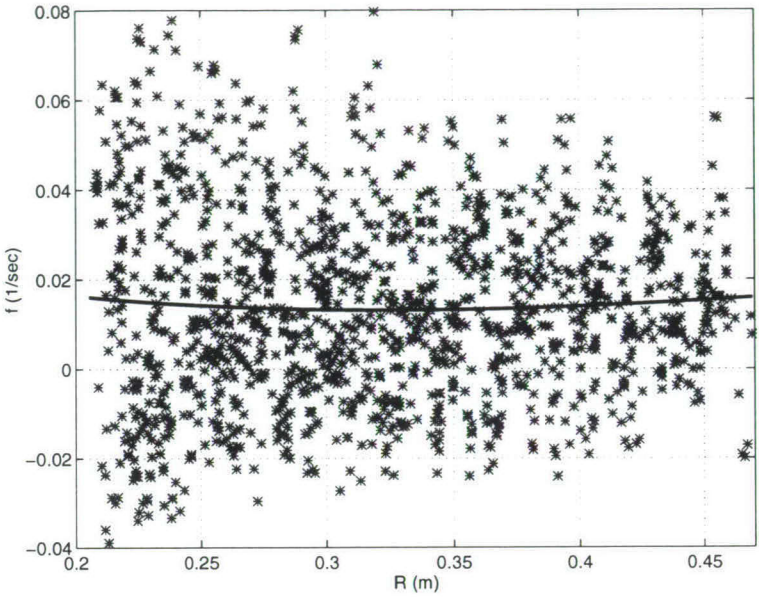

Figure 5.17: Local differences in friction.

friction coefficient f_r (for the motion along the rim) is constant, per orbit. This constant is estimated by means of an LS-procedure, applied to equation $(5.4)^2$. The result is given in $(5.7)^1$.

5.5.3 The spin

By substituting friction function f from (5.38) and oblique position (β, φ_β) from (5.42) into equation $(5.14)^1$, we obtain a rough estimate of the unobserved spin $\dot{\psi}$. This estimate is presented as the thin line graph in figure 5.18. Apart from a relatively large variation, we observe a spin which rapidly drops to zero, ensued by a clearly visible sign flip. This phenomenon can be accounted for by posing that the ball, while moving down the drum, experiences a winding momentum caused by the surface grooves. This extra momentum can be represented as

$$M_w = wI/(aR\dot{\varphi}), \tag{5.44}$$

where I is the central moment of inertia, and w is a winding coefficient of the same dimension as spin friction coefficient h in $(5.14)^3$. Note that

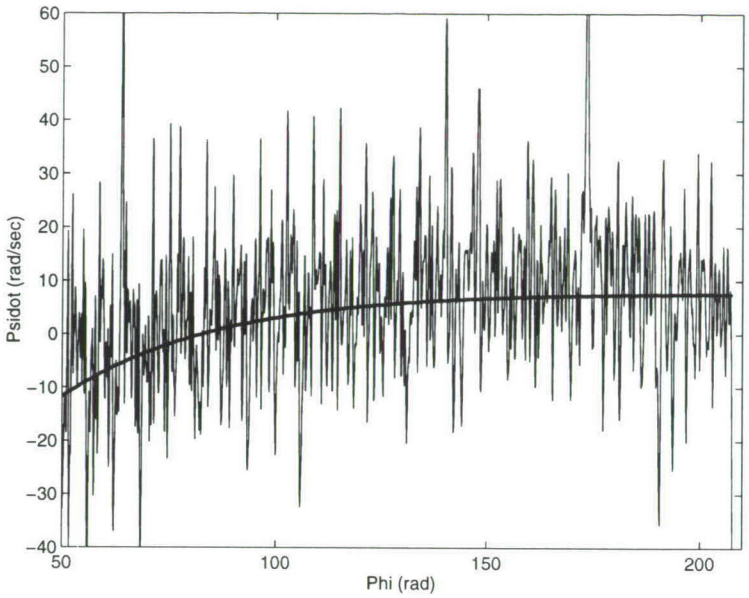

Figure 5.18: Global course of the spin.

the sign of w should in fact be opposite to that of the radial velocity $\dot{R}$, but since $\dot{R}$ is predominantly negative - and also for reasons of simplicity - we choose w to have a constant, positive value.

Winding coefficient w can be estimated by determining a smoothing spline for the estimated spin data, and by employing an LS-procedure, based on equation $(5.37)^3$. This procedure yields simultaneous estimates for h and w, according to $(5.15)^2$ and (5.39), respectively. This smoothing spline provides us also with an estimate for the initial spin, see $(5.13)^2$. The thick solid graph in figure 5.18 represents the numerically calculated spin with the above-mentioned estimates, substituted into the deterministic version of (5.37). On cursory inspection, the fit appears to be very reasonable.

5.5.4 Random forces

With the parameters estimated above, and the deterministic version of the stochastic model in (5.37), we can generate an orbit that closely resembles standard orbit T11B21. See figure 5.19, where the thin line graph

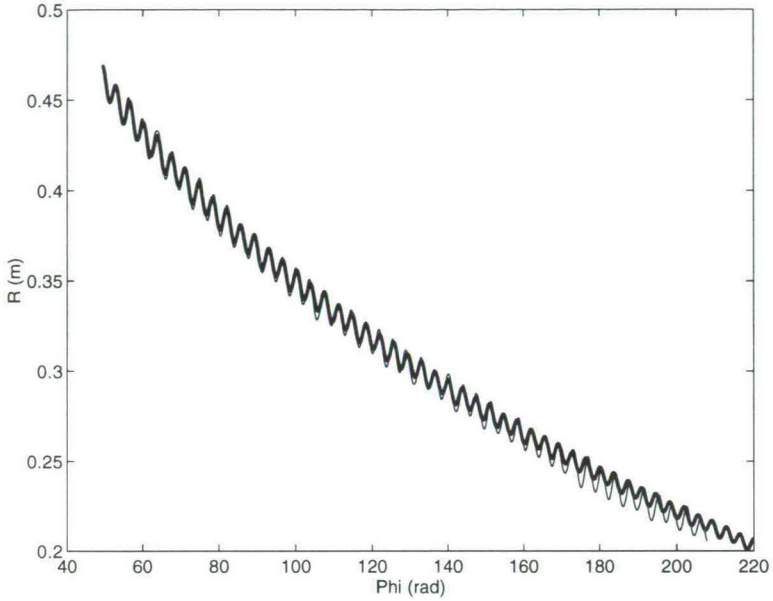

Figure 5.19: Deterministic orbit (based on the complete model), compared to experiment T11B21. The thick line represents the deterministic orbit.

represents the particular experiment, and the thick line graph represents the outcome of an RK-routine. However, the two orbits are not exactly equal. The difference can be thought of as caused by a conglomerate of small, random forces and momentums, and can be modelled as a standard Brownian motion, in accordance with (5.25) and (5.37).

Although the elusive variables ε_i themselves cannot be observed directly, we can estimate the outcomes of the Brownian motion for $i = 1, 2$ by using the smoothing splines. Observations for $i = 3$ are not available, since we have added the corresponding disturbances to ε_1. Direct LS-estimation of σ_1 and σ_2 from all 338 orbits yields values exactly twice the size of those in (5.26). Because of the relatively large measurement errors in chapter 4, which are in fact of the same order of magnitude, and the independence of the two kinds of error terms, we simply divide the estimates by two. This decision may seem to be arbitrary, but it is in fact corroborated by the simulation results, see e.g. figures 5.20-5.23. Note that a larger (or smaller) value for σ_1 would have resulted in crookeder

(or less crooked) orbits, and that a larger (or smaller) value for σ_2 would have generated larger (or smaller) amplitudes.

5.5.5 Trenches

The random forces from subsection 5.5.4 are not the only stochastic components of the motion, since the events of getting stuck into a trench and getting out of it are also stochastic. The observed relative frequencies of these events immediately provide the estimates of P_t in tables 5.2 to 5.5. The partitioning into segments has been arranged in such a way as to yield a more or less balanced number of observations per segment.

The nature of the motion through a trench is slightly different for local minima, local maxima, and for the trench along the rim. Along the rim we have a different nature of friction force, which is characterized by coefficients f_{t1} and h_{t1} in (5.12), as opposed to f_t and h_t in (5.35). The friction coefficients f_{t1} and f_t can be estimated by employing a simple LS-procedure based on equations $(5.11)^2$ and $(5.34)^2$. Coefficient h_{t1} can be estimated by substituting the observed values of $\dot{\psi}_1$ and $\dot{\psi}_2$ into $(5.11)^3$. For coefficient h_t, all we can say is that it is small and of minor importance, wherefore we simply take $h_t = 0$, according to $(5.35)^2$. Note that for local minima on the surface (away from the rim), the friction coefficient is apparently lower than for local maxima, which is probably due to the way in which the surface grooves are cut on the milling-machine.

For the trench times τ_k, for all $k \geq 1$, we pose an explicit positive dependency on velocity $R_k\dot{\varphi}_k$. For $k = 1$, this velocity is almost constant for all 338 orbits, so we simply estimate τ_1 with the observed mean value. For $k > 1$, we use a standard LS-procedure. The distribution of the error terms (i.e. corrected trench times, see subsection 5.3.1) appears to be the same for both cases, which supports the correctness of our assumptions. Although the distribution somewhat resembles a χ^2-distribution, we do not have to try to find a fit, since we have no cause to believe that it really is a χ^2-distribution (or a normal distribution, for that matter). The estimation results are given in equations (5.24) and (5.36), and table 5.1. Note that the trench times in local minima are usually longer than in local maxima. This is due to the fact that the magnitude of the upward, centrifugal force in a minimum is lower than that of the downward, centripetal force in a maximum.

5.5.6 The downfall

While falling down from the surface towards the number disc, the ball may keep rolling along the edge of the drum for some time, or not. Furthermore, before actually coming down in the final compartment, it may bounce on one or more partition lamellae. This means that the last part of the motion is rather capricious, wherefore we consider it to be - at least partially - stochastic.

From the experimental data we find that the difference between the compartment number where the ball leaves the surface and the number corresponding to the final outcome, ranges from 1 to 3. Although the nature of this difference is stochastic, it is obvious that it must also - at least to some extent - depend on velocity $R\dot{\varphi}$, as well as on fractional compartment position γ, as in (5.28). Since the exact physical characteristics of the fall are unknown, we estimate the difference in compartment numbers according to an ordered probit model (see e.g. Amemiya [2]), with threshold values $1\frac{1}{2}$ and $2\frac{1}{2}$. The result is given in (5.31) and (5.32).

5.6 Simulation results

Section 5.4 describes a complete stochastic simulation model, based on the mechanical, deterministic model in chapter 3, and fitting to the experimental data in chapter 4. This model is complete in the sense that it deals with a wide variability in environmental conditions, such as a tilted drum, a grooved drum surface, and a varying air friction coefficient. Examples of simulated orbits are given in figures 5.20- 5.23. The simulaton program is written in the MATLAB programming language (see The Mathworks [18]), and listed in appendix D.2.

When the game is played under ideal circumstances, i.e. without any of the above-mentioned oddities, we can stick to the basic stochastic model in section 5.3 (the listing is given in appendix D.1). In chapter 6 we will use this basic model to derive optimal prediction strategies and calculate expected gains. The complete model then serves as an indicator for the success of these strategies under less ideal circumstances. Since both models are very flexible, we can easily adjust the required parameters to fit virtually any Golden-Ten game site conceivable.

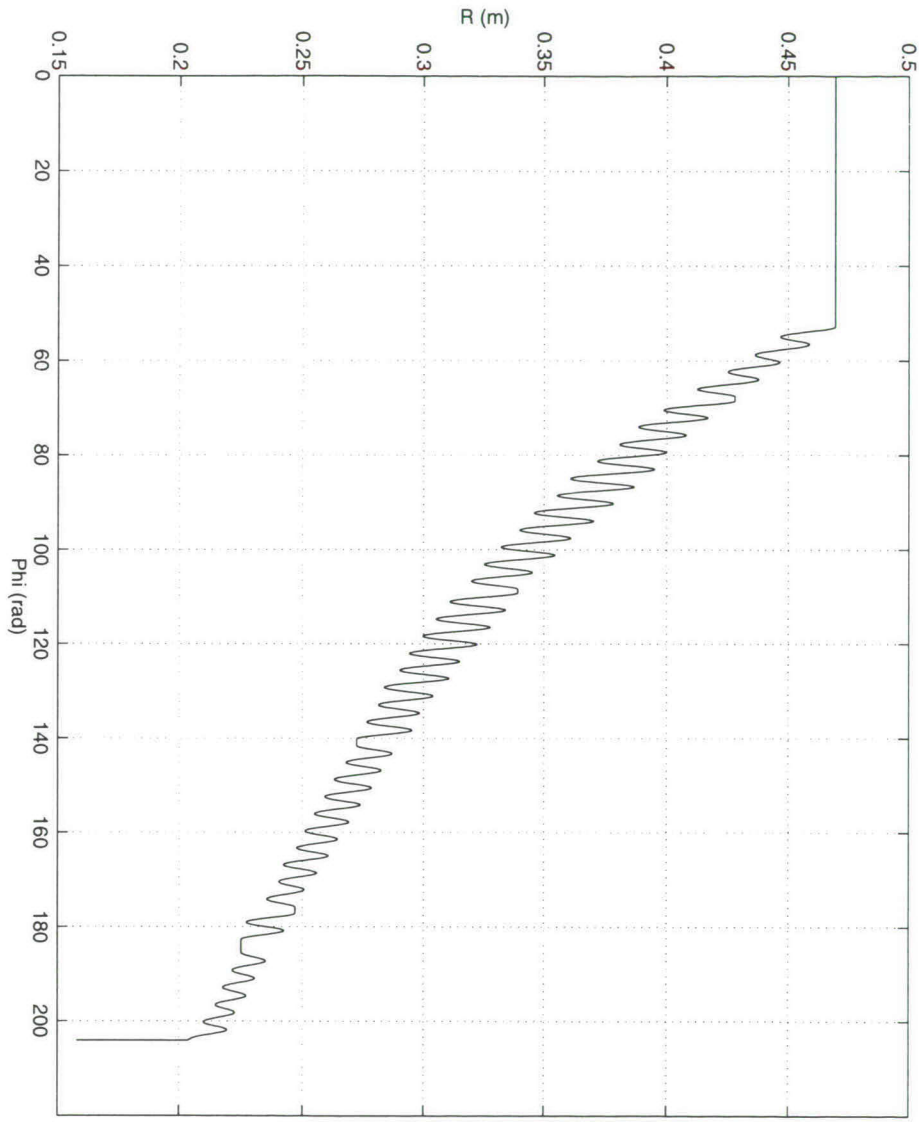

Figure 5.20: First graph of simulated orbit COMP8246 (generated by simulation of the complete model).

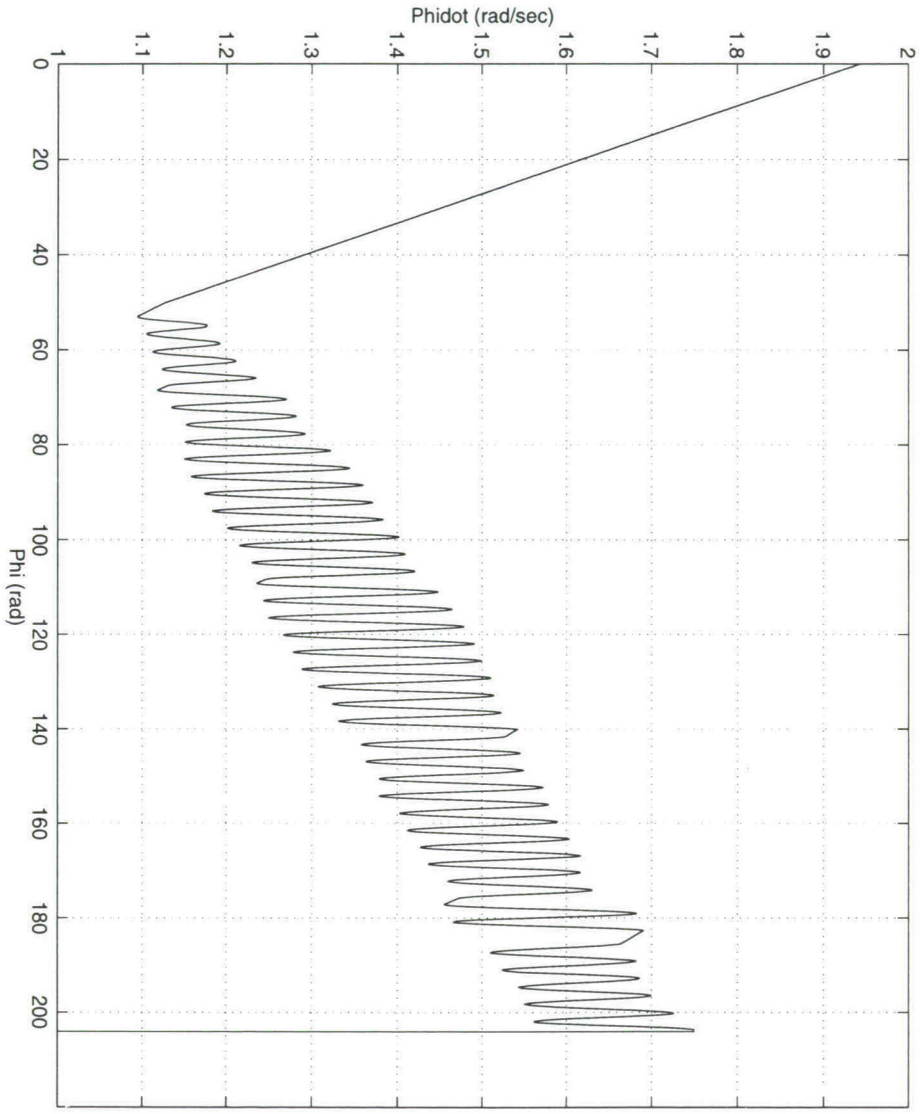

Figure 5.21: Second graph of simulated orbit COMP8246 (generated by simulation of the complete model).

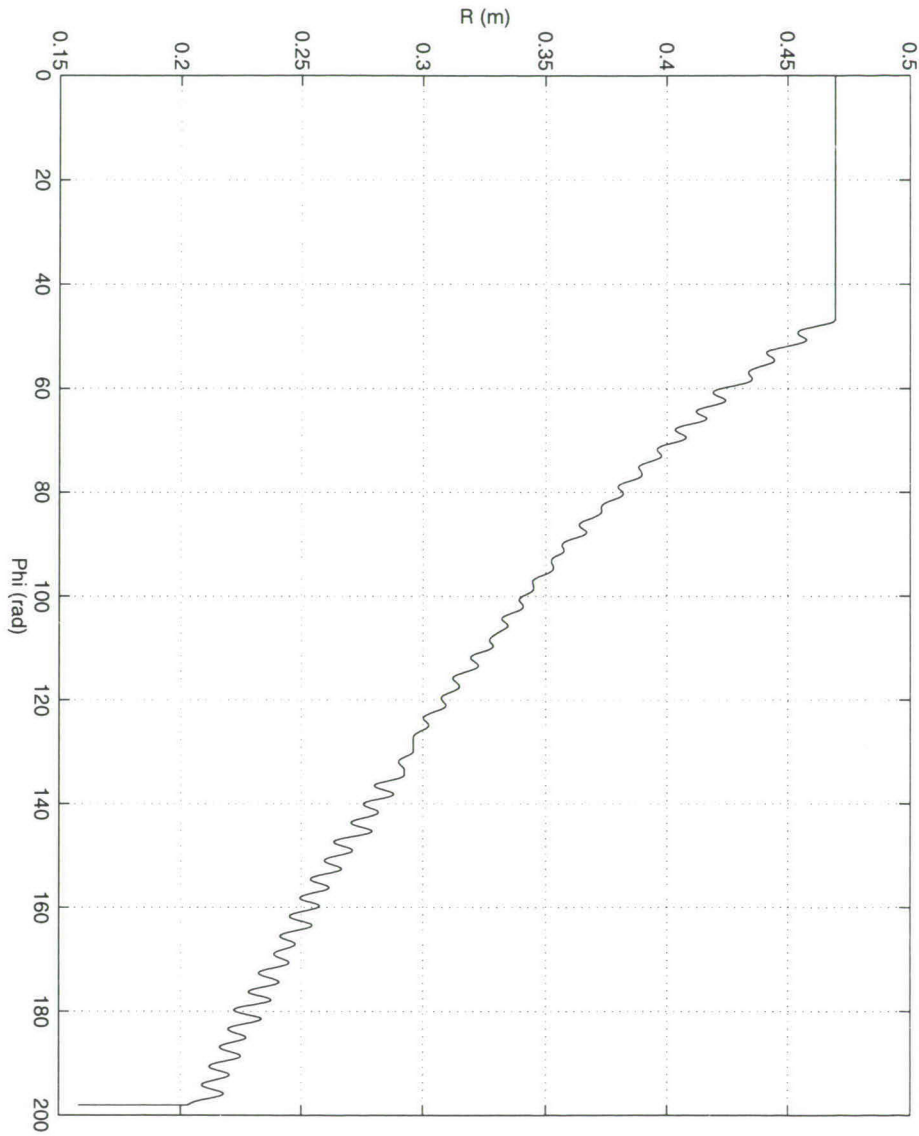

Figure 5.22: First graph of simulated orbit COMP8248.

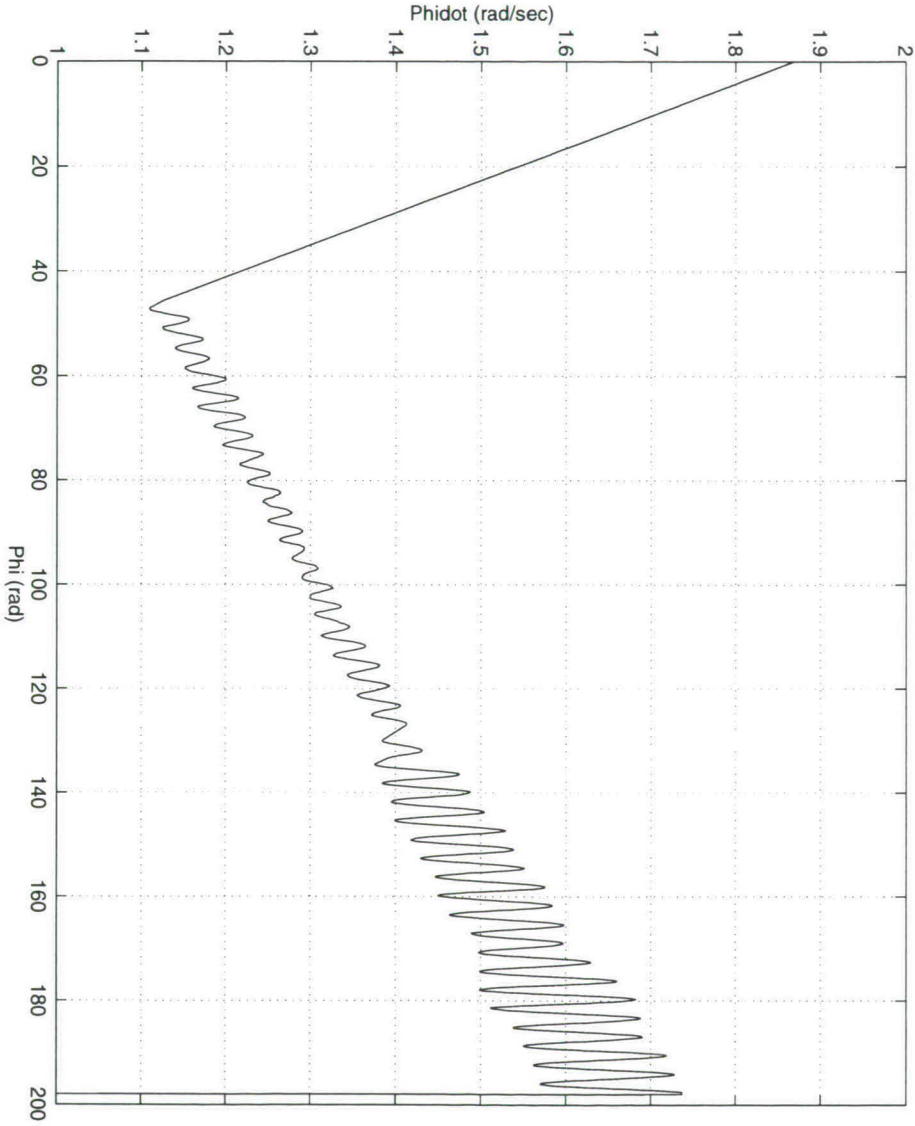

Figure 5.23: Second graph of simulated orbit COMP8248.

Chapter 6

Estimation and prediction

6.1 Practical strategies

As a result of 10,000 simulations of our complete model (described in section 5.4), it becomes immediately clear that a prediction strategy purely based on the angular position of the point where the ball leaves the rim makes no sense. Figure 6.1 depicts the distribution of the final outcome (modulo 26), relative to the compartment number where the bal left the rim; it shows that there is simply no clear relationship between these two numbers. On the other hand, figure 6.2 reveals that a prediction strategy purely based on the compartment number corresponding to the intersection point with the limit ring, can lead to a fairly large gain: by putting a bet on the compartment that lies 5 numbers further than that of the intersection point, the standard payment rule (see subsection 2.1.2) yields an expected gain of approximately $0.06 \times 24 - 1 = 0.44$. This positive result roughly agrees with conclusions from Albers [1], Boer [3], Embrechts et al. [13], Gill & Oudshoorn [14], LaFors & Derksen [16] and Wagenaar & Groeneweg [33]. Furthermore, figure 6.2 demonstrates that the distribution of the relative outcome is bimodal, with a difference of 14 numbers. This is not in accordance with the behaviour of most players, who usually bet on a difference of 13 numbers, see e.g. Delbaen & Haezendonck [7], NSC [19] and Van der Genugten & Borm [26]. We will return to this subject in sections 6.4 and 6.6.

In order to feed all available information into some prediction strategy, one should observe the trajectories as accurately and as long as possible. Since bets can be put until the ball intersects the inner edge of the limit ring (according to the rules of the game, see subsection 2.1.2),

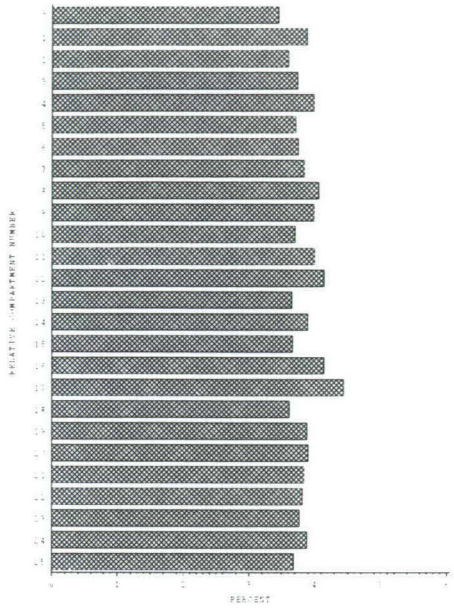

Figure 6.1: From rim to number disc, modulo 26 (complete model, low friction level).

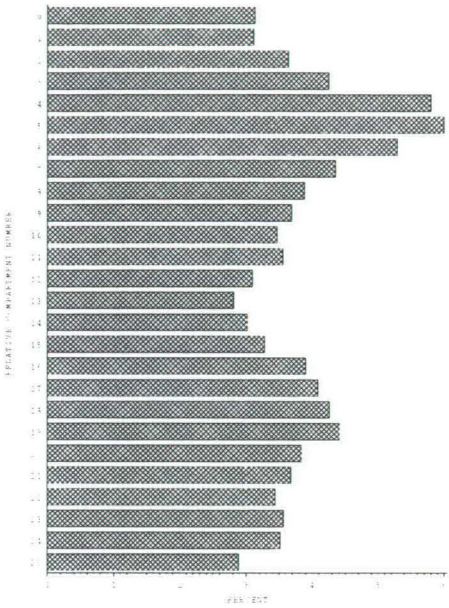

Figure 6.2: From limit ring to number disc, modulo 26 (complete model, low friction level).

the most practical time to stop observing is when the ball intersects the outer edge of the limit ring, which leaves the players a few seconds to place their bets (see chapter 3, equations (3.33) and (3.115): $\Phi_m/\omega_m = 2\pi/(\cos\alpha\sqrt{3})/1.55 = 2.3$ (sec)). The first intersection of the outer edge of the limit ring happens during some stage, say $m+1$, after time t_{m+1} and before time t_{m+2} (see section 5.2 and figure 6.3). On the analogy of symbol R_{lim}, we define $t_{lim} \in (t_{m+1}, t_{m+2})$ as the intersection time of the outer edge of the limit ring, and accordingly

$$\boldsymbol{x}_{lim} = \boldsymbol{x}(t_{lim}), \tag{6.1}$$

for the five-vector $\boldsymbol{x} = (R, \dot{R}, \varphi, \dot{\varphi}, \dot{\psi})$. Thus, for any variable, index lim indicates the value of that variable on time t_{lim}. Note that index m indicates the last local minimum before the limit ring (if such a minimum

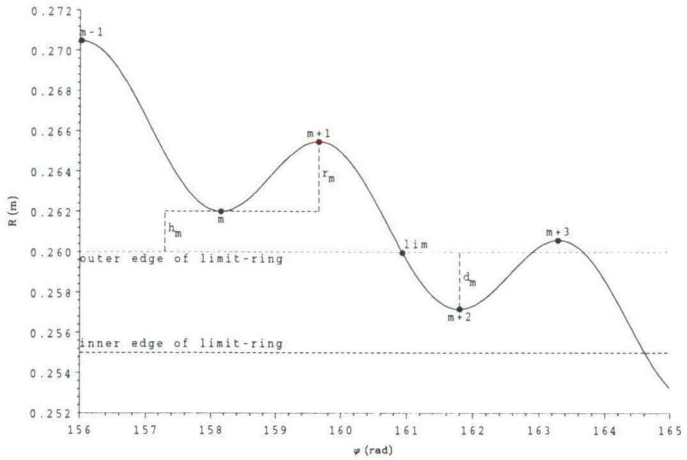

Figure 6.3: Trajectory near the limit ring, in polar coordinates.

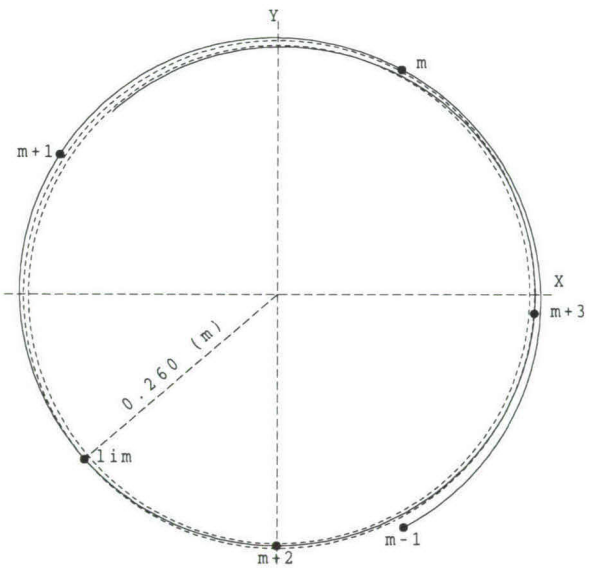

Figure 6.4: Trajectory near the limit ring, in cartesian coordinates (according to the reference system $\{O_{XYZ}\}$, see figure 4.1).

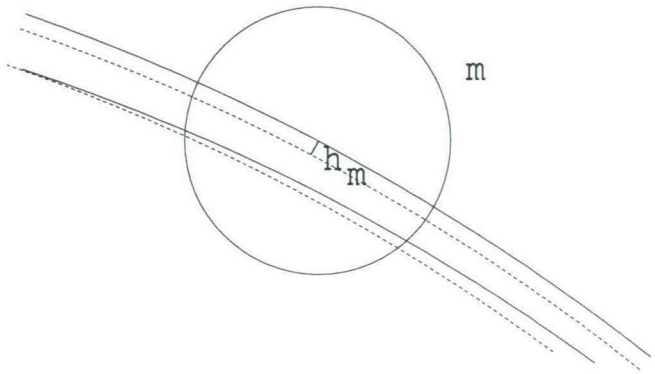

Figure 6.5: Full-scale detail of a trajectory near the limit ring (the same trajectory as in figures 6.3 and 6.4). The centre of the ball passes the limit ring at height $h_m = 2$ (mm).

exists, otherwise we have $m = 0$, or $m+1 = 1$, representing the last stage along the rim).

Subject to investigation is the variable

$$\Delta\varphi(t) = \varphi_{n+2} - \varphi(t),\ t \leq t_{lim}, \tag{6.2}$$

for some moment of time t close to t_{lim} (index $n+2$ represents the end of stage $n+1$, when the ball lies still in the final compartment, see section 5.2). Our first option is to take $t = t_{lim}$, such that $\Delta\varphi(t) = \Delta\varphi_{lim}$, representing the total angle from the limit ring intersection point to the middle of the final compartment. As alternatives to t_{lim} we think of t_m and t_{m+1}, which are also well defined observation points, see figures 6.3 and 6.4. A variable closely related to $\Delta\varphi$, but easier observable (from a player's point of view), is

$$\Delta N(t) = N_{n+2} - N(t) \bmod 26,\ t \leq t_{lim}, \tag{6.3}$$

which represents the total number of compartments (from t to t_{n+2}), modulo 26. For any observed trajectory $\{\boldsymbol{x}(s)\}_{s \leq t}$ and any time $t \leq t_{lim}$,

ΔN is a stochastic variable with a conditional probability distribution given by

$$p_k = P[\Delta N = k | \{\boldsymbol{x}(s)\}_{s \leq t}], \; k = 0, \ldots, 25. \tag{6.4}$$

This distribution, for some moment of time t, determines the value (or expected gain) of all strategies based on that particular time t.

The probability distribution of ΔN depends on the specific drum and the environment in which the game is played. This particularly applies to the coefficient of air friction, which roughly determines the length of the trajectory from limit ring to edge. In the first instance, we therefore only consider the specific drum and environment pertaining to the experimental setup in chapter 4. This leads to a set of environmental conditions of which only the coefficient of air friction may vary; differences can occur when the game is played on different days, or different parts of a day, see section 6.3. In order to be able to compare the results for the basic and the complete stochastic model from chapter 5, we here define the (average) *friction level* as

$$\overline{f} = (R_{lim} - R_{num})^{-1} \int_{R_{num}}^{R_{lim}} \mathcal{F}(R) dR, \tag{6.5}$$

where $\mathcal{F}$ is a quadratic function when the complete model is considered (see subsection 5.4.2), and a constant when the basic model is considered (see subsection 5.3.2).

A general *strategy* is defined as a function

$$\boldsymbol{S} : \; \{\{\boldsymbol{x}(t)\}_{t \leq t_{lim}}\} \; \rightarrow \; [0,1]^{26}. \tag{6.6}$$

Such a function is characterized by its components $(S_0, \ldots, S_{25})$, which represent the proportional stakes $(\sum_k S_k = 1)$ on the relative compartment numbers $0, \ldots, 25$. Together with the probability distribution $(p_0, \ldots, p_{25})$ in (6.4), this vector determines the *expected gain* ***per unit of stake*** of a strategy, expressed as

$$G(\boldsymbol{S}) = 24 \sum_{k=0}^{25} p_k S_k - 1. \tag{6.7}$$

Hence, the maximum expected gain is reached for those strategies that bet only on the mode. This is the reason why we will concentrate on practical, single-number strategies. The strategies will be derived from the basic stochastic model, and tested on the basic model as well as on the complete model.

A single-number strategy is defined by the way it transforms the information in the observed part of the trajectory into a prediction of the final outcome. We have derived three of those strategies, based on observation of either $\boldsymbol{x}_m$, or $\boldsymbol{x}_{lim}$, or on both. Considering $\boldsymbol{x}_m$, we define the observable variable *height* as

$$h_m = R_m - R_{lim}, \tag{6.8}$$

and the observable variable *rise* as

$$r_m = R_{m+1} - R_m, \tag{6.9}$$

see figures 6.3 and 6.4. Table 6.1 defines three strategies: the *minimum strategy* called *Min*, the *intersection strategy* called *Int*, and the *advanced strategy* called *Adv*. For example: in table 6.1 we read that *Int* is based on observation of N_{lim}, and bets on relative compartment number $\Delta N_{lim} = 5$ in case the friction level is 0.0152 $\sec^{-1}$, and on relative number $\Delta N_{lim} = 16$ if the friction level is different. So, if for example $N_{lim} = 22$ and $\overline{f} = 0.0152$ $(\sec^{-1})$, *Int* bets on $22 + 5 \bmod 26 = 1$. *Int* and *Min* will be extensively discussed in section 6.5, *Adv* in section 6.2. The expected gains of the three strategies are given in table 6.2.

Table 6.2 reveals that all three strategies are fairly profitable, even when applied to the complete model. We see for example that on friction level $\overline{f} = 0.0152$ $(\sec^{-1})$, $G(Int) = 24p_5 - 1 = 0.45$; see also table 6.1 and figure 6.2 (showing that $p_5 \approx 0.06$). Table 6.2 also demonstrates that not only the strategies themselves, but also their expected gains depend on the friction level. We will return to this subject in section 6.3. The most profitable strategy is the advanced strategy, as it should be since it exploits the most information. Concerning the other, more naive strategies: neither of them always leads to a higher gain, but the minimum strategy is rather difficult to play (see figure 6.4): the descent per compartment in the neighbourhood of a local minimum is very small, which makes it hard to determine the exact position of the minimum itself. However, this slow descent is quite useful for application of the advanced strategy, since it gives the players some time to estimate the height above the limit ring, see figure 6.5.

The rise r_m, which is in fact a measure of the local ellipticity, does not play a role in any of the strategies (see also section 6.2). However, it is quite an important variable, since table 6.3 shows that it affects the expected gains in the sense that high and low rises correspond to high and

strategies	*Min*	*Int*	*Adv*						
observe	N_m	N_{lim}	N_{lim}, h_m						
$\overline{f}$ ↓	h_m →		0	1	2	3	4	5	≥ 6
0.0152	18	5	6	5	5	5	5	4	3
0.0161	3	16	17	17	16	16	15	4	4
0.0170	14	16	2	2	2	16	15	15	15

Table 6.1: Three practical single-number strategies, based on observation of compartment number N_m or N_{lim} (and height h_m), and represented by their prediction of the relative outcome ΔN_m or ΔN_{lim}. (Coefficient $\overline{f}$ represents the friction level, h_m is rounded to mm; if h_m is Not Available, then $Adv = Int$.)

expected gains		strategy		
model	$\overline{f}$ ↓	*Min*	*Int*	*Adv*
basic	0.0152	1.79	1.82	1.94
	0.0161	1.99	1.89	1.99
	0.0170	1.63	1.23	2.15
complete	0.0152	0.28	0.45	0.46
	0.0161	0.24	0.25	0.27
	0.0170	0.24	0.22	0.37

Table 6.2: Expected gains of three practical single-number strategies (cf. table 6.1).

low gains, respectively. While the mean expected gain for the intersection strategy for the basic model with $\overline{f} = 0.0161$ ($\sec^{-1}$) is 1.99, it can be as high as 3.10 for rises higher than 14 mm, or as low as 0.88 for rises lower than 3 mm. This means that more money can be made when the stakes are higher for high rises, regardless of the strategy. The curved air friction function in the complete model (see subsection 5.5.2) appears to partly override this effect, but the expected gain turns out to be positive in all cases (according to table 6.2). This implies that our strategies are always profitable, so that players who want to get rich, just have to stake as much money as possible, even regardless of the rise.

model	$r_m \downarrow$	$G(Min)$	$G(Int)$	$G(Adv)$
basic	≤ 2	0.42	0.77	0.89
	$3-6$	1.51	1.61	1.54
	$7-10$	1.54	2.03	2.37
	$11-14$	3.20	2.81	3.03
	≥ 15	3.42	3.45	3.03
complete	≤ 2	0.11	0.22	0.14
	$3-6$	0.20	0.06	0.16
	$7-10$	0.38	0.31	0.37
	$11-14$	0.23	0.42	0.61
	≥ 15	0.39	0.40	0.23

Table 6.3: Expected gains, as depending on the rise r_m (rounded to mm; friction level $\overline{f}$ fixed to 0.0161 $\sec^{-1}$.)

6.2 The optimal strategy

Any trajectory is in fact a Markov process, which means that $E[\Delta N|\{\boldsymbol{x}(s)\}_{s\leq t}] = E[\Delta N|\boldsymbol{x}(t)]$ for all times t, especially t_{lim}. Hence we can introduce the *optimal strategy*, called *Opt*, which simply bets on the mode of the conditional distribution of the final outcome, given all components of the trajectory at the time it intersects the outer edge of the limit ring. Although this strategy is clear, it is also hard to determine since this requires large numbers of simulations for all possible sets of coordinates. For this reason, we will only take an overall view of this strategy, and search for a workable approximation.

As possibly (almost) optimal, we first consider the *numerical strategy* called *Num*, which is defined as the output of a Runge-Kutta routine, based on the system of equations (5.14), with the initial conditions equal to $\boldsymbol{x}_{lim}$. As an estimator of the mode, this strategy may be biased however, since the actual equations of motion in (5.37) contain stochastic factors of which the cumulative effects are still largely unknown to us. Application of *Num* to simulations of the same models as in table 6.2 confirms that the expected gain is usually lower than that of the simple strategies *Min* and *Int*, and always lower than that of *Adv*. Hence, *Num* is biased, and certainly not optimal.

In order to get a better understanding of *Opt*, and in search of a way

r_m	3			7			13		
d_m	1	2	4	1	2	4	1	2	4
Opt	16	17	17	3	16	17	4	16	17
$G(Opt)$	0.73	1.38	1.40	2.12	2.55	2.70	2.94	3.13	3.18
Num	3	3	18	3	4	17	4	17	17
$G(Num)$	0.49	0.01	1.21	2.12	1.30	2.70	2.94	2.24	3.18

Table 6.4: The optimal and the numerical strategy, represented by their prediction of ΔN_{lim} (for the basic model with $\overline{f} = 0.0161$ (sec^{-1})). Rise r_m and depth d_m are both in mm.

to put this strategy into practice, we replace the coordinates of vector $\boldsymbol{x}_{lim}$ with easily observable quantities. At time t_{lim}, R is equal to the radius of the limit ring, and φ is observed as compartment number N. This in fact leaves us with three components (i.e. $\dot{R}$, $\dot{\varphi}$ and $\dot{\psi}$). Firstly, we simply eliminate $\dot{\psi}$, since it turns out that its absolute value is very low (in all simulations of the basic model lower than 3 rad/sec), and thus negligible (see also subsection 3.3.3). Secondly, we translate $\dot{\varphi}$ - according to the results in section 3.4 - into the rise r_m, and the remaining variable $\dot{R}$ into the variable *depth*, defined as

$$d_m = R_{lim} - R_{m+2}, \tag{6.10}$$

see figure 6.3. It would have been more consistent to translate $\dot{R}$ into the height h_m, but on the other hand, we know from equation (3.141) that $h_m + d_m = R_m - R_{m+2}$ is almost constant (see section 3.4). Extra simulations on a balanced design of 3×3 different levels of (r_m, d_m) eventually give us table 6.4. The table shows for example, that the combination of rise and depth of 13 and 2 mm yields a modal relative outcome of 16 (hence $Opt_{16} = 1$), whereas the numerical strategy predicts 17 ($Num_{16} = 0$, $Num_{17} = 1$). Since *Num* is apparently biased, its expected gain for this particular set of initial conditions is lower than that of *Opt* (2.24 is lower than 3.13).

From table 6.4 we learn that the optimal strategy depends on the depth, or - equivalently - on the height. This phenomenon has a straightforward explanation, since a longer radial distance to the edge of the drum expectedly leads to a longer trajectory. Furthermore, we learn that the expected gain of *Opt* depends on the rise, indicating that a strongly

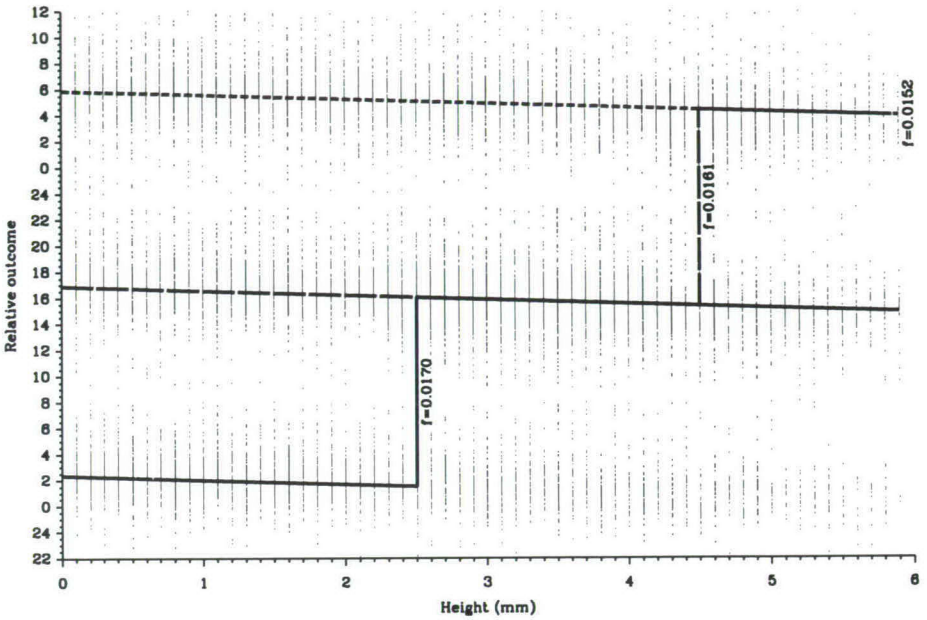

Figure 6.6: The advanced strategy *Adv* (represented by its prediction of relative outcome ΔN_{lim}), as the sum of a continuous function and a step function of height h_m. (Note that the position of the step depends on the value of friction level $\overline{f}$.)

elliptical trajectory is less sensitive to small disturbances than a weakly elliptical trajectory. Table 6.4 also contains information on strategy *Num*, which appears to be biased in the sense that it usually predicts a slightly shorter trajectory. We have found that the overall expected gain of *Num* for the model in question is exactly 1.62, which is clearly less than the expected gains in tabel 6.2.

The optimal strategy depends strongly on the depth d_m (or, equivalently, on the height h_m). Figure 6.6 shows the correspondence between the relative final outcome ΔN_{lim} and the height h_m for simulations of the basic model on three different friction levels. The main effect, i.e. that of higher heights corresponding to higher outcomes (or longer trajectories), is clearly visible in the big jumps for friction levels 0.0161 and 0.0170 $\sec^{-1}$, at the heights 2.5 and 4.5 mm, respectively. The second effect, which shows a slightly increasing trajectory length (or slightly

higher outcomes) for lower heights, is local (near $t = t_{lim}$), and fades away along the remaining part of the trajectory. It is explained by the fact that lower heights correspond to lower phases (or angular positions) at $t = t_{lim}$, which - in the end - yield slightly longer trajectories. To see this, redraw the trajectory in figure 6.3 with a 1 mm lower radius R.

Starting from the $3 \times 10,000$ observations of $(h_m, \Delta N_{lim})$ in our three simulation sets of the complete model (represented by the $\pm 30,000$ small dots in figure 6.6), we estimate the slope by means of a linear regression model. We furthermore estimate the jump positions by roughly estimating the change in the modal relative outcome. The result of this estimation procedure is an approximation of the optimal strategy. We have presented this result as the advanced strategy *Adv* in table 6.1, with its expected gain in table 6.2. Note that on friction level $\overline{f} = 0.0170$ (sec^{-1}), the gain of *Adv* is apparently much higher than that of the two other practical strategies, *Min* and *Int*. The reason for this is that this particular friction level is *critical* in the sense that the distribution of the final relative outcome has two modes of approximately the same frequency (in contrast with figure 6.2, where the frequencies are clearly different). By taking into account the observed jump on height $h_m = 2.5$ (mm), the advanced strategy is able to indicate (given this observed height) which one of the two modes is more likely. So, if the observed height is smaller than 2.5 mm, then the lowest mode is the more likely one, and else the highest mode.

6.3 The influence of air friction

The level of friction usually varies per session (i.e. per afternoon, evening, etc.). Figure 6.7 gives an impression of this variation: it shows the estimated levels of friction for the set of the 338 fully available orbits in chapter 4. The level was assessed by re-estimating the level of the friction function $\mathcal{F}(R)$ in (5.17) for each individual orbit, and by calculating $\overline{f}$ according to (6.5). It appears that the level of friction (in our laboratory) was usually 0.0161 sec^{-1}, although on some occasions it was as low as 0.0152 sec^{-1}, or as high as 0.0167 sec^{-1} (note that the small fluctuations in figure 6.7 are largely due to measurement errors). To investigate the effects of low as well as high levels, and for reasons of symmetry, we simulated sets of 10,000 orbits for the three levels 0.0152, 0.0161 and 0.0170 sec^{-1} (see also tables 6.1 and 6.2). We also simulated small sets for some intermediate levels, but their number was unfortunately too small

to produce accurate results.

However, the above-mentioned small sets did show some interesting effects. Figure 6.8 sketches the impact of a slowly increasing friction level on the mode frequency of ΔN_{lim}: it depicts the evolution of the mode and its frequency, or - equivalently - the evolution of strategy *Int* and its expected gain $G(Int)$. Note that figure 6.8 is only a sketch, since the only accurate values are those for $\overline{f} = 0.0152, 0.0161, 0.0170$ (sec^{-1}). For $\overline{f} = 0.0161$ (sec^{-1}), we read that the modal relative outcome $\Delta N_{lim} = 16$ (i.e. $Int_{16} = 1$), and that $G(Int) = 24p_{16} - 1 = 24 \times 0.1203 - 1 = 1.89$, exactly as in tables 6.1 and 6.2. The figure also shows that on friction level $\overline{f} = 0.0171$ (sec^{-1}), the modal relative outcome is 15, whereas the intersection strategy predicts 16. This explains why the corresponding expected gain in table 6.2 is lower than $24 \times 0.1096 - 1 = 1.63$. The fact that *Int* bets on 16 will be justified in sections 6.4 and 6.5.

The modal relative outcome is appears to be usually 16 or 5, depending on the friction level. Higher friction levels lead to shorter trajectories, thus to lower modal outcomes (note that $5 - 15 \mod 26 = 16$). When the friction level becomes critical, the outcome distribution becomes strongly bimodal, as in figure 6.2, which actually corresponds to $\overline{f} = 0.0152$ (sec^{-1}), i.e. the low friction level. Somewhere around the critical level 0.0158 (see figure 6.8), the mode changes from 5 to 16, and probably changes again around level 0.0170. Furthermore, we have a low expected gain for critical values of $\overline{f}$, since then we have lots of trajectories that would have ended in the smallest (largest) mode if $\overline{f}$ were slightly larger (smaller), which would have yielded a higher frequency of the mode. Finally note that the highest gain is reached around $\overline{f} = 0.0164$ (sec^{-1}): approximately $24 \times 0.1240 - 1 = 1.98$, see figure 6.8.

6.4 A robust strategy

The exact level of friction in a casino is usually not known. The players can either try to estimate this level and then use an appropriate strategy (see section 6.5), or they can play a robust strategy, i.e. one that does not depend on the actual friction level, but still yields some profit. Since the expected gain of a strategy depends on the level of friction, the most attractive robust strategy is the minimax strategy, i.e. the one that maximizes the minimum gain (for all possible levels of friction). Since we only have data from simulations on the three levels 0.0152, 0.0161 and 0.0170 sec^{-1}, we here only present the solution that maximizes the

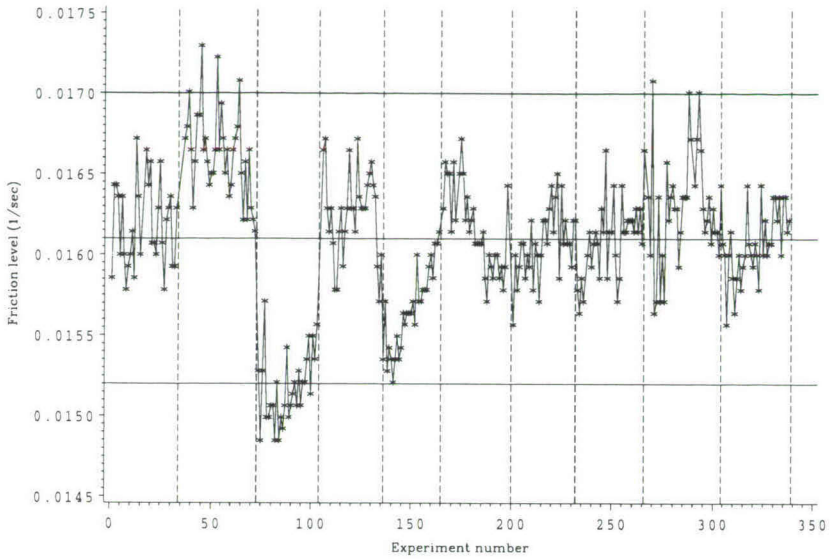

Figure 6.7: Estimated levels of friction. the dashed lines are dividing lines between series of games.

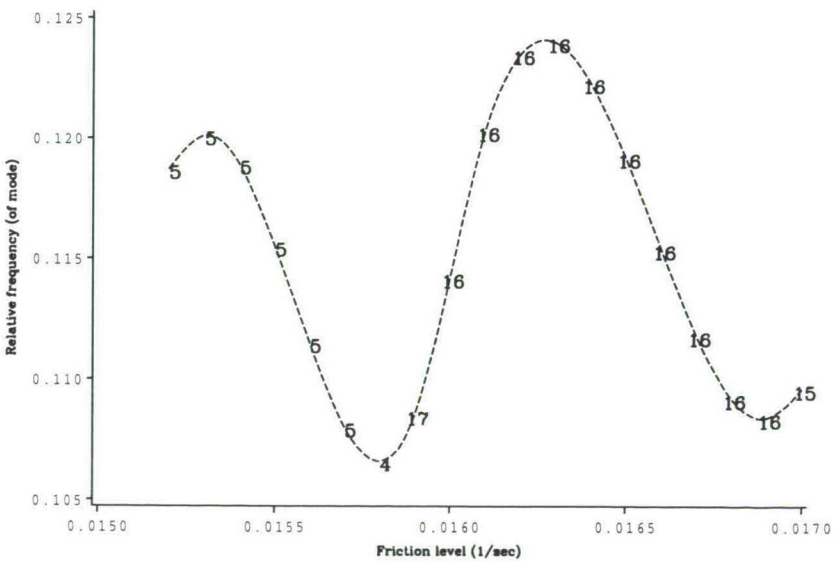

Figure 6.8: Modal relative outcomes ΔN_{lim} and corresponding relative frequencies (i.e. probabilities), as depending on friction level $\overline{f}$.

perc.	$\Delta N_{lim} = k$							$G(Rob)$	
$\overline{f}\downarrow$	4	5	6	$\cdots$	15	16	17	basic	compl.
0.0152	9.17	11.73	9.07		2.78	5.75	8.27	0.77	0.08
0.0161	9.08	7.08	3.93	$\cdots$	9.02	12.03	10.02	1.56	0.20
0.0170	4.66	2.35	1.56		11.09	9.29	5.75	0.77	0.13
Rob	0	0.274	0	$\cdots$	0	0.726	0	0.77	0.08

Table 6.5: The robust strategy, as derived from the probability distribution of the relative outcome ΔN_{lim} (percentages $100 \times p_k$), and expressed in the components Rob_k, for $k = 0, \ldots, 25$.

minimum gain for these three particular levels.

The three different modal relative outcomes on the three considered friction levels are 5, 16 and 15 (see figure 6.8). We therefore only need to focus our attention on the numbers around 5 and 16, as in table 6.5, which presents part of the probability distribution of ΔN_{lim}: e.g. $p_{16} = 0.1203$, in case $\overline{f} = 0.0161$ (sec^{-1}). We define the *robust strategy*, called *Rob*, as the minimax solution based on the three probability distributions of the relative outcomes for the three different levels 0.0152, 0.0161 and 0.0170 sec^{-1}. According to table 6.5, the robust strategy bets only on the numbers 5 and 16: $Rob_5 + Rob_{16} = 0.274 + 0.726 = 1$.

In case the friction level $\overline{f} = 0.0152$ (sec^{-1}), the expected gain of the robust strategy is $G(Rob) = 0.77$ when the basic model is concerned, and $G(Rob) = 0.08$ when the complete model is concerned (see table 6.5). In the two other cases, the expected gain is higher (or - more precisely - not lower) than 0.77 or 0.08. Figure 6.8 indicates that *Rob* is not only robust for variation on the three levels 0.0152, 0.0161 and 0.0170 sec^{-1}, but even for variation on the entire interval $[0.0152, 0.0169]$ sec^{-1}. The proportional stakes Rob_5 and Rob_{16} may then be slightly different from those in table 6.5, but they still add up to 1.

6.5 A practical strategy for Golden-Ten variants

Until now, all strategies were derived from the simulation results for one particular drum, in one particular environment. However, from the analytic results in chapter 3 we can find some overall characteristics (of the elliptically spiralling orbits) that lead to generalizations of the two previously discussed strategies *Min* and *Int*, which can in fact also be

played in different environments on different drums. The leading part here is played by the periodicity of the orbits, or the angular distance from one local maximum (minimum) to the next. According to (3.140), the periodicity equals

$$\Phi_m = \frac{26}{\cos\alpha\sqrt{3}} \text{ (rad)} \approx 15\tfrac{1}{16} \text{ (compartments)}. \tag{6.11}$$

Note that the periodicity is superimposed on a steady descent, and both of these components contain random factors, so there may not always exist two extrema within one period. However, this does not affect the periodicity itself. Although the periodicity can be affected by the occurrence of grooves, this appears not to happen frequently enough to gloss over the overall structure completely (see figure 6.2, which is clearly not a uniform distribution).

Instead of directly investigating the behaviour of ΔN, we first consider the conduct of the related variable

$$\Delta P(t) = [\tfrac{\cos\alpha\sqrt{3}}{26}\Delta N(t) + \tfrac{1}{2}],\ t \leq t_{lim}. \tag{6.12}$$

As an example, we first consider ΔP_{lim}, which represents the rounded number of periods, from limit ring intersection point to final compartment. Due to the periodicity, the ball usually passes through the limit ring (for the first time) after it has completed approximately three quarters of a period following the last local minimum, as in figure 6.3. The same angular distance applies to where the ball falls off of the edge of the drum, which means that the length of a trajectory from limit ring to edge often corresponds to an integer number of periods of approximately $15\frac{1}{16}$ compartments. This explains why the modes for the friction levels 0.0152 and 0.0161 differ 15 numbers (see table 6.1). To simplify the counting of numbers, we finally also introduce

$$\Delta n(t) = N_{n+2} - N(t),\ t \leq t_{lim}, \tag{6.13}$$

on the analogy of definition (6.3).

A trajectory only ends after completion of stage $n+1$, representing the downfall into the number disc (see subsection 5.3.3). The motion during this stage has been modelled in equation (5.31), which usually leads to a fall of two compartment numbers: sixty-six percent of the orbits in chapter 4 appear to have this property. This directly leads to an intersection strategy that adds to the observed intersection point an integer number of

ΔP_{lim}	11	12	13	14	15	16
Δn_{lim}	168	183	198	213	228	243
ΔN_{lim}	12	1	16	5	20	9

Table 6.6: Variants of the intersection strategy (i.e. the prediction of relative outcome ΔN_{lim}) based on the corresponding observed mode of ΔP_{lim} (i.e. the rounded number of periods). Note that $\Delta N_{lim} = \Delta n_{lim} \bmod 26$.

periods (of $15\frac{1}{16}$ compartments) plus another two compartments for the downfall. Similar reasoning applies to the minimum strategy: because of the periodicity, the ball leaves the edge approximately one eighth of a period, or two compartment numbers, before completing yet another full period. Hence, since the fall adds two extra numbers, the trajectory often ends exactly after an integer number of periods (of $15\frac{1}{16}$ compartments) following the position of the last observed minimum.

The modal number of periods depends on the ratio of friction level $\overline{f}$ and radial distance $R_{lim} - R_{num}$. Just like we varied $\overline{f}$ in order to obtain figure 6.8, we could also have varied R_{lim} in order to get practically the same image. According to equations (3.33), (3.115) and (3.143), the descent per full period in the neighbourhood of the limit ring is $\Delta R \approx 20\pi\overline{f}/(21\cos\alpha\sqrt{3}) \times R_m/\omega_m = 4.4$ (mm), for $\overline{f} = 0.0152$ ($\sec^{-1}$). So, on this friction level, we can shift the distribution of ΔN_{lim} with one period (or 15 numbers) to the right by raising R_{lim} with 4.4 mm. We can acquire approximately the same result by raising $\overline{f}$ to 0.0166 $\sec^{-1}$, and keeping R_{lim} constant (see figure 6.8). Although an extra period can slightly increase the cumulative effects of the random disturbances, it does not affect the periodicity, so it leaves strategies based on the mode unchanged.

We can now easily extend our intersection strategy to Golden-Ten played under different circumstances (i.e. with a different $\overline{f}$), or Golden-Ten variants with a different R_{lim}, or variants that force the players to bet before the touching point with the limit ring instead of the intersection point. This extended intersection strategy simply bets on a modal relative outcome ΔN_{lim} that corresponds (at least for non-critical ratios of $\overline{f}$ and $R_{lim} - R_{num}$) to an integer number of periods (of $15\frac{1}{16}$ numbers), plus two numbers more. This strategy must be applied after estimation of the ratio of $\overline{f}$ and $R_{lim} - R_{num}$, which can be done (indirectly) by determining

probability distribution		ΔP_{lim}				expected
model	$f \downarrow$	12	13	14	15	gain
basic	0.0152	0.00	0.06	0.85	0.09	1.59
	0.0161	0.01	0.75	0.24	0.00	1.58
	0.0170	0.37	0.63	0.00	0.00	1.29
complete	0.0152	0.00	0.08	0.74	0.18	0.31
	0.0161	0.04	0.59	0.37	0.00	0.17
	0.0170	0.38	0.61	0.01	0.00	0.25

Table 6.7: Probability distribution of the observed modal rounded number of periods after sixteen games, and the expected gain of the corresponding intersection strategy (cf. table 6.6).

the mode of the rounded number of periods ΔP_{lim} in a series of - say sixteen - games. Note that sixteen games take about three quarters of an hour, see section 5.2. After the estimation, the corresponding number of compartments ΔN_{lim} in table 6.6 serves as the outcome of the strategy. For example, an observed modal ΔP_{lim} of 14 corresponds to a prediction for ΔN_{lim} of 5.

Strictly speaking, the relationship between the first and the two next rows in table 6.6 depends on α. For example: $16 \times 26/(\cos\alpha\sqrt{3}) + 2 \bmod 26 \approx 243 \bmod 26 = 9$, for $\alpha = 0.0831$ (rad), as in table 2.1. So, for $\alpha = 0.0831$ (rad), $\Delta P_{lim} = 16$ corresponds to $\Delta n_{lim} = 243$ and $\Delta N_{lim} = 9$. However, for larger or smaller values of α this correspondence may be different. Since α can vary from 0.105 down to 0.0698 rad - according to Teugels [24] and Urban [25], respectively - this implies that table 6.6 can not be extended independently of α.

The expected gain of the above-described strategy depends on the probability distribution of the modal rounded number of periods, as well as on the characteristics of the drum surface (see section 5.4). We can get an impression of this gain by playing the strategy in our laboratory casino, the result of which is given in table 6.7. This table shows, for example, that in the basic model on friction level 0.0152 sec^{-1} the players estimate the mode to be 14 (which it actually is) in 85% of all occasions. They sometimes find 13 (6%) or 15 (9%), but in the long run, this strategy yields a gain of 1.59, which is still fairly high.

6.6 The gains of experienced players

The strategies practised most frequently - even by experienced players - are multiple-number strategies that bet on two diametrical sectors (see subsection 2.2.1). Since at best one of these numbers is the mode, these strategies yield a lower gain than single-number strategies that bet only on the mode. On the other hand, multiple-number strategies have a higher rate of success, which explains their popularity. But betting on diametrical sectors is really suboptimal, for two reasons. First we note that according to section 6.5, the modes of two relative outcome distributions usually differ by a multiple of 15 numbers, not 13. Secondly, we have seen in figure 6.2 that such a distribution has two modes that differ 14 numbers, again not 13.

If the rounded number of periods in a trajectory is not the modal number, then it is usually one higher or lower. Starting from friction level $\overline{f} = 0.0152$ ($\sec^{-1}$) in table 6.7, we find that the corresponding modal number of periods is 14. Furthermore, we find that 13 and 15 are also quite frequent, especially 15. This accounts for the second peak in figure 6.2, although the two peaks show a difference of 14 numbers, instead of 15. If we raise $\overline{f}$, the peak around 14 periods becomes lower, whereas the peak around 13 periods becomes higher. Again the difference is 14 numbers, since figure 6.8 shows modal number $17 = 5 - 14 \mod 26$, for level $\overline{f} = 0.0159$ ($\sec^{-1}$). Similar reasoning accounts for the modal numbers 16 and 4 in figure 6.8, when $\overline{f}$ is lowered from 0.0161 to 0.0158 $\sec^{-1}$. Figure 6.8 also indicates that around the critical level 0.0158, we have two modes with a difference of 13 numbers. Hence, in very special cases (i.e. for critical ratios of $\overline{f}$ and $R_{lim} - R_{num}$), a diametrical multiple-number strategy can be optimal after all.

By playing some of these multiple-number strategies in our laboratory casino, and comparing the results to those reported by Albers [1], Boer [3], Embrechts et al. [13] and LaFors & Derksen [16], we can get an impression of the actual skills of experienced, real-life players. Apart from a few test persons described in Embrechts et al. [13], all of these players are reported to have used some kind of intersection strategy, so we can compare their results to ours by defining a few simple variants of our strategy *Int*. Table 6.8 gives five diametrical intersection strategies, which are all derived from the basic simulation model with friction level 0.0152 $\sec^{-1}$. For the two even-number sector strategies $Int^{2\times4}$ and $Int^{2\times2}$, we especially reckon with number 19, since this number corresponds to the second mode of the

relative outcome distribution in figure 6.2. So, for strategy $Int^{2\times 2}$ for example, we take $Int_k^{2\times 2} = \frac{1}{4}$ for $k = 5, 6, 18, 19$, and $Int_k^{2\times 2} = 0$ for all other k.

Table 6.9 presents the reported gains as well as the expected gains of the strategies defined in table 6.8. To be sure, it is not easy to compare the gains, since the games were not played according to the same set of rules, nor were they played with exactly the same attributes. Nevertheless, table 6.9 first of all clearly shows that the expected gains get higher when bets are put on smaller sectors (the highest expected gain is reached by betting on one number only, cf. table 6.2). Secondly, it shows that the gains reported by Embrechts et al. [13] are very low. This is explained by the fact that some of these players did not observe the trajectories beyond the observation ring, or even not beyond the rim. All other reported gains in table 6.9 lie between the corresponding gains for our basic and our complete simulation model. This means that when the game is played on a brand-new, very smoothly polished drum (corresponding to our basic model, cf. the fictitious game Super-Ten defined in subsection 2.1.3), experienced players can make high profits. But even when the game is played on a normal drum with a rough surface and fair-sized grooves, like the one we used (corresponding to our complete model), the profits are still high.

stakes	k										
strategy	3	4	5	6	7	$\cdots$	16	17	18	19	20
$Int^{2\times5}$	$\frac{1}{10}$	$\frac{1}{10}$	$\frac{1}{10}$	$\frac{1}{10}$	$\frac{1}{10}$		$\frac{1}{10}$	$\frac{1}{10}$	$\frac{1}{10}$	$\frac{1}{10}$	$\frac{1}{10}$
$Int^{2\times4}$	0	$\frac{1}{8}$	$\frac{1}{8}$	$\frac{1}{8}$	$\frac{1}{8}$		0	$\frac{1}{8}$	$\frac{1}{8}$	$\frac{1}{8}$	$\frac{1}{8}$
$Int^{2\times3}$	0	$\frac{1}{6}$	$\frac{1}{6}$	$\frac{1}{6}$	0	$\cdots$	0	$\frac{1}{6}$	$\frac{1}{6}$	$\frac{1}{6}$	0
$Int^{2\times2}$	0	0	$\frac{1}{4}$	$\frac{1}{4}$	0		0	0	$\frac{1}{4}$	$\frac{1}{4}$	0
$Int^{2\times1}$	0	0	$\frac{1}{2}$	0	0		0	0	$\frac{1}{2}$	0	0

Table 6.8: Five straightforward multiple-number variants of the intersection strategy, represented by their stakes on the relative compartment numbers $k = 0, \cdots, 25$ (friction level $\overline{f} = 0.0152$ (sec^{-1})).

strategy	expected gain		reported	reported	report
	basic	complete	strategy	gain	source
$Int^{2\times5}$	0.85	0.11	2×5	0.26	[3]
$Int^{2\times4}$	1.07	0.15	2×4	0.09	[13]
$Int^{2\times3}$	1.23	0.18	2×3	0.64	[1]
$Int^{2\times2}$	1.38	0.23	2×2	0.02	[13]
$Int^{2\times1}$	1.46	0.23	2×1	0.56	[16]

Table 6.9: Reported and expected gains, per model, of five straightforward multiple-number intersection strategies (cf. table 6.8).

Appendix A

Asymptotic power series

This appendix contains the coefficient lists of the power series in (3.72). The formulas have been derived by employing the techniques described in section 3.3. Most of the calculations have been done using software package MATHEMATICA (see Wolfram [35]).

$$u_0 = (1+\tfrac{1}{3}\varphi_2)^2, \tag{A.1}$$

$$v_0 = (1+\tfrac{1}{3}\varphi_2)^3, \tag{A.2}$$

$$w_0 = \varphi_2(1+\tfrac{1}{3}\varphi_2)^{-1}, \tag{A.3}$$

$$\begin{aligned} u_1 &= \tfrac{1}{9}(d_1-\tfrac{6}{5}d_2)\varphi_2(1-\tfrac{1}{3}\varphi_2)(1+\tfrac{1}{3}\varphi_2) \\ &- \tfrac{2\sqrt{3}}{9}(1+\tfrac{1}{3}\varphi_2)^2\sin(\sqrt{3}\varphi_1-\Omega_1), \end{aligned} \tag{A.4}$$

$$v_1 = -\tfrac{1}{9}(d_1-\tfrac{6}{5}d_2){\varphi_2}^2(1+\tfrac{1}{3}\varphi_2)^2, \tag{A.5}$$

$$\begin{aligned} w_1 &= -\tfrac{1}{3}(d_1-\tfrac{6}{5}d_2)\varphi_2(1+\tfrac{2}{3}\varphi_2)(1+\tfrac{1}{3}\varphi_2)^{-2} \\ &+ (d_1-\tfrac{6}{5}d_2)\log(1+\tfrac{1}{3}\varphi_2), \end{aligned} \tag{A.6}$$

$$\begin{aligned} u_2 &= \tfrac{8}{27}+(\tfrac{8}{27}+\tfrac{2}{27}{d_1}^2-\tfrac{1}{45}d_1d_2-\tfrac{2}{25}{d_2}^2)\varphi_2 \\ &+ (\tfrac{2}{81}-\tfrac{2}{45}d_1d_2+\tfrac{4}{75}{d_2}^2){\varphi_2}^2 \\ &- \tfrac{2}{243}(d_1+\tfrac{27}{10}d_2)(d_1-\tfrac{6}{5}d_2){\varphi_2}^3+\tfrac{1}{729}(d_1-\tfrac{6}{5}d_2)^2{\varphi_2}^4 \\ &+ \tfrac{2}{15}d_2(d_1-\tfrac{6}{5}d_2)(1+\tfrac{1}{3}\varphi_2)^3\log(1+\tfrac{1}{3}\varphi_2) \\ &- (1+\tfrac{1}{3}\varphi_2)\{\lambda_1\sin(\sqrt{3}\varphi_1-\Omega_1)+\lambda_2\cos(\sqrt{3}\varphi_1-\Omega_1)\} \\ &+ \tfrac{2}{81}(1+\tfrac{1}{3}\varphi_2)^2\cos(2\sqrt{3}\varphi_1-2\Omega_1), \end{aligned} \tag{A.7}$$

$$
\begin{aligned}
v_2 &= \Big\{\tfrac{4}{9} + (\tfrac{10}{27} - \tfrac{2}{15}d_1d_2 + \tfrac{4}{25}{d_2}^2)\varphi_2 \\
&+ (\tfrac{2}{81} - \tfrac{2}{27}{d_1}^2 - \tfrac{2}{15}d_1d_2 + \tfrac{4}{15}{d_2}^2){\varphi_2}^2 \\
&- \tfrac{1}{81}(d_1 + 6d_2)(d_1 - \tfrac{6}{5}d_2){\varphi_2}^3 + \tfrac{2}{243}(d_1 - \tfrac{6}{5}d_2)^2{\varphi_2}^4\Big\}(1 + \tfrac{1}{3}\varphi_2) \\
&+ \tfrac{2}{5}(d_1 - \tfrac{6}{5}d_2)(1 + \tfrac{1}{3}\varphi_2)^4 \log(1 + \tfrac{1}{3}\varphi_2) \\
&- \tfrac{4}{9}(1 + \tfrac{1}{3}\varphi_2)^2 \cos(\sqrt{3}\varphi_1 - \Omega_1), \qquad \text{(A.8)} \\
w_2 &= \Big\{\tfrac{2}{9} - \tfrac{13}{15}d_2(d_1 - \tfrac{6}{5}d_2)\varphi_2 - (\tfrac{10}{81} + \tfrac{1}{27}{d_1}^2 + \tfrac{32}{45}d_1d_2 - \tfrac{68}{75}{d_2}^2){\varphi_2}^2 \\
&- (\tfrac{14}{729} + \tfrac{23}{135}d_1d_2 - \tfrac{46}{225}{d_2}^2){\varphi_2}^3\Big\}(1 + \tfrac{1}{3}\varphi_2)^{-3} \\
&+ d_2(d_1 - \tfrac{6}{5}d_2)\Big\{\tfrac{13}{5} - \tfrac{1}{5}\log(1 + \tfrac{1}{3}\varphi_2)\Big\}\log(1 + \tfrac{1}{3}\varphi_2) \\
&- \tfrac{2}{9}(1 + \tfrac{1}{3}\varphi_2)^{-2} \cos(\sqrt{3}\varphi_1 - \Omega_1), \qquad \text{(A.9)}
\end{aligned}
$$

$$
\Omega_1 = \tfrac{\sqrt{3}}{3}(d_1 + \tfrac{3}{2}d_2)\varphi_2 + \tfrac{\sqrt{3}}{18}(d_1 - \tfrac{6}{5}d_2){\varphi_2}^2, \qquad \text{(A.10)}
$$

$$
\begin{aligned}
\lambda_1 &= \tfrac{\sqrt{3}}{9}(d_1 + \tfrac{3}{5}d_2) + \tfrac{2\sqrt{3}}{27}(d_1 - \tfrac{3}{10}d_2)\varphi_2 - \tfrac{\sqrt{3}}{243}(d_1 - \tfrac{6}{5}d_2){\varphi_2}^2 \\
&+ \tfrac{2\sqrt{3}}{45}d_2(1 + \tfrac{1}{3}\varphi_2)\log(1 + \tfrac{1}{3}\varphi_2), \qquad \text{(A.11)} \\
\lambda_2 &= \tfrac{26}{81} - (\tfrac{2}{243} + \tfrac{1}{27}{d_1}^2 + \tfrac{7}{45}d_1d_2 + \tfrac{3}{100}{d_2}^2)\varphi_2 \\
&+ (\tfrac{2}{729} - \tfrac{1}{81}{d_1}^2 - \tfrac{5}{54}d_1d_2 + \tfrac{7}{180}{d_2}^2){\varphi_2}^2 \\
&+ \tfrac{1}{243}(d_1 - \tfrac{9}{2}d_2)(d_1 - \tfrac{5}{6}d_2){\varphi_2}^3 + \tfrac{1}{729}(d_1 - \tfrac{6}{5}d_2)^2{\varphi_2}^4 \\
&+ \tfrac{2}{15}d_2(d_1 - \tfrac{6}{5}d_2)(1 + \tfrac{1}{3}\varphi_2)^3 \log(1 + \tfrac{1}{3}\varphi_2). \qquad \text{(A.12)}
\end{aligned}
$$

Appendix B

Tracking parameters

```
                Base output file name: t10b03
                     Experiment title: Tape 10, Ball 3
                   Total tracking time:  1830.000000
       Spacing between acquired images:          2
Experimental time at start of tracking:       .000000
                  Top of tracking window:         18
               Bottom of tracking window:        496
                 Left of tracking window:        113
                Right of tracking window:        441
               Lower particle size limit:       -100
               Upper particle size limit:        300
               Minimum horizontal extent:         11
                   Minimum vertical size:         16
    Lower particle location threshold:         96
    Upper particle location threshold:        128
                  Minimum ellipticity:      1.000000
                  Maximum ellipticity:      1.000000
           Maximum centroid mismatch:       1.000000
                           Lost cost:      60.000000
                       Pricing policy: 1
         Previous velocity weighting:        .500000
         Premium for small particles:       1.000000
         Premium for large particles:       1.000000
     Premium for elliptical particles:      1.000000
         Premium for faint particles:       1.000000
  Expected x velocity for new parts.:        .000000
```

```
      Expected y velocity for new parts.:       .000000
       Max velocity error for new parts.:   1000.000000
Ratio of y to x velocity error for new p:      1.000000
         Max rms error in reference map:     -2.000000
                        Centroid type: A
                     Particle polarity: G
                   Rewind in background: F
             Type of background removal: N
                    Time for background:     10.000000
       Type of ALU operation for removal:            15
     Result table for background removal:             0
           Type of background recording: N
                Display paths/cost etc.: M
                Display paths plot type: L
        Buffer containing particle paths:             0
                  Paths intensity change:             6
                          Type of filter: 0
```

Appendix C

Image transformation

```
/* ********************************************************** */
/* THIS IS THE SAS PROGRAMME E:\MYSAS\G10\DIGTODAT.SAS.       */
/* IT READS DIGIMAGE FILES, CORRECTS THE TIME CODE,           */
/* SHIFTS THE IMAGE, SPLITS OFF AND TRANSFORMS TRAJECTORIES,  */
/* WRITES THE TRAJECTORIES TO ASCII FILES, AND PLOTS THEM.    */
/* ********************************************************** */

*  DETERMINE THE FILE NAMES  ;
   DM 'LOG; CLEAR; OUTPUT; CLEAR; PGM';
%WINDOW INFO COLOR=RED IROW=8 ICOLUMN=1 ROWS=7 COLUMNS=78
   #1 @1 'DigImage name     : ' INNAME 40 COLOR=YELLOW REQUIRED=YES
     @60 '(Without extension)'
   #3 @1 'Exp. nr. correct?: ' YN 1 COLOR=YELLOW REQUIRED=YES
     @60 '(Y/N)'
   #5 @1 'Time step         : 0.' STEP 2 COLOR=YELLOW REQUIRED=YES
     @60 '(seconds)';
%DISPLAY INFO;
   %LET NR1=%SUBSTR(&INNAME,%LENGTH(&INNAME)-1,1);
   %LET NR2=%SUBSTR(&INNAME,%LENGTH(&INNAME),1);
   %LET TAPE=%SUBSTR(&INNAME,%LENGTH(&INNAME)-4,2);
   %LET DIR=.\;
%WINDOW EXPNR COLOR=RED IROW=12 ICOLUMN=1 ROWS=3 COLUMNS=78
   #1 @1 "Exp. number: T&TAPE.B" NR 2 COLOR=WHITE REQUIRED=YES;
%MACRO NAMES;
   %IF (&YN=n OR &YN=N) %THEN %DO;
      %DISPLAY EXPNR;
      %LET NR1=%SUBSTR(&NR,1,1);
      %LET NR2=%SUBSTR(&NR,2,1);
   %END;
   %IF %LENGTH(&INNAME)>6 %THEN
       %LET DIR=%SUBSTR(&INNAME,1,%LENGTH(&INNAME)-6);
%MEND NAMES;
```

```
   %NAMES;
*  READ IND FILE  ;
DATA INDEX;
   INFILE "&INNAME..IND" FIRSTOBS=2 END=LAST;
   RETAIN T 0;
   IF _N_ NE 1 THEN T=T+&STEP;
   INPUT SAMPLE $ START END RMS N BUFFER;
   RECORD=START; OUTPUT;
   IF START NE END THEN DO; RECORD=END; OUTPUT; END;
   IF LAST THEN CALL SYMPUT('NUMBER',MAX(START,END));
   KEEP T RECORD BUFFER;
RUN;
PROC SORT DATA=INDEX;
   BY RECORD;
RUN;
*  DETERMINE THE COORDINATE SYSTEM  ;
   %LET TOP=18;
   %LET BOTTOM=496;
   %LET LEFT=113;
   %LET RIGHT=441;
   %LET XRANGE=%EVAL(&RIGHT-&LEFT);
   %LET YRANGE=%EVAL(&BOTTOM-&TOP);
DATA _NULL_;
   INFILE "&INNAME..WLD" RECFM=N;
   DO I=1 TO 3;
      INPUT BYTE PIB2.;
   END;
   CALL SYMPUT('RCODE',BYTE);
   STOP;
RUN;
%MACRO REFLECT;
   %IF &RCODE=0 %THEN %LET TOP=%EVAL(511-&BOTTOM);
   %ELSE %DO;
       %LET YRANGE=%EVAL(-&YRANGE);
       %LET TOP=%EVAL(511-&TOP);
   %END;
%MEND REFLECT;
   %REFLECT;
*  READ PRT FILE  ;
DATA POSITION;
   INFILE "&INNAME..PRT" RECFM=N;
   DO RECORD=1 TO &NUMBER;
      DO I=1 TO 3;
         INPUT BYTE PIB2.;
         IF I=2 THEN XDIG=1.447*(BYTE*&XRANGE/65535+&LEFT-255.5);
         ELSE IF I=3 THEN YDIG=BYTE*&YRANGE/65535+&TOP-255.5;
      END;
      OUTPUT;
```

```
   END;
   STOP;
   KEEP RECORD XDIG YDIG;
RUN;
*  DISTINGUISH THE TWO BALLS  ;
DATA BALL;
   MERGE INDEX POSITION;
   BY RECORD;
   IF (XDIG-30.85)**2+(YDIG-1.72)**2>50 THEN OUTPUT;
   DROP RECORD;
RUN;
PROC DATASETS LIBRARY=WORK;
   DELETE INDEX POSITION;
QUIT;
PROC SORT DATA=BALL;
   BY T;
RUN;
*  CORRECT THE TIME CODE  ;
   %LET PI= 3.14159265358979;
   %LET TWOPI=6.28318530717958;
   %LET LAGS=%STR(
   LF=LAG(F);
   IF LF<-3 AND F>0 THEN LF=LF+&TWOPI; );
%MACRO TIME;
   %IF &STEP=4 %THEN %LET LAGS=&LAGS%STR(
       F4=  4*F-3*LF;
       F3= (7*F-5*LF)/2;
       F2=  3*F-2*LF;
       F1= (5*F-3*LF)/2;
       F0=  2*F-  LF;
       F_1=(3*F-  LF)/2;
       F_2=   F;
       F_3=  (F+  LF)/2;
       F_4= LAG1(F);
       F_5=(LAG1(F)+LAG2(F))/2;
       F_6= LAG2(F);
       F_7=(LAG2(F)+LAG3(F))/2;
       F_8= LAG3(F); );
   %ELSE %IF &STEP=8 %THEN %LET LAGS=&LAGS%STR(
       F4=  3*F-2*LF;
       F3=(11*F-7*LF)/4;
       F2= (5*F-6*LF)/2;
       F1= (9*F-5*LF)/4;
       F0=  2*F-  LF;
       F_1=(7*F-3*LF)/4;
       F_2=(3*F-  LF)/2;
       F_3=(5*F-  LF)/4;
       F_4=   F;
```

```
      F_5=(3*F+  LF)/4;
      F_6=(  F+  LF)/2;
      F_7=(  F+3*LF)/4;
      F_8=       LF; );
   %ELSE %LET LAGS=&LAGS%STR(
      F4=  (8*F-5*LF)/3;
      F3= (15*F-9*LF)/6;
      F2=  (7*F-4*LF)/3;
      F1= (13*F-7*LF)/6;
      F0=   2*F-  LF;
      F_1=(11*F-5*LF)/6;
      F_2= (5*F-2*LF)/3;
      F_3= (9*F-3*LF)/6;
      F_4= (4*F-  LF)/3;
      F_5= (7*F-  LF)/6;
      F_6=    F;
      F_7= (5*F+  LF)/6;
      F_8= (2*F+  LF)/3; );
%MEND TIME;
   %TIME;
*  AND COUNT THE NUMBER OF TRAJECTORIES  ;
DATA BALL;
   SET BALL END=LAST;
   ARRAY FF F4 F3 F2 F1 F0 F_1-F_8;
   RETAIN M 1 IMAGE FLAGBUF DT 0 F R0;
   IMAGE=IMAGE+1;
   FDIG=ATAN((YDIG-1.72)/(XDIG-30.85));
   IF XDIG LE 30.85 THEN FDIG=FDIG-&PI;
   RDIG=SQRT((XDIG-30.85)**2+(YDIG-1.72)**2);
   &LAGS;
   IF BUFFER LT LAG(BUFFER) AND IMAGE GT 4 THEN DO;
      DIST=&PI-ABS(MOD(ABS(FDIG-F0),&TWOPI)-&PI);
      IF &PI-ABS(MOD(ABS(FDIG- F1),&TWOPI)-&PI) LT DIST OR
         &PI-ABS(MOD(ABS(FDIG-F_1),&TWOPI)-&PI) LT DIST THEN DO;
         XDIG=30.85+R0*COS(F0);
         YDIG= 1.72+R0*SIN(F0);
         FDIG=ATAN((YDIG-1.72)/(XDIG-30.85));
         IF XDIG LE 30.85 THEN FDIG=FDIG-&PI;
         RDIG=SQRT((XDIG-30.85)**2+(YDIG-1.72)**2);
         FLAGCOR=1;
      END;
      FLAGBUF=1;
   END;
   ELSE DO;
      IF FLAGBUF=1 AND IMAGE GT 5 THEN DO;
         MIN=&PI;
         DO I=1 TO 13;
            DIST=&PI-ABS(MOD(ABS(FDIG-FF{I}),&TWOPI)-&PI);
```

```
            IF DIST<MIN THEN DO; INDEX=I; MIN=DIST; END;
          END;
          DT=DT-2*(INDEX-5);
       END;
       FLAGBUF=0;
    END;
    T=T+DT;
    F=FDIG; RO=RDIG;
    PX=-66.868288+2.091377*XDIG-0.002287*YDIG;
    PY= -0.093121+0.001293*XDIG+2.090268*YDIG;
    PRHO=SQRT(PX*PX+PY*PY);
    IF PRHO-LAG(PRHO)>250 THEN DO;
       M=M+1;
       IMAGE=0;
    END;
    _TYPE_='FINAL';
    IF LAST THEN CALL SYMPUT('FILES',M);
    IF FLAGCOR NE 1 AND IMAGE GT 3 THEN OUTPUT;
    KEEP T XDIG YDIG _TYPE_;
RUN;
PROC SORT DATA=BALL NODUPKEY;
    BY T;
RUN;
*  ADJUST DEFAULT SYSTEM OPTIONS  ;
    OPTIONS NONUMBER PS=63 LS=78;
    GOPTIONS DEVICE=HPLJS2;
    AXIS2 ORDER=(100 TO 500 BY 100) LABEL=('R');
    AXIS3 ORDER=(1 TO 2 BY 0.1) LABEL=(F=CGREEK 'Df/D' F=SIMPLEX 't');
    SYMBOL1 V=NONE I=JOIN;
*  SPLIT OFF TRAJECTORIES  ;
    %LET FIRST=1;
%MACRO WRITE;
    %DO I=1 %TO &FILES;
    *  FIND THE SHIFT  ;
       %LET NO1=&FIRST;
       DATA CIRCLE;
          SET BALL (FIRSTOBS=&FIRST) END=LAST;
          RETAIN N 0;
          X1=-66.868288+2.091377*XDIG-0.002287*YDIG;
          Y1= -0.093121+0.001293*XDIG+2.090268*YDIG;
          PHI=ATAN(Y1/X1);
          IF X1<0 THEN PHI=PHI-&PI;
          IF (PHI-LAG(PHI)> 3) THEN N=N+1;
          IF (PHI-LAG(PHI)<-3) AND (_N_ NE 1) THEN N=N-1;
          IF N=1 THEN OUTPUT;
          RHO=SQRT(X1*X1+Y1*Y1);
          IF RHO-LAG(RHO)>250 OR LAST THEN DO;
             CALL SYMPUT('FIRST',_N_+&FIRST-1);
```

```
        %IF &FIRST>1 %THEN %DO;
            %IF &NR2=9 %THEN %DO;
                %LET NR1=%EVAL(&NR1+1);
                %LET NR2=0;
            %END;
            %ELSE %LET NR2=%EVAL(&NR2+1);
        %END;
        STOP;
    END;
    KEEP XDIG YDIG;
RUN;
PROC NLIN DATA=CIRCLE OUTEST=B;
    PARMS XS=0
          YS=0;
    A11= 1.0032119404E+00;
    A12= 1.3562415386E-03;
    A21= 4.3645268283E-03;
    A22= 9.9678761234E-01;
    A31=-4.6472509465E-02;
    A32= 8.8859632522E-02;
    A1= -8.2386070451E+01;
    A2=  1.4580318470E+02;
    A3= -1.8025764000E+03;
    X0 = 1.0559229131E+02;
    Y0 =-3.0562048483E+02;
    Z0 = 3.7882919356E+03;
    Z  = 470/12;
    CONST=220900-X0*X0-Y0*Y0;
    DZ=Z-Z0;
    N =A31*(XDIG-XS)+A32*(YDIG-YS)+A3;
    TX=A11*(XDIG-XS)+A12*(YDIG-YS)+A1;
    TY=A21*(XDIG-XS)+A22*(YDIG-YS)+A2;
    T =X0*TX+Y0*TY;
    T2=TX*TX+TY*TY;
    MODEL CONST=(DZ/N)*(2*T+(DZ*T2/N));
    DER.XS=(DZ/N)*((2*A31*T)/N-2*(A11*X0+A21*Y0)+
                   (2*DZ*A31*T2)/N**2-(2*DZ/N)*(A11*TX+A21*TY));
    DER.YS=(DZ/N)*((2*A32*T)/N-2*(A12*X0+A22*Y0)+
                   (2*DZ*A32*T2)/N**2-(2*DZ/N)*(A12*TX+A22*TY));
RUN;
    DM 'OUTPUT; CLEAR; PGM';
*   KEEP THE SHIFT  ;
    %LET SHFTNAME=&DIR.SHIFT&TAPE;
    %LET OUTNAME=%SUBSTR(&INNAME,1,%LENGTH(&INNAME)-2)&NR1&NR2;
DATA B;
 SET B (KEEP=_TYPE_ XS YS);
 FILE "&SHFTNAME..PAR" MOD;
 IF _TYPE_='FINAL' THEN DO;
```

```
      PUT "%SUBSTR(&OUTNAME,%LENGTH(&INNAME)-5) " (XS YS) (13.10 +1);
      OUTPUT;
    END;
   RUN;
*  CREATE DAT FILE  ;
   %IF &I=&FILES %THEN %LET NO2=&FIRST;
                 %ELSE %LET NO2=%EVAL(&FIRST-1);
   DATA BALL&I;
      MERGE BALL
           (KEEP=T XDIG YDIG _TYPE_ FIRSTOBS=&NO1 OBS=&NO2)
            B END=LAST;
      BY _TYPE_;
      FILE "&OUTNAME..DAT";
      RETAIN N T0 0;
      IF _N_=1 THEN T0=T;
      T=(T-T0)/100;
      XDIG=XDIG-XS-0.0234904199;
      YDIG=YDIG-YS+0.1997646069;
      A11= 1.0032119404E+00;
      A12= 1.3562415386E-03;
      A21= 4.3645268283E-03;
      A22= 9.9678761234E-01;
      A31=-4.6472509465E-02;
      A32= 8.8859632522E-02;
      A1= -8.2386070451E+01;
      A2=  1.4580318470E+02;
      A3= -1.8025764000E+03;
      X0 = 1.0559229131E+02;
      Y0 =-3.0562048483E+02;
      Z0 = 3.7882919356E+03;
      TX=A11*XDIG+A12*YDIG+A1;
      TY=A21*XDIG+A22*YDIG+A2;
      NZ=A31*XDIG+A32*YDIG+A3;
      ALFA1=X0-TX*Z0/NZ;
      ALFA2=TX/NZ;
      BETA1=Y0-TY*Z0/NZ;
      BETA2=TY/NZ;
      A=BETA2*BETA2+ALFA2*ALFA2-144;
      B=2*ALFA1*ALFA2*BETA2-2*ALFA2*ALFA2*BETA1+288*BETA1;
      C=ALFA1*ALFA1*BETA2*BETA2-2*ALFA1*ALFA2*BETA1*BETA2+
        ALFA2*ALFA2*BETA1*BETA1-144*BETA1*BETA1;
      PY=(-B+SQRT(B*B-4*A*C))/(2*A);
      IF (PY-BETA1)/BETA2 < 0 THEN PY=PY-SQRT(B*B-4*A*C)/A;
      PX=ALFA2*PY/BETA2+ALFA1-ALFA2*BETA1/BETA2;
      PRHO=SQRT(PX*PX+PY*PY);
      PPHI=ATAN(PY/PX);
      IF PX<0 THEN PPHI=PPHI-&PI;
      IF (PPHI-LAG(PPHI)> 3) THEN N=N+1;
```

```
        ELSE IF (PPHI-LAG(PPHI)<-3) AND (_N_ NE 1) THEN N=N-1;
        PHI_TOT=-PPHI+N*&TWOPI;
        PUT T 8.2 +1 PRHO 8.3 +1 PHI_TOT 8.3;
        IF PHI_TOT GE 0 THEN OUTPUT;
        IF LAST THEN CALL SYMPUT ('PHIMAX',10*FLOOR(PHI_TOT/10+1));
        PHI_DOT=(PHI_TOT-LAG(PHI_TOT))/(T-LAG(T));
        KEEP T PRHO PHI_TOT PHI_DOT;
     RUN;
  *  PLOT THE TRAJECTORY  ;
        AXIS1 ORDER=(0 TO &PHIMAX BY 10) LABEL=('Phi');
     PROC GPLOT DATA=BALL&I;
        PLOT PRHO*PHI_TOT /GRID HAXIS=AXIS1 VAXIS=AXIS2;
        FOOTNOTE J=R "%SUBSTR(&OUTNAME,%LENGTH(&OUTNAME)-5)";
     RUN;
     PROC GPLOT DATA=BALL&I;
        PLOT PHI_DOT*PHI_TOT /GRID HAXIS=AXIS1 VAXIS=AXIS3;
     RUN;
  *  DELETE BALL#I  ;
     PROC DATASETS LIBRARY=WORK;
        DELETE BALL&I;
     QUIT;
  %END;
%MEND WRITE;
  %WRITE;
  FOOTNOTE '';
*  DELETE TEMPORARY DATA SETS  ;
PROC DATASETS LIBRARY=WORK;
  DELETE CIRCLE B;
RUN;
*  SOUND THE SIREN  ;
DATA _NULL_;
  DO I=0 TO 12.5664 BY .062832;
     CALL SOUND(3000-2000*COS(I),55);
  END;
RUN;

/* END OF PROGRAMME */
```

Appendix D

Simulation programs

D.1 Simulating the basic model

```
% This program simulates the basic model (10,000 x).

% The Fehlberg coefficients:
alpha = [1/4  3/8  12/13  1  1/2]';
beta  = [ [    1      0      0     0      0    0]/4
          [    3      9      0     0      0    0]/32
          [ 1932  -7200   7296     0      0    0]/2197
          [ 8341 -32832  29440  -845      0    0]/4104
          [-6080  41040 -28352  9295  -5643    0]/20520 ]';
gamma = [902880  0  3953664  3855735  -1371249  277020]'/7618050;
f = zeros(5,6);

% Trench times:
trtime = [-1.476 0.000; -1.350 0.017; -1.050 0.054; -0.750 0.131;
          -0.450 0.330; -0.150 0.576;  0.150 0.713;  0.450 0.840;
           0.750 0.913;  1.050 0.955;  1.350 0.978;  1.650 0.990;
           1.950 0.994;  2.250 0.998;  0.255 0.999;  2.850 1.000];

% Physical dimensions.
Rrim=0.487; Rnum=0.205; Rcom=0.158;
sina=sin(0.0831); cosa=cos(0.0831);
AA=0.0175; R0=Rrim-AA;

% Estimated constants.
Fr=0.0163; F1=0.0115; H1=0.3;
```

```
% Random components;
dt=0.08;
rand('seed',7065);
randn('seed',7065);
S1=0.0040*cosa; S2=0.0029;
Sstar=0.2938;

for nr=0:9999, disp(nr)

% Rolling along the rim (1a).
Fdot1=0.7723482/sqrt(R0);
Fdot0=Fdot1+10*pi*Fr*(1+rand(1));
t1=log(Fdot0/Fdot1)/Fr;
T1a=[[0:dt:t1]';t1]; n1a=length(T1a);
c1=ones(size(T1a)); exp1=exp(-Fr*T1a);
X1a=[R0*c1,0*c1,Fdot0/Fr*(1-exp1),Fdot0*exp1,...
     -(1-sina)/cosa*R0*Fdot0*exp1/AA];
x1=[X1a(n1a,3),X1a(n1a,5)];

% Slipping along the rim (1b).
tau1=1.476+table1([trtime(:,2),trtime(:,1)],rand(1));
T1b=[[dt:dt:tau1]';tau1];
c1=ones(size(T1b)); exp1=exp(-F1*T1b);
X1b=[R0*c1,0*c1,x1(1)+Fdot1/F1*(1-exp1),Fdot1*exp1,...
     x1(2)*exp(-H1*T1b)];
T1=[T1a;T1a(n1a)+T1b]; X1=[X1a;X1b]; n1=length(T1);
clear c1 exp1 T1a T1b X1a X1b

% Rolling on the surface (2).
% (Fixed friction level 0.0161)
T2=zeros(3000,1); X2=zeros(3000,5);
ti=T1(n1); xi=X1(n1,:)';
i=1; X2(i,:)=xi';
while xi(1)>Rnum
      % Compute the slopes
      f(:,1) = simp(ti,xi)';
      for j = 1:5
         f(:,j+1) = simp(ti+alpha(j)*dt, xi+dt*f*beta(:,j))';
      end
      % Update the solution
      ti = ti + dt;
      xi = xi + dt*f*gamma;
      % Add disturbances
      xi(2)=xi(2)+randn(1)*S1*dt;
```

D.2 Simulating the complete model

```
% This program simulates the complete model (10,000 x).

% The Fehlberg coefficients:
alpha = [1/4  3/8  12/13  1  1/2]';
beta  = [ [    1      0      0     0      0    0]/4
          [    3      9      0     0      0    0]/32
          [ 1932  -7200   7296     0      0    0]/2197
          [ 8341 -32832  29440  -845      0    0]/4104
          [-6080  41040 -28352  9295  -5643    0]/20520 ]';
gamma = [902880  0  3953664  3855735  -1371249  277020]'/7618050;
f = zeros(5,6);

% Trench times:
trtime = [-1.476 0.000; -1.350 0.017; -1.050 0.054; -0.750 0.131;
          -0.450 0.330; -0.150 0.576;  0.150 0.713;  0.450 0.840;
           0.750 0.913;  1.050 0.955;  1.350 0.978;  1.650 0.990;
           1.950 0.994;  2.250 0.998;  0.255 0.999;  2.850 1.000];

% Trench tables
load drumhigh.tab
load drumlow.tab
load ringhigh.tab
load ringlow.tab

% Physical dimensions.
Rrim=0.487; Rnum=0.205; Rcom=0.158;
sina=sin(0.0831); cosa=cos(0.0831);
AA=0.0175; R0=Rrim-AA;

% Estimated constants.
Fr=0.0163; F1=0.0115; H1=0.3;

% Random components;
dt=0.08;
rand('seed',0);
randn('seed',0);
S1=0.0040*cosa; S2=0.0029;
Sstar=0.2938;

for nr=0:9999, disp(nr)
```

```
      xi(4)=xi(4)+randn(1)*S2*dt/xi(1);
      i=i+1; T2(i)=ti; X2(i,:)=xi';
end
T2=T2(1:i); X2=X2(1:i,:);
tn1=table1([X2(i-1:i,1),T2(i-1:i)],Rnum);
xn1=[Rnum,table1(X2(i-1:i,:),Rnum)];
T2=T2(2:i-1); X2=X2(2:i-1,:);
Gamma=13/pi*xn1(3)-floor(13/pi*xn1(3));

% Bouncing onto a lamella (3).
Nustar=-9.279+31.63*Rnum*xn1(4)+1.198*Gamma+Sstar*randn(1);
if Nustar<1.5, Nu=1; elseif Nustar<2.5, Nu=2; else Nu=3; end
tnp=(Nu-Gamma+0.5)*pi/13/xn1(4);
T3=[[0:dt:tnp]';tnp]; c3=ones(size(T3));
X3=[xn1(1)+T3*xn1(2),c3*xn1(2),...
    xn1(3)+T3*xn1(4),c3*xn1(4),c3*xn1(5)];
T3=tn1+T3; n3=length(T3);
clear c3

% Rolling through a compartment (4).
taunp=1.2-tnp;
X3(n3,2)=(Rcom-X3(n3,1))/taunp; X3(n3,4:5)=[0 0]; xnp=X3(n3,:);
T4=[dt:dt:taunp]'; c4=ones(size(T4));
X4=[xnp(1)+T4*xnp(2),c4*xnp(2),c4*xnp(3),c4*0,c4*0];
T4=tn1+tnp+[T4;taunp]; X4=[X4;[Rcom,0,xnp(3),0,0]];
clear c4

% Save results.
t=[T1;T2;T3;T4]; x=[X1;X2;X3;X4];
name=sprintf('c:\\matlab\\basic\\bas%-4.0f',nr);
fid=fopen(name,'a');
fwrite(fid,[t x],'float32');
fclose(fid);
clear T1 T2 T3 T4 t X1 X2 X3 X4 x

end
```

```
% Rolling along the rim (1a).
Fdot1=0.7723482/sqrt(R0);
Fdot0=Fdot1+10*pi*Fr*(1+rand(1));
t1=log(Fdot0/Fdot1)/Fr;
T1a=[[0:dt:t1]';t1]; n1a=length(T1a);
c1=ones(size(T1a)); exp1=exp(-Fr*T1a);
X1a=[R0*c1,0*c1,Fdot0/Fr*(1-exp1),Fdot0*exp1,...
     -(1-sina)/cosa*R0*Fdot0*exp1/AA];
x1=[X1a(n1a,3),X1a(n1a,5)];

% Slipping along the rim (1b).
tau1=1.476+table1([trtime(:,2),trtime(:,1)],rand(1));
T1b=[[dt:dt:tau1]';tau1];
c1=ones(size(T1b)); exp1=exp(-F1*T1b);
X1b=[R0*c1,0*c1,x1(1)+Fdot1/F1*(1-exp1),Fdot1*exp1,...
     x1(2)*exp(-H1*T1b)];
T1=[T1a;T1a(n1a)+T1b]; X1=[X1a;X1b]; n1=length(T1);
clear c1 exp1 T1a T1b X1a X1b

% Rolling on the surface (2).
% (Fixed friction level 0.0161)
T2=zeros(3000,1); X2=zeros(3000,5);
ti=T1(n1); xi=X1(n1,:)';
i=1; X2(i,:)=xi';
while xi(1)>Rnum
      % Compute the slopes
      f(:,1) = compfr(ti,xi)';
      for j = 1:5
         f(:,j+1) = compfr(ti+alpha(j)*dt, xi+dt*f*beta(:,j))';
      end
      % Update the solution
      ti = ti + dt;
      xi = xi + dt*f*gamma;
      % Add disturbances
      xi(2)=xi(2)+randn(1)*S1*dt;
      xi(4)=xi(4)+randn(1)*S2*dt/xi(1);

% Drawing a trench lot.
si=(sign(xi(2))-sign(X2(i,2)))*sign(abs(X2(i,2)))*(xi(1)<=R0);
if si~=0 % Local extremum
   tk=table1([X2(i,2) T2(i);xi(2) ti],0);
   xk=table1([T2(i) X2(i,:);ti xi'],tk); xk(2)=0;
   if si<0 % Local maximum
      if ((xk(1)<0.390 & xk(1)>0.385) |
```

```
         (xk(1)<0.260 & xk(1)>0.255))
         p=table2(ringhigh,xk(1),rem(xk(3),2*pi));
      else
         p=table2(drumhigh,xk(1),rem(xk(3),2*pi));
      end
   else % Local minimum
      if ((xk(1)<0.390 & xk(1)>0.385) |
         (xk(1)<0.260 & xk(1)>0.255))
         p=table2(ringlow,xk(1),rem(xk(3),2*pi));
      else
          if xk(1)>Rnum
             p=table2(drumlow,xk(1),rem(xk(3),2*pi));
          else, p=0; end
      end
   end
   % Rolling through a trench.
   if rand(1)<p
      i=i+1; T2(i)=tk; X2(i,:)=xk; si=sign(si);
      Fk=0.0113-0.0017*si;
      tauk=max(0,0.4301+1.699*xk(1)*xk(4)+0.3149*si+...
                 table1([trtime(:,2),trtime(:,1)],rand(1)));
      ti=tk+tauk; xi=[xk(1:2)';xk(3)+xk(4)/Fk*(1-exp(-Fk*tauk));
                                 xk(4)*exp(-Fk*tauk);xk(5)];
   end
end

      i=i+1; T2(i)=ti; X2(i,:)=xi';
end
if X2(i-1,2)==0, i=i-1; end
T2=T2(1:i); X2=X2(1:i,:);
tn1=table1([X2(i-1:i,1),T2(i-1:i)],Rnum);
xn1=[Rnum,table1(X2(i-1:i,:),Rnum)];
T2=T2(2:i-1); X2=X2(2:i-1,:);
Gamma=13/pi*xn1(3)-floor(13/pi*xn1(3));

% Bouncing onto a lamella (3).
Nustar=-9.279+31.63*Rnum*xn1(4)+1.198*Gamma+Sstar*randn(1);
if Nustar<1.5, Nu=1; elseif Nustar<2.5, Nu=2; else Nu=3; end
tnp=(Nu-Gamma+0.5)*pi/13/xn1(4);
T3=[[0:dt:tnp]';tnp]; c3=ones(size(T3));
X3=[xn1(1)+T3*xn1(2),c3*xn1(2),...
    xn1(3)+T3*xn1(4),c3*xn1(4),c3*xn1(5)];
T3=tn1+T3; n3=length(T3);
clear c3
```

```
% Rolling through a compartment (4).
taunp=1.2-tnp;
X3(n3,2)=(Rcom-X3(n3,1))/taunp; X3(n3,4:5)=[0 0]; xnp=X3(n3,:);
T4=[dt:dt:taunp]'; c4=ones(size(T4));
X4=[xnp(1)+T4*xnp(2),c4*xnp(2),c4*xnp(3),c4*0,c4*0];
T4=tn1+tnp+[T4;taunp]; X4=[X4;[Rcom,0,xnp(3),0,0]];
clear c4

% Save results.
t=[T1;T2;T3;T4]; x=[X1;X2;X3;X4];
name=sprintf('c:\\matlab\\complete\\comp%-4.0f',nr);
fid=fopen(name,'a');
fwrite(fid,[t x],'float32');
fclose(fid);
clear T1 T2 T3 T4 t X1 X2 X3 X4 x

end
```

Appendix E

List of symbols

The list of symbols is ordered alphabetically, where capitals precede small letters, and Greek precedes Roman. Throughout this dissertation, vectors are printed in bold face type (e.g. $\boldsymbol{v}$), their lengths in normal type (e.g. v), and their components are denoted with subscripts. Time dependent variables are sometimes denoted as explicit time functions (e.g. $R(t)$), but usually not (e.g. R). Time derivatives are indicated with a dot (e.g. $\dot{R}$). Tildes and circumflex signs indicate transformed variables (e.g. $\tilde{R}$); these signs are usually omitted after the variables have been properly introduced. Unless explicitly defined otherwise, subscripts indicate components (of vectors, e.g. x_1, or of asymptotic power series, e.g. u_1), quantities belonging to specific points (e.g. $\boldsymbol{v}_o$), or quantities belonging to specific times (e.g. $R_0 = R(t_0)$).

α	surface inclination angle
Adv	advanced strategy
a	radius of the ball
β	tilt angle
γ	fractional compartment position
c	dimensionless constant of order 1; camera constant
$\Delta\varphi$	total covered angle
ΔN	total number of compartments, modulo 26
Δn	total number of compartments
ΔP	rounded total number of periods
ΔR	descent per full period

δ	small, dimensionless parameter
d_1, d_2	dimensionless constants of order 1
d_m	depth (of a trajectory near the limit ring)
ε	small, dimensionless parameter
ε_1, ε_2, ε_3	processes of standard Brownian motion
e_1, e_2, e_3	moving axes
e, e_m	ellipticity
Φ, Φ_m	periodicity
φ	angular ball position
φ_1, φ_2	slow, and fast angular scale
φ_β	angular tilt position
$\mathcal{F}$	air friction function
F_a, F_d, F_g, F_n	forces: due to air friction, dry friction, gravitation, and normal force, respectively
$\overline{f}$	level of friction
f_l, f_q, f_r, f_t f_{t1}	air friction coefficients: linear and quadratic, along the rim, for surface trenches, and the first trench, respectively
G	expected gain
g	gravitation constant
η	corrected trench time
h_m	height (of a trajectory near the limit ring)
h_t, h_{t1}	spin friction coefficients: for surface trenches, and the first trench, respectively
I	central moment of inertia
Int, $Int^{i\times j}$	intersection strategies: single-number, and multiple-numbers (bets on $i \times j$ diametrical compartments)
lim	index of the limit ring intersection time
M_d, M_r, M_w	momentums: due to dry friction, rolling resistance, and winding, respectively
Min	minimum strategy
m	mass of the ball; index of the last local minimum before the limit ring intersection time
ν, ν^*	compartment jump during the downfall
N	compartment number position; size of the normal force
Num	numeric strategy

n	number of stages between rim and edge
num	index of the edge intersection time
O	(imaginary) drum apex; order symbol
Opt	optimal strategy
o	centre of the ball; centre of projection
obs	index of the observation ring intersection time
p	conditional probability distribution of the total number of compartments; smoothing parameter
P	point of contact between ball and surface
P_t	trench probability
Q	point of contact between ball and rim
R	radial ball position
Rob	robust strategy
r_m	rise (of a trajectory near the limit ring)
rim	index of the time of descent (from the rim)
$\sigma_1,\ \sigma_2,\ \sigma_3,\ \sigma^*$	standard deviations: of the three processes of Brownian motion, and of the compartment jump, respectively
$\mathcal{S}$	level of skill
τ	trench time
$TijBkl$	experiment code (tape ij, orbit kl)
t	time
t_f	final time (of a trajectory between rim and edge)
$u,\ v,\ w$	asymptotic power series
v	velocity
Ω	angular velocity of the moving axes
Ω_1	asymptotic power series representing a phase shift
ω	angular velocity of the ball
w	winding coefficient
$X,\ Y,\ Z$	fixed axes (in the real world); real-world coordinates
$X_0,\ Y_0,\ Z_0$	real-world coordinates of the centre of projection
x	position of the ball; momentary state vector
$x,\ y,\ z$	fixed axes (in the projection image); image coordinates
$\dot{\psi}$	spin
$y_1,\ (y_2,\ y_3)$	total covered area per time unit, (and two additional variables)

Bibliography

[1] W. Albers, *Behendigheid bij Eurobsgame; een tussenrapportage.* Enschede: Technische Universiteit (1994)

[2] T. Amemiya, *Studies in Econometric Theory.* Vermont: Edgar Elgar Publishing Ltd. (1994)

[3] L.C. Boer, *Eurobsgame.* Soesterberg: IZF-TNO, report C-38 (1993)

[4] P.E.M. Borm and B.B. Van der Genugten, *On a measure of skill for games with chance elements.* Tilburg: Tilburg University, report FEW 721 (1996)

[5] S.B. Dalziel, *DigImage Particle Tracking.* University of Cambridge (1992)

[6] C. De Boor, *A Practical Guide to Splines.* New York: Springer Verlag (1978)

[7] F. Delbaen & J. Haezendonck, *Bespreking van de rapporten van prof.dr. W.A. Wagenaar.* Brussel: Vrije Universiteit (1987)

[8] J.C. De Vos, *A thousand Golden Ten orbits.* Tilburg: Tilburg University, report FEW 654 (1994)

[9] J.C. De Vos, Using the SAS system to acquire a set of Golden-Ten orbits. *SEUGI Proceedings* 13 (1995) 902-913

[10] J.C. De Vos and B.B. Van der Genugten, *Fitting a stochastic model for Golden-Ten.* Tilburg: Tilburg University, report FEW 735 (1996)

[11] J.C. De Vos and A.A.F. Van de Ven, The Golden-Ten equations of motion. *Journal of Engineering Mathematics* (1997)

[12] H.L. Dryden, F.P. Murnaghan and H. Bateman, *Hydrodynamics.* Dover Publications (1956)

[13] P. Embrechts, W. Stahel & M. Aebi, *Beurteilung des Spiels "Dix d'Or".* Zürich: IFOR, Dokument A 930531 (1993)

[14] R.D. Gill & C.G.M. Oudshoorn, Behendigheid bij Fantasie 24? *Kwantitatieve Methoden* 46 (1993) 3-13

[15] J. Kevorkian and J.D. Cole, *Perturbation Methods in Applied Mathematics.* New York: Springer Verlag (1981)

[16] F.P.G.M. LaFors & G.B. Derksen, *Golden Ten, een kansspel of behendigheidsspel?* 's Gravenhage: IWIS-TNO, report D-81 ST 55 33 (1981)

[17] P.W. Likins, *Elements of Engineering Mathematics.* New York: McGraw-Hill (1973)

[18] The MathWorks, *Matlab Reference Guide.* Natick: The MathWorks Inc. (1993)

[19] N(ationale) S(tichting) C(asinospelen), *Golden Ten; een onderzoek gedaan naar de spelresultaten van Golden Ten na toepassing van de betalingsregel.* Hoofddorp: Holland Casino's (1986)

[20] H. Rouse, *Elementary Mechanics of Fluids.* New York: John Wiley and Sons (1959)

[21] SAS Institute, *SAS Language Reference.* Cary: SAS Institute (1990)

[22] Z. Schuss, *Theory and Applications of Stochastic Differential Equations.* New York: John Wiley & Sons (1980)

[23] K. Schwidefsky & F. Ackermann, *Photogrammetrie.* Stuttgart: Teubner (1976)

[24] J.L. Teugels, *Untitled; research on Golden Ten.* Leuven: Katholieke Universiteit (1994)

[25] N.N. Urban, *Gewerbeordnung für das Spiel "Roulette Opta II A".* Wiesbaden: Bundeskriminalamt, Unbedenklichkeitsbescheinigung Nr. ZV 33/5153.02/3335/87 (1988)

[26] B.B. Van der Genugten & P.E.M. Borm, Golden Ten: een kans- of behendigheidsspel. *Kwantitatieve Methoden* 38 (1991) 61-80

[27] B.B. Van der Genugten & P.E.M. Borm, *Een vergelijking van de behendigheid in spelen met een kanselement.* Tilburg: Katholieke Universiteit Brabant (1993)

[28] B.B. Van der Genugten, *Blackjack in Holland Casino's: hoe de dealer te verslaan.* Tilburg: Tilburg University Press (1993)

[29] B.B. Van der Genugten, *Een keuringsmethode voor behendigheidsautomaten.* Tilburg: Katholieke Universiteit Brabant, EIT report (1997)

[30] B.B. Van der Genugten, Blackjack in Holland Casino's: basic, optimal and winning strategies. *Statistica Neerlandica* (1997)

[31] B.B. Van der Genugten, P.E.M. Borm and W. Grossman, *Addendum to two reports on games of skill.* Tilburg: Katholieke Universiteit Brabant (1997)

[32] W.A. Wagenaar, *Is het spel "Golden Ten" een kansspel?* Soesterberg: IZF-TNO, report C-29 (1982)

[33] W.A. Wagenaar & J. Groeneweg, *Is het "kogelspel" een kansspel?* Soesterberg: IZF-TNO, report C-23 (1983)

[34] W.A. Wagenaar & G. Keren, *Het onderscheid tussen kans- en behendigheidsspelen.* Soesterberg: IZF-TNO, report C-5 (1985)

[35] S. Wolfram, *Mathematica, a System for Doing Mathematics by Computer.* Redwood City: Adddison-Wesly Publishing Co. (1991)

Summary

Golden-Ten bears some resemblance to Roulette. The main differences are that the orbit of the ball is not disturbed by any obstacles, that the number disc is not rotating, and that the players do not have to bet before they have observed the first part of the total orbit. Accurate observation allows the players to make a better than random guess on the outcome, and thus to earn some money. It is therefore not obvious that Golden-Ten and related trajectory games as Eurobsgame and Dromus-24 are games of chance, nor that they are games of skill.

The main issue in this research work is the determination of the exact level of skill in Golden-Ten and related trajectory games, thereby simplifying the decision whether or no such a game should be classified as a game of chance. Note that the decision itself is up to law-makers and judges. More specific questions in this research work are where the possible elements of skill in Golden-Ten eventually come through, how the players can employ these skills, and which is the optimal strategy, i.e. the one that renders the highest possible gain.

The research work starts off with a deterministic mechanical model to describe the motion of the ball in the drum. This model leads to a system of second order, non-linear ordinary differential equations, completed with a set of theoretical initial conditions. This system can be solved numerically, and - after it has been rewritten - part of it can even be solved exactly. However, solving the remaining part requires asymptotic approximation techniques. The results show that the orbit of the ball is a spiralling ellipse, with a clearly perceptible ellipticity and a uniformly rotating orientation.

The dissertation proceeds with a description of the setup and elaboration of an experiment to acquire a large set of accurately measured trajectories of real Golden-Ten balls in a real, used Golden-Ten drum. This set is the basis on which the validity of the theoretical assumptions

in the deterministic model can be tested, as well as the basis on which this model can be extended. The final result of the experiment is a fair-sized database of time series of two-dimensional ball coordinates, the accuracy of which appeared to be amply sufficient to compute time derivatives also.

A comparison of the experimental results to the the analytic results shows that the global characteristics are quite similar, but also that the local differences are relatively large. The small differences in the global course of the orbit can be modelled by extending the mechanical model with a number of deterministic factors. The local irregularities can be modelled as a standard Brownian motion, during which the ball occasionally gets stuck in one of the many concentric surface grooves. A few simple, extra extensions eventually lead to a complete stochastic model for the entire motion of the ball, from the launch up to and including the downfall in the number disc.

Analysis of the structure of the stochastic model leads to a number of practical players strategies, whereas simulations of this model yield the corresponding expected gains. One of the strategies is the advanced strategy, which is considered to be practically optimal. However, all strategies and their expected gains appear to be influenced by the prevailing level of air friction. For situations in which this level is not known, there are two alternatives. One is a robust strategy; another is an observation method to estimate the unknown friction level. The latter alternative leads to a strategy that is also applicable for trajectory games other than Golden-Ten.

One of the final results is the value of the level of skill in Golden-Ten. Skill is defined in such a manner that it links up closely to the code of the applicable Act on Games of Chance. This definition leads to an objective, quantitative measure to assess the level of skill in many games, not only trajectory games. The level of skill in Golden-Ten appears to be lower than that in Blackjack, which is generally known as a game of chance. However, the level of skill in Eurobsgame is higher, and that in (the yet fictitious game) Super-Ten is even much higher. Hence, the final word is up to the judge.

Samenvatting

Golden-Ten is een Roulette-achtig spel. De belangrijkste verschillen met Roulette zijn dat de baan van de kogel niet door obstakels wordt gehinderd, dat de getallenkrans niet ronddraait, en dat de spelers kunnen inzetten nadat ze het eerste deel van de kogelbaan gezien hebben. Met behulp van nauwkeurige observatie zijn de spelers in staat om een enigszins trefzekere voorspelling te doen, en daarmee geld te verdienen. Voor Golden-Ten en aanverwante kogelbaanspelen als Eurobsgame en Dromus-24 is het dus niet op voorhand duidelijk of het hier kansspelen dan wel behendigheidsspelen betreft.

Het doel van dit onderzoek is het bepalen van het behendigheidsniveau van Golden-Ten en aanverwante kogelbaanspelen, om daardoor de beslissing of een dergelijk spel wel of niet kan worden aangemerkt als een kansspel te vereenvoudigen. Merk op dat de beslissing zelf alleen kan worden genomen door de opstellers en de handhavers van de wet. Afgeleide onderzoeksvragen zijn welke vormen van behendigheid er eventueel kunnen worden aangewend, hoe deze kunnen worden aangewend, en welke strategie voor spelers optimaal is in die zin dat zij een maximale winst oplevert.

In dit proefschrift wordt de baan van de kogel in eerste instantie beschreven op grond van een deterministisch, fysisch bewegingsmodel. Hieruit worden de bewegingsvergelijkingen afgeleid als een stelsel tweede-orde, niet-lineaire gewone differentiaalvergelijkingen, met bijbehorende theoretische beginvoorwaarden. Dit stelsel kan numeriek worden opgelost, en door het te herschrijven kan een deel zelfs exact worden opgelost. Voor het overige deel wordt echter een asymptotische benaderingswijze gebruikt. De resultaten tonen aan dat de deterministische kogelbaan een spiralende ellips is, met een duidelijke waarneembare ellipticiteit, en een wentelende orientatie.

Vervolgens beschrijft dit proefschrift de opzet en de uitwerking van een

experiment ter verkrijging van een groot bestand van nauwkeurig opgemeten banen van echte Golden-Ten-kogels in een werkelijk als zodanig gebruikte Golden-Ten-ketel. Dit bestand is de basis waarop de geldigheid van de theoretische aannamen in het deterministische bewegingsmodel kan worden getoetst, alsmede de basis voor uitbreidingen van dit model. Het experiment heeft uiteindelijk geresulteerd in een behoorlijk bestand van tijdreeksen van twee-dimensionale kogelposities. De nauwkeurigheid bleek ruim voldoende te zijn om hieruit tevens tijdsafgeleiden te distilleren.

Vergelijking van de experimentele met de analytische resultaten leert dat de globale baankarakteristieken redelijk goed met elkaar overeenkomen, maar ook dat de lokale verschillen relatief groot zijn. De kleine verschillen in het globale baanverloop kunnen worden gemodelleerd door het fysische model uit te breiden met een aantal deterministische factoren. De onregelmatigheden in het lokale baanverloop kunnen gemodelleerd worden als een Brownse beweging, gedurende welke de kogel af en toe blijft steken in één van de vele concentrische oppervlaktegroefjes. Met enkele eenvoudige, extra uitbreidingen ontstaat er een stochastisch bewegingsmodel voor de volledige baan van de kogel.

Uit de structuur van het stochastische bewegingsmodel worden een aantal praktische spelersstrategieën afgeleid, en met behulp van simulaties worden de bijbehorende verwachte winsten bepaald. Eén van de strategieën is dermate geavanceerd dat zij kan worden beschouwd als optimaal. Het blijkt echter dat alle strategieën, alsmede hun verwachte winsten, beïnvloed kunnen worden door het heersende luchtweerstandsniveau. Voor gevallen waarin dit niveau onbekend is worden er twee alternatieven geboden: men kan een robuuste strategie spelen, of men kan het weerstandsniveau schatten door middel van observatie. De laatstgenoemde methode leidt tot een strategie die tevens bruikbaar is voor andere kogelbaanspelen dan Golden-Ten.

Tenslotte wordt het behendigheidsniveau van Golden-Ten bepaald. Het begrip behendigheid wordt hier op zodanige wijze gedefinieerd dat het nauw aansluit bij de letterlijke bepalingen in de Wet op de Kansspelen. Deze definitie leidt tot een objectieve, kwantitatieve maat voor het meten van behendigheid in velerlei spelen. Het behendigheidsniveau van Golden-Ten blijkt lager te zijn dan bijvoorbeeld dat van Blackjack, dat algemeen bekend staat als een kansspel. Het niveau van Eurobsgame is echter hoger, en dat van (het tot nu toe fictieve spel) Super-Ten is zelfs fors hoger. Het woord is nu dus aan de rechter.

Golden-Ten bears some resemblance to Roulette. The main differences are that the orbit of the ball is not disturbed by any obstacles, that the number disc is not rotating, and that the players do not have to bet before they have observed the first part of the total orbit. Accurate observation allows the players to make a better than random guess on the outcome, and thus to earn some money. It is therefore not obvious that Golden-Ten and related trajectory games as Eurobsgame and Dromus-24 are games of chance, nor that they are games of skill.

The main issue in this research work is the determination of the exact level of skill in Golden-Ten and related trajectory games, thereby simplifying the decision whether or no such a game should be classified as a game of chance. Note that the decision itself is up to lawmakers and judges. More specific questions in this research work are where the possible elements of skill in Golden-Ten eventually come through, how the players can employ these skills, and which is the optimal strategy, i.e. the one that renders the highest possible gain.

ISBN 90-361-0016-X

(Side-view on drum, ball and number disc)